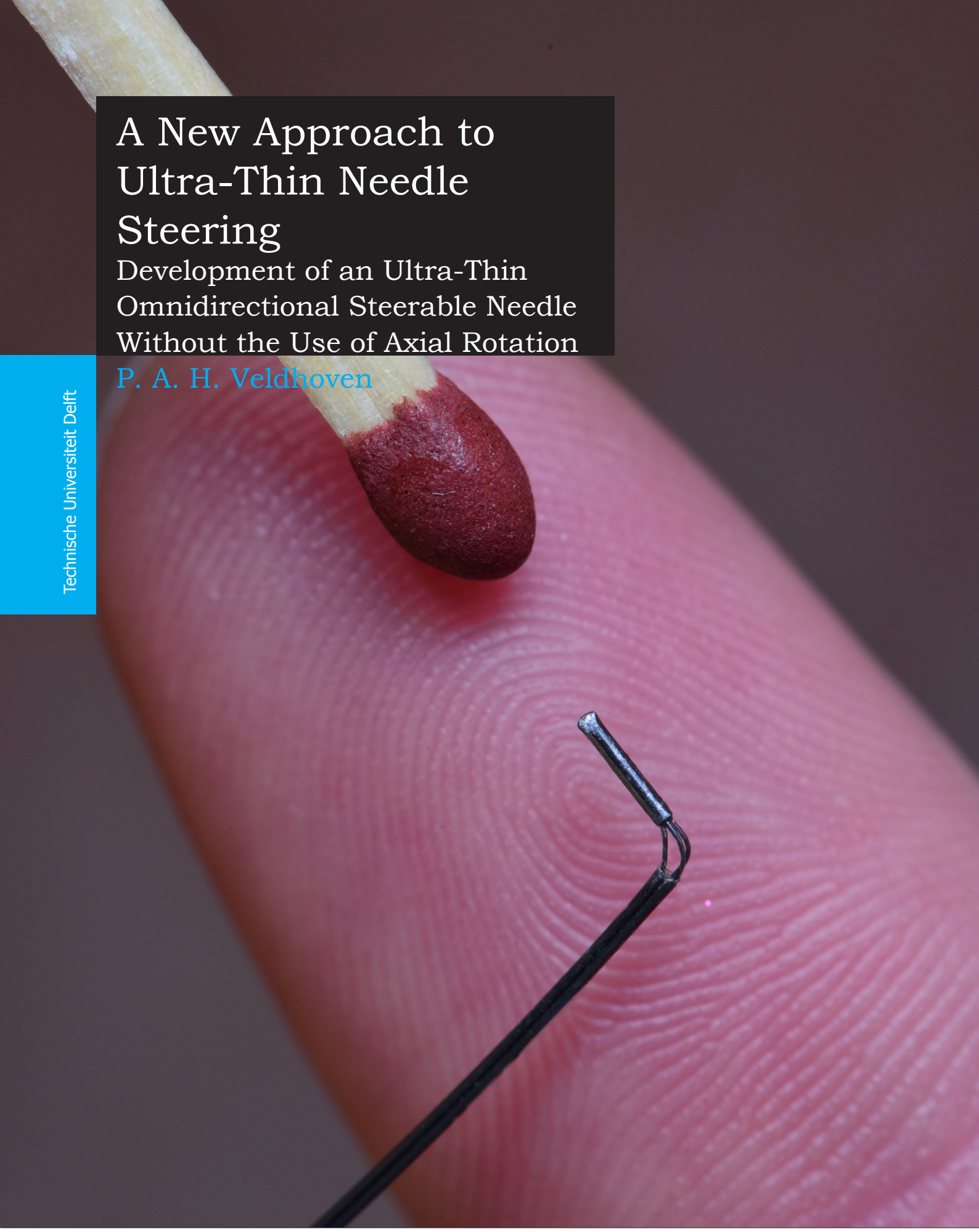

A New Approach to Ultra-Thin Needle Steering

Development of an Ultra-Thin Omnidirectional Steerable Needle Without the Use of Axial Rotation

P. A. H. Veldhoven

Technische Universiteit Delft

TU Delft Delft University of Technology

Challenge the future

A New Approach to Ultra-Thin Needle Steering

Development of an Ultra-Thin Omnidirectional Steerable Needle Without the Use of Axial Rotation

by

P. A. H. Veldhoven

in partial fulfillment of the requirements for the degree of

Master of Science
in Biomedical Engineering

at the Delft University of Technology,
to be defended publicly on Wednesday November 29, 2017 at 1:00 PM.

Supervisors:	Ir. M. Scali	
	Ir P.W.J. Henselmans	
	Prof. dr. ir. P. Breedveld	
Thesis committee:	Prof. dr. ir. P. Breedveld,	TU Delft
	Ir. M. Scali,	TU Delft
	Ir. P.W.J. Henselmans,	TU Delft
	Dr. ir. D. H. Plettenburg,	TU Delft

This thesis is confidential and cannot be made public until November 29, 2022.

TU Delft Delft University of Technology

Contents

Abstract

Flexible steerable needles can follow curved paths inside the human body, allowing to steer around objects, to adjust for mispunctures, and to reach multiple targets. However, the designs of existing ultra-thin (diameter < 1 mm) steerable needles require axial rotation of the needle to steer in 3D space causing needle twisting, which results in difficulties in needle trajectory control. Therefore, the goal of this paper is to design and experimentally evaluate an ultra-thin steerable needle, which can steer omnidirectional without the need of axial rotation.

This study describes a new way of ultra-thin needle steering by a retractable steering mechanism inside a flexible cannula. The steering mechanism prototype consists of three Nitinol wires with a small custom-made curvature at the tip to increase the internal bending moment. Pulling one or multiple elements results in reorientation of the tip , thereby allowing to steer without axial rotation of the needle. An experimental prototype was made, which includes the needle together with a control unit. The final needle prototype has a total of three elements to steer in three-dimensional space and has an outer diameter of 0.5 mm.

The prototype was tested in porcine gelatine phantoms (10 wt%) to evaluate the performance of the needle in terms of steering direction and curvature. The needle was able to steer towards the direction of the retracted element. Increasing the level of element retraction resulted in a higher steering curvature.

The maximal median deflection was 62.76 mm for an insertion of 65 mm into the gelatine. The proposed needle showed good potential in omnidirectional steering with high curvature and it is able to follow multi-curved trajectories. Future improvements can be done to refine the design and make it user-friendly. Possibly, this will allow the proposed needle to compete with ultra-thin standard bevel-tip and pre-curved needles.

Keywords: medical needles, steerable needles, ultra-thin needles, percutaneous procedures, soft tissue steering

1

Introduction

1.1. Medical Background

In recent years, there has been growing interest in steerable instruments for medical applications due to an increase in application of minimal invasive procedures [1] and the challenge to steer medical instruments through a body with limiting factors, such as size and safety. Percutaneous interventions are examples of minimal invasive procedures, where access to inner organs or other tissue is done via needle-puncture of the skin, rather than by using an "open" approach where inner organs or tissue are exposed [2].

Brachytherapy [3], tumour biopsy [4] and nerve blocking [5] are typical percutaneous procedures where medical needles are used to introduce radioactive seeds, to extract tissue samples or to inject fluids. Accurate needle placement is necessary to avoid treatment of unintended tissue, and biopsy of unintended tissue (resulting in misdiagnosis) [6]. The needles used in interventions can be categorised in straight rigid needles and flexible steerable needles. As rigid needles are not able to bend, the insertion position and the angle of needle insertion determine the needle trajectory inside the tissue. Steerable needles can deviate from the straight path during needle insertion, allowing more positioning freedom.

In some cases, straight rigid needles can not reach their targets because a straight path to the desired target is not realisable without crossing hard or sensitive structures, such as bone or blood vessels [7]. However, by utilising a flexible steerable needle, the obstacles can be avoided by steering around it (Figure 1.1 a).

Even when a target is reachable by a straight pathway, a rigid needle can be misplaced by tissue deformation, tissue in-homogeneity, physiological processes (e.g. fluid flow and respiration), image limitations, needle deflections, or misestimating of the puncture angle by the surgeon [7–9]. As the needle penetrates the tissue, the surrounding tissue deforms, and therefore, even when working with straight rigid needles, the target can be missed [10]. Especially in soft tissues such as breast tissue, tissue movement is noticeable [11], which leads to an increased chance of mispuncturing [12]. The mispuncturing of the needle requires retraction and reinsertion of the needle which, eventually, leads to elongation of procedure times, increase of tissue damage and increase of discomfort of the patient. Steerable needles are able to correct the pathway when the needle is misplaced (Figure1.1 b), avoiding reinsertion of the needle. Additionally, steerable needles enable access to multiple targets within a single insertion (Figure1.1 c).

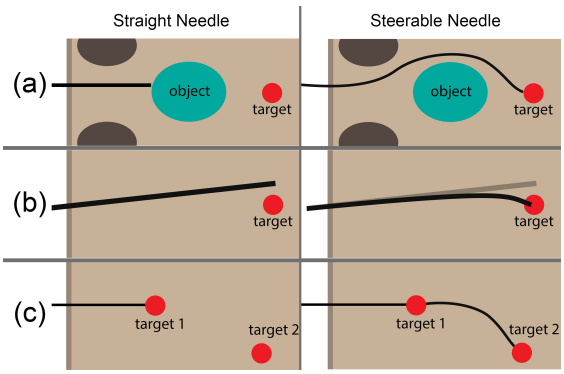

Figure 1.1: Comparison between rigid needle and steerable needle performances in three different situations: (a) Steering around an object, (b) correcting for mispuncture, (c) reaching multiple targets.

1.2. Needle-Tissue Interactions

The insertion of a needle can be categorised in four phases: the deformation phase, the penetration phase, the relaxation phase and the extraction phase [13] (Figure 1.2).

- **Phase 1: Deformation Phase**

In this phase, the needle pushes against the tissue causing deformation of the tissue. However, the needle does not puncture the tissue.

- **Phase 2: Penetration Phase**
  In the penetration phase the needle enters the tissue and moves forward. The needle needs to cut the tissue and has to overcome friction forces from the surrounding tissue during forward motion.

- **Phase 3: Relaxation Phase**
  This phase occurs after the needle is stationary. Due to viscoelastic properties of the tissue, the tissue will relax and forms partially back to its original position.

- **Phase 4: Extraction Phase**
  This phase covers the extraction of the needle. Friction forces between tissue and needle act on the needle when it is retracted from the tissue. Due to the friction forces the tissue will deform.

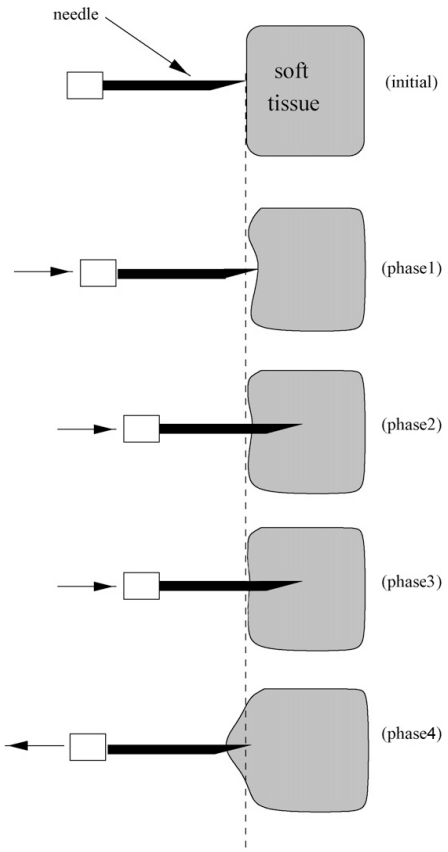

Figure 1.2: The initial phase and the four phases of needle insertion: deformation phase (phase 1), penetration phase (phase 2), relaxation phase (phase 3) and extraction phase (phase 4). Modified from [13].

This thesis will mainly focus on the penetration phase, where the needle is inside the tissue and needs to be steered towards a set target. During this phase, needle-tissue interaction forces affect the needle steering.

When the needle is inside tissue, the tissue acts with compression force on the needle. While moving the needle, the needle experiences a friction force ($F_{friction}$) along its shaft due to tissue adhesion and clamping [6] [14] (Figure 1.3). Soft tissue is considered to be viscoelastic, which means that the friction force increases as the velocity of the needle increases relative to the tissue [6]. While moving the needle, a cutting force is generated at the tip, which is necessary to cut through the tissue ($F_{cutting}$) (Figure 1.3) [6].

As the needle is pushed through the tissue, the total force on the needle is considered as a combination of frictional and cutting forces (1.2).

$$F_{needle}(x) = F_{friction}(x) + F_{cutting}(x) \quad (1.1)$$

When an asymmetric force is applied to the tip of a flexible needle, the needle will deflect into transverse direction. By controlling the transverse deflection, the needle can be steered towards a desired direction. The asymmetric force is often determined by the design of the tip of the needle. When a needle with an asymmetric tip shape is inserted into tissue, the shape of the tip and its interaction with the tissue creates an imbalance in lateral force [15].

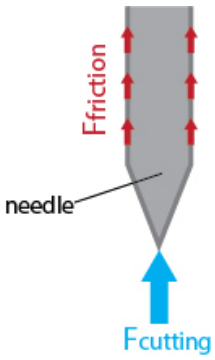

Figure 1.3: Needle-tissue interaction forces during needle insertion. The blue arrow represents the cutting force ($F_{cutting}$) at the tip of the needle and the red arrows represent the friction forces ($F_{friction}$) along the needle shaft.

1.3. State of the Art in Steerable Needles

Several studies focus on the development of new steering principles in percutaneous interventions to replace the traditional rigid needles with steerable needles. However, the diversity in designs decreases within miniaturised steerable needles.

1.3.1. Steering Principles

At the moment, some reviews on steerable needles exist, which show a large variety of steerable needles designs. The reviews of Scali et al. [9] and van de Berg et al. [8] give a comprehensive overview of steering principles and available designs for needle steering.

Scali et al. [9] provides a systematic classification of possible mechanical solutions for three-dimensional steering through solid organs, which results in seven distinct groups of steering: bevel-tip needles, one-plane pre-curved needles, two-plane pre-curved needles, needles with one on-demand deflection angle, needles with two on-demand deflection angles, and needles with one on-demand angle and one predefined deflection angle.

The planes in which the needle can steer are defined by the planes in which the needle deflects without rotation. One-plane steering means that the deflection of the needle is on one single plane, whereas deflection in a perpendicular plane can be achieved by rotation of the needle about its longitudinal axis [9]. Two plane steering allows deflection of the needle in two perpendicular planes, thereby increasing the steerability of the needle to follow more complex 3D trajectories [9].

Van de Berg et al. [8] classified needle designs found in literature on their steering technique and gives an overview of currently existing needle designs. Examples are, bevel tips, pre-curved stylets, active cannulas, programmable bevels, and tendon actuated tips (Figure 1.4).

Combining these two reviews, it can be concluded that all steering designs are based on three main principles of steering: bevel tip steering, pre-curved steering, and on-demand steering (Figure 1.5).

Bevel tip A bevel tip introduces asymmetric forces by introducing an angle at the tip. By pushing the needle through tissue, reaction forces are exerted on the surface of the needle (Figure 1.5 b). Due to the asymmetric reaction forces exerted on the surface of the bevel, the needle deflects in the direction of the bevel [9].

Pre-Curved

Various designs of pre-curved needles exist. Often the inner tube has a predefined curvature and is fed through an outer tube. This outer tube can be straight or pre-curved (e.g. concentric tubes). As the pre-curved stylet is fed through the cannula, it returns into its initial pre-curved shape, which allows the needle to follow the curved trajectory (Figure 1.5 a).

On-Demand

Needles with on-demand steering have at least one actuated part which causes deflection of the needle on demand [9]. The deflection can be locally and actively controlled. By actuation of the tip asymmetry is created, which makes the needle deflect when pushed forwards (Figure 1.5 c). There are numerous ways for on-demand actuation, such as mechanical, electrical, thermal and magnetic actuation [9]. Examples of on-demand steering principles are tendon-driven needles (mechanical), shape-memory alloy actuation (thermal), piezo-electric actuation (electrical) [8].

1.3.2. Limitations of Miniaturisation

Previous studies examined the relationship between post-biopsy complications and biopsy needle diameter [16] [17]. The study shows that less serious complications occur with fine biopsy needles (less than 1 mm) than with higher diameter needles [16] [17]. Furthermore, thin needles cause less damage to the tissue and facilitate highly curved trajectories due to their lower bending stiffness. Therefore, thin needles can be advantageous over thicker needles.

When we look at the dimensions of existing steerable needles, there is a large variety. In case of active cannulas (i.e. multiple pre-bend cannulas), and tendon actuated needles, the tubes and tendons takes up space in the shaft, which enlarges the overall diameter of the needle. Only bevel tip and pre-curved needle solutions provide diameters lower than 1 mm [18].

For standard bevel tip and one-plane pre-curved needles, the steering direction is controlled by rotation of the needle about its shaft at the base (outside the tissue). Thereby, reorienting the tip, allowing two-plane steering [19]. However, the rotation of the needle along

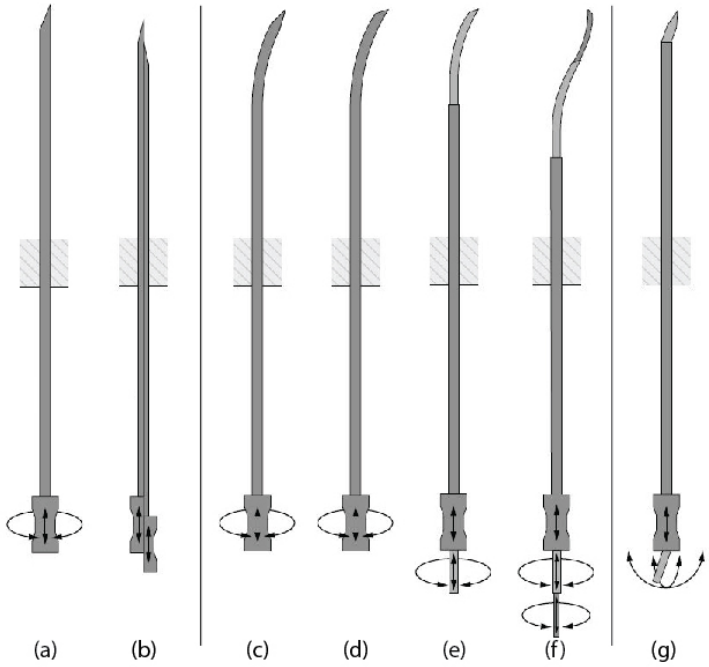

Figure 1.4: Steerable needles and their degrees of freedom in actuation. The depicted techniques are, respectively, bevel tip (a), programmable bevel tip (b), pre-curved needle (c), pre-curved bevel tip (d), pre-curved stylet (e), active cannula/concentric tubes (f) and on demand tendon actuated tip steering (g). The programmable bevel is here presented with two segments, versions with four segments are available as well. Modified from van de Berg et al. [8].

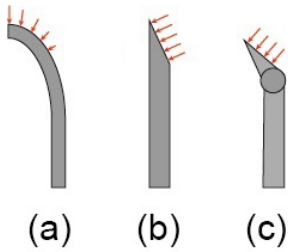

Figure 1.5: The red arrows represent the (asymmetric) forces on the needle tip during needle insertion into tissue of a pre-curved tip (a), bevel tip (b), and a conical on-demand tip (c).

its shaft may cause damage to the tissue, it can introduce inaccuracies due to torsion, and it makes the control of the needle trajectory challenging [20].

Of all needle designs only programmable bevel tips, concentric tubes, and on-demand actuated needles provide steering without rotation (Figure 1.4). However, the diameter of existing programmable bevel tips ranges from 4 mm up to 12 mm [21], and the diameter of tendon actuated needles from 1.67 mm [22] up to 2.2 mm [18] [23].

Torsion

When a needle is rotated at the base, torsion applies on the needle due to frictional forces of the tissue along the shaft of the needle. This torsion induces twist of the needle along the length of the needle. Reed et al. [19] showed that rotation of a bevel tip needle results in a significant discrepancy up to 45° between the orientation of the needle tip and the base where the needle angle is controlled, for an insertion depth of 10 cm (1.6).

The angle of twist of the needle caused by torsion can be calculated by

$$\phi = TL/JG \tag{1.2}$$

where T is the internal torque $[N * mm]$, J the polar moment of inertia $[mm^4]$, L the length of the object where the torque is applied to $[mm]$, and G the shear modulus [MPa].

The polar moment of inertia of a hollow cylindrical shaft can be calculated by

$$J = \pi(D^4 - d^4)/32 \tag{1.3}$$

where D is the outer diameter [mm] and d the inner diameter of the hollow cylinder. So, when the length (l) and torque (T) remain the same, the polar moment of inertia (J) and the shear modulus (G) determine the angle of twist.

When miniaturised, the shear modulus stays the same because it is a material property and does not change. The polar moment of inertia decreases when miniaturised, resulting in an increase of the angle of twist (ϕ) during rotation. Therefore, small needles experience increased twisting of the needle tip caused by torsion. This twist introduces positioning errors during needle insertion resulting in poor performance and control difficulties.

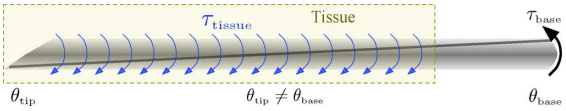

Figure 1.6: Angle deviation from the base by rotation of the needle due to friction along the tissue-needle interface where τ_{tissue} is the torsional friction, τ_{base} the torsion caused by the rotation at the base, θ_{tip} the angle at the tip, and θ_{base} the angle at the base [19].

Control Difficulties

For standard bevel tip needles (Figure 1.4 a) and standard pre-curved needles (Figure 1.4 c & d), the direction of steering is determined by the orientation of the tip. When the needle is moved forward without rotation, it bends into the direction of the bevel tip or pre-curve. To follow a straight trajectory, the needle needs to be rotated with a rate that is higher than the insertion rate. To allow in-between curvatures and to follow trajectories the needle is controlled by altering between insertion with and without rotation. This control strategy is known as 'duty cycling'. The duty cycle is defined as the period in which the needle is inserted while being rotated divided by the period of insertion without rotation [9]. Duty cycling of the needle is non-intuitive, which results in control difficulties [17]. A way to solve the problem of control difficulties requires development of a computerised robotic system that can plan and perform insertions of thin flexible needles [17].

Tissue Damage

Duty cycling of pre-curved or bevel needles cuts a local helical path into tissue when axially rotated, thereby introducing tissue damage (figure1.7) [24][23]. A straight pathway of bevel tip needles can be seen as a helical path with a small pitch [9]. To change steering direction, the needle has to be rotated, which lead to cutting of the tissue.

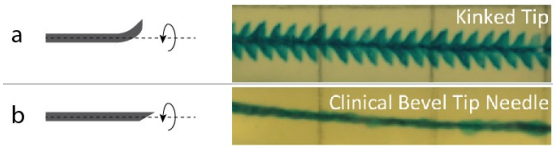

Figure 1.7: Tissue damage comparison of kinked bevel-tip needle (a) and clinical bevel-tip needle (b) by duty cycling. Modified from [24].

1.4. Problem Statement

Medical needles are often used in procedures, such as brachytherapy, tumour biopsy and drug delivery, for which accurate needle placement is necessary for the success of the procedure. However, reaching targets with straight needles can be challenging because of obstacles, image limitations and tissue deformations. Therefore, steerable needles have been introduced to steer around objects, to adjust for mispunctured needles, and to reach multiple targets.

Looking at existing steerable needles, three options exist for needle steering: bevel steering, pre-curved steering and on-demand steering. Small needles have the advantage of less tissue damage, less post-operation pain and provide larger curvature. When we look at steerable needles under 1 mm cross-sectional diameter, only bevel tip and pre-curved needle designs exist in such small dimensions. However, steering bevel and pre-curved needles in two planes requires rotation of the needle, leading to needle twisting and tissue damage [24][23]. These drawbacks of existing thin steerable needles imply the need for small needles with omnidirectional steering without the use of axial rotation.

1.5. Aim of the Thesis

The aim of this thesis is to develop an ultra-thin steerable needle which can steer in 3D (omnidirectional steering) without axial rotation. For the sake of finding the boundaries of miniaturisation, the aim is to design a needle with a maximum diameter of 0.5 mm, which is comparable to ultra-thin standard bevel tip needles.

1.6. Layout of the Thesis

Chapter 2 describes the development of the steering mechanism made from moving long slender elements. It covers the idea generation up to the concept choice. Chapter 3 describes the experiment which was performed in order

to select the best steering mechanism. In this experiment four tip designs were evaluated based on their angle and forces during retraction. In Chapter 4 the chosen steering mechanism was combined with a cannula and a control unit to make it into a fully working prototype. Chapter 5 describes an experiment which investigates the steering direction and deflection of the needle in porcin gelatine, to asses the performance of the needle design. Chapter 6 discusses the proposed design, the experiment, the limitations, and future work. Finally, in Chapter 7, the conclusions of this thesis are presented.

2

Steering Mechanism: Development Process

2.1. Requirements & Wishes

The objective in this study was to design a prototype of an ultra-thin needle that can steer in 3D (omnidirectional steering) without the use of axial rotation. A list of wishes and requirements for the needle can be found below.

Requirements

1. ***Omnidirectional steering***
   The needle should be able to steer in in 3D space, which means that it needs to steer in at least two planes.

2. ***Diameter smaller than 0.5 mm***
   Small needles have the advantages of less tissue damage, less post-operation pain and provide smaller bending radii. In terms of dimension, we set ourselves the aim of maximal cross-sectional diameter of 0.5 mm, which is comparable to ultra-thin standard bevel needles found in literature [18].

3. ***No axial rotation***
   Axial rotation of the needle causes needle twisting, resulting in inaccuracies and difficulties in control of the needle during needle steering (see section 1.3.2).

4. ***Central lumen***
   When reaching the target, the needle needs to have a lumen which can act as a working channel to deliver drugs, radioactive seeds, or to insert small instruments such as biopsy tools.

5. ***Flexible shaft***
   The asymmetric tip forces determine the amount of steering. However, the shaft must be flexible to let the needle bend. Therefore, the material of the shaft of the needle needs to be flexible to make steering possible.

6. ***Bio-compatible***
   Because needles are inserted into the human body, the materials cannot be toxic for human beings.

Wishes

1. ***Continuous steering***
   Continuous steering means that the needle is not limited to certain steering directions (i.e. north/east/south/west), but can also steer into in-between directions to increase the steerability.

2. ***Simple design***
   When miniaturised, a simple design is beneficial for manufacturing and assemble possibilities with high accuracy [25]. Therefore we can say that a low number of components and simple shapes are beneficial.

3. ***Prevent tissue damage***
   The goal is to reach a certain target, while trying to reduce as much harm as possible to surrounding tissue. Preferably, less than pre-curved bevel tips, which cut tissue when reorienting the needle tip.

4. ***Small bending radius***
   A smaller bending radius increases the steerability of the needle. The smallest bending radius found in literature is 34 mm for a pre-curved bevel tip needle [26]. Therefore, we strive to reach at least the same radius.

2.2. Biological Inspiration: Wasp Ovipositor

This work builds upon previous work in the field of ovipositor-inspired steerable needles. Wasp ovipositors are thin and flexible needle-like structures used for penetrating wood to lay eggs inside hosts (e.g. larvae) (Figure 2.1 a). Wasp ovipositors are composed out of longitudinal segments (Figure 2.1 b), called "valves", which can be actuated individually and independently of each other with musculature located in the abdomen of the insect [27]. Steering is achieved by offsetting the valves, resulting in an asymmetric tip. In this way, the wasp can move the ovipositor forward along curved trajectories inside different substrates without the need for rotatory motion or axial push.

Previous work of Sprang et al. [28] (Figure 2.1 c) and Scali et al. [18] (Figure 2.1 d) proposed a multiple-segmented needle design inspired by the ovipositor of a parasitic wasp. The design described in this thesis makes use of multiple sliding elements to steer in 3D without the need of axial rotation of the needle.

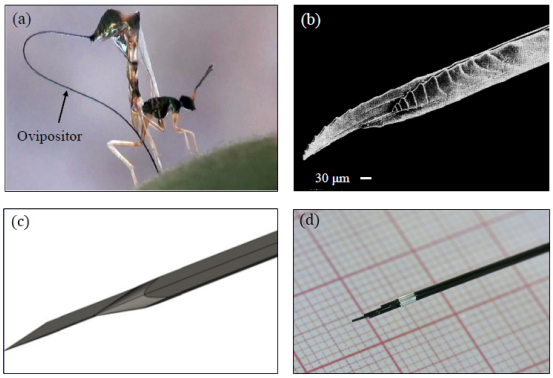

Figure 2.1: Steerable needles inspired by the ovipositor of a parasitic wasp. (a) Wasp inserting its ovipositor into a fig. Adapted from from [28], (b) Close-up of the valves of an ovipositor (c) Design of an ovipositor inspired steerable needle by Sprang et al. Adapted from [28]. (d) Design of an ovipositor inspired steerable needle by Scali et al. [18]. Adapted from [18].

2.3. Conceptual Design

Most tendon actuated needles maximise the moment created by the tendon by placing the tendons as far from the axis of the needle as possible (i.e. on the outside of the needle) [20]. However, the tendons require additional space, thus, increasing the overall diameter of the needle. For example, the needle design of van de Berg et al. [29] required additional notches for the tendons to guide the tendons, which increases the diameter. The conceptual design for this thesis makes efficient use of the available space, by using the space inside lumen of the needle for the steering mechanism. The conceptual design of the needle consists of a cannula containing multiple long flexible elements inside its lumen. The long, slender elements can be pushed and pulled, thereby providing transmission of movement from the base all the way to the steerable tip (Figure 2.2).

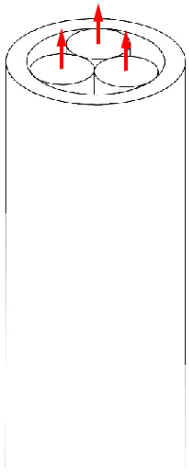

Figure 2.2: Conceptual design of a single cannula with a lumen containing multiple elements which allow up and down movement. The arrows represent the motion of the elements.

The idea is to steer towards the target and retract the steering mechanism when the target is reached, leaving an open lumen behind (Figure 2.3). In this case, no additional space is required for the steering mechanism, allowing a small diameter of the needle.

Ideally, the elements are sector-shaped to prevent rotation of the elements inside the lumen. However, manufacturing of long and well-aligned sector-shaped needle segments within the dimension is technically challenging. Therefore, off-the-shelf round elements were used. When increasing the amount of elements a more homogeneous round shape is formed (Figure 2.4).

The conceptual design can be divided into the needle and the control unit. The needle is the part that enters the tissue and consists of the cannula together with the steering mechanism (i.e. the long and slender elements inside the lumen of the cannula). The control unit is located at the distal end of the needle and is responsible for the accurate control of the

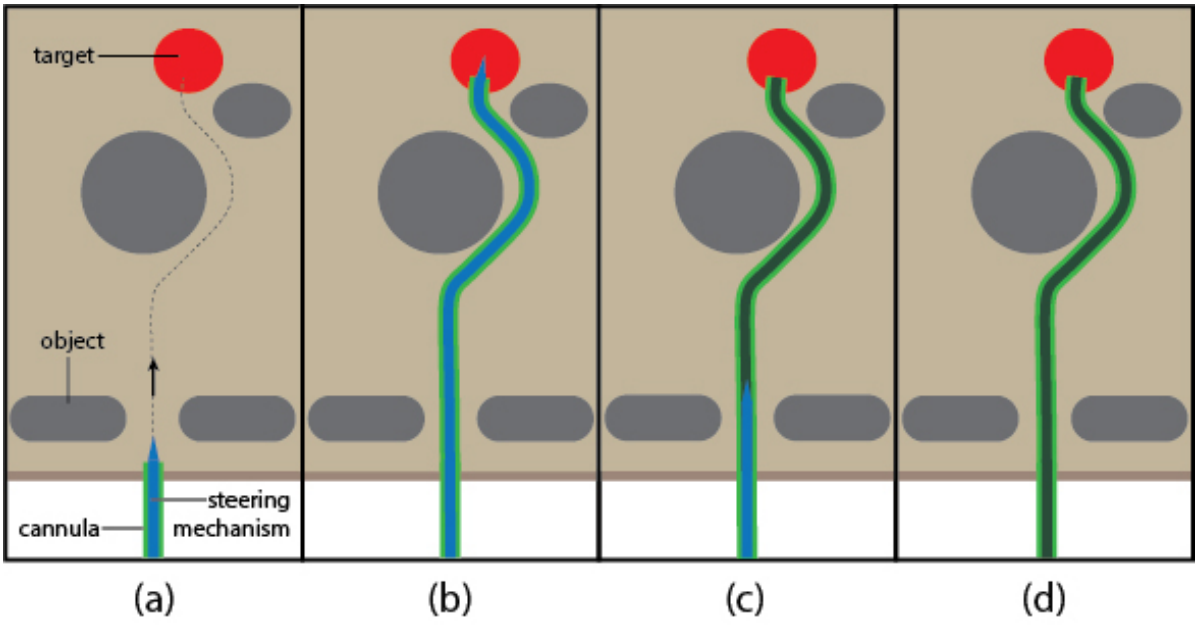

Figure 2.3: Steps of needle insertion with a retractable mechanism. Green represents the cannula, blue represents the steering mechanism made of multiple elements, red represents the target, grey represents objects and light brow represents the tissue in which the needle is inserted. The steps are as followed: The needle is inserted into the tissue (a), and steered towards the target (b). When reaching the target the steering mechanism is retracted (c), leaving an open lumen is left behind (d).

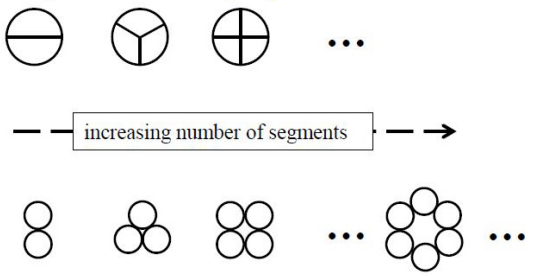

Figure 2.4: Replacement of sector shaped elements with round elements with increasing the amount of elements. On the top the cross-section of a needle with sector shaped needle segments is represented. On the bottom, the simplification with round of-the-shelf elements is represented. Modified from [30].

element displacement. The design of the control unit is dependent on the design of the steering mechanism. Therefore, the initial focus of the design process is on the steering mechanism.

2.3.1. Idea Generation

Steering occurs by the generation of asymmetric forces at the tip of the needle. The tip of the needle can be varied by movement of the long slender elements, which run from the base all the way to the tip of the needle through the needle cannula. A brainstorm was performed to come up with viable solutions for steering with multiple round elements.

The ideas were clustered by grouping them into designs containing straight or pre-curved elements. Each idea of the brainstorm was extended by increasing the number of elements, to vary between a fixed and loose configuration and by placing the elements inside our outside the cannula (Figure 2.5). A fixed configuration means that the elements are connected to each other at end of the elements, so a movement of one element will influence the movement of the other elements. A loose configuration means that the elements are not connected to each other and they are free to move along each other. By placing the distal end of the elements outside the cannula, the distal end can move freely along the radial direction. By placing the elements inside the cannula, the elements are restricted in movement in the radial direction.

2.3.2. Concepts

Each group was evaluated based on the list of requirements and wishes. Since loose straight wires inside a cannula do not result in steering, that idea was excluded. The three most promising groups were the straight

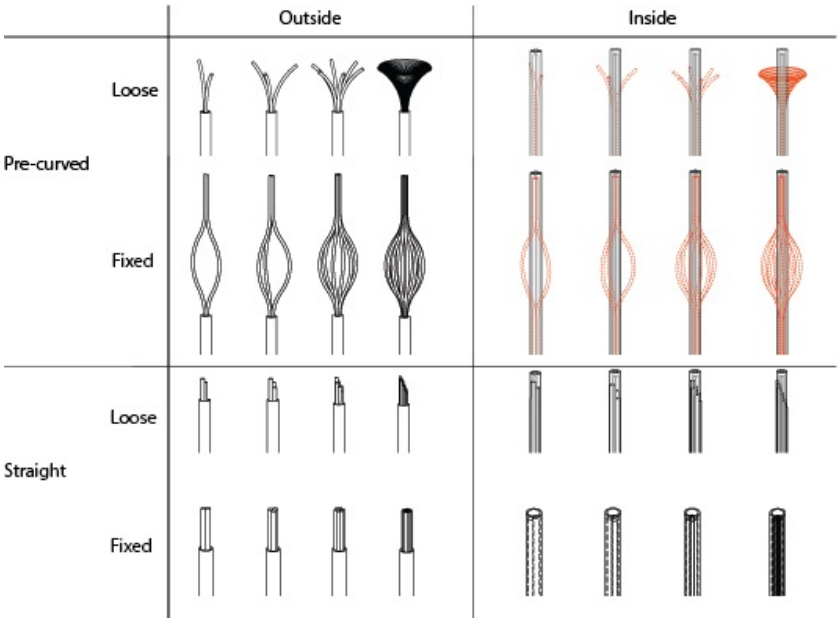

Figure 2.5: Brainstorm for idea generation for needle tip consisting of a single cannula with multiple elements inside its lumen. The ideas were generated by variations between pre-curved and straight element configurations, loose en fixed elements, and by placing the elements in- or outside the cannula. Each idea was expanded by increasing the amount of elements.

loose elements (resulting in a configurable bevel tip), elements pre-curved inside the cannula, and fixed pre-curved elements outside the cannula. The three concepts are described below, elaborating on their main working principle.

Concept 1: Bevel Tip

Previous work on the ovipositor inspired needle of Scali et al. [18] already showed that steering occurs by creating an offset between two adjacent needle elements resulting in a discrete bevel-tip (Figure 2.1 d). The angle of the bevel can be controlled by changing the offset between the elements. However, the steering shows little curvature (Figure 2.6).

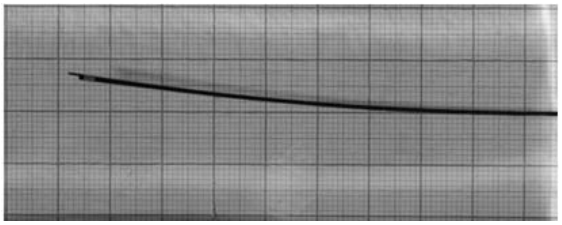

Figure 2.6: Needle steering of a needle composed of 7 Nitinol elements configured in a discrete bevel-tip by offsetting the needle elements. Adopted from [9].

The bevel tip consists of multiple elements. Increasing the number of elements results in a more continuous bevel tip (Figure 2.7). By using smaller elements, the stiffness of each element decreases which may increase the deflection of the elements, and thereby the steerability.

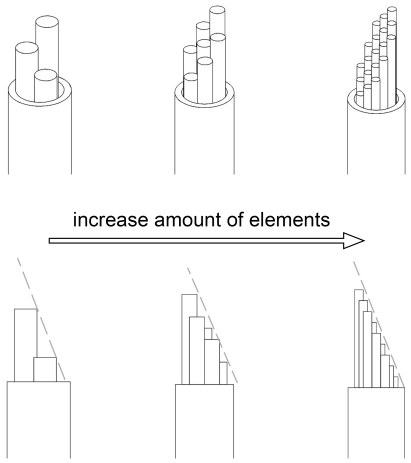

Figure 2.7: Discrete bevel tip composed of multiple elements. Increasing the amount of elements results in a more continuous bevel tip. The bevel is shown by the dashed gray line.

Concept 2: Pre-curved Wires in Tube

The second concept contains multiple pre-curved elements inside the cannula. The elements are pre-curved into the radial direction of the element crossection. When they are all at the same height, all forces are in equilibrium and cancel each other out

(Figure 2.8 a). By pushing and pulling the elements, this balance is disturbed, resulting in asymmetric force distributions of the forces on the cannula. Since the cannula is flexible, it will bend (Figure 2.8 b). The curvature of the cannula is variable by varying the amount of displacement of each element.

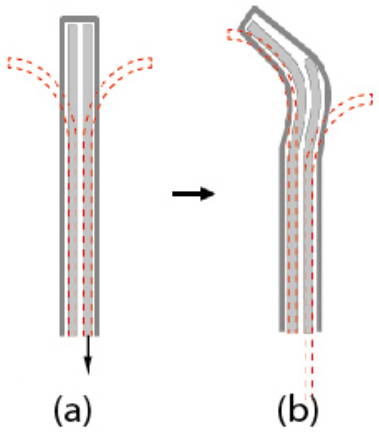

Figure 2.8: Bending of a tip consisting of pre-curved elements inside a cannula. By moving one of the elements (a), the force equilibrium is disturbed, resulting in bending of the tip of the needle (b).

Concept 3: Pre-curved Fixed Wires

Tendon-driven actuated needles make use of a push-pull mechanism. However, on such small scales the moment generated by the pushing and pulling of the tendons decreases, leading to very high operating forces. Therefore, by pre-curving the elements outwards, the internal moment generated by pushing and pulling increases, leading to less operating forces compared to the straight wire configuration. By retracting one of the elements the tip tends to bend into the direction of the retracted element (Figure 2.9).

2.3.3. Proof of Concepts: Prototyping

In order to make a proper decision between the three different concepts, experimental prototypes for each concept were made to test their proof of principle. All prototypes were made of 0.125 mm or 0.25 mm diameter Nitinol wires (Flexmet, Belgium). To pre-curve the Nitinol elements, shape setting was done by Joule heating or by a heating the elements by arework station (Appendix A).

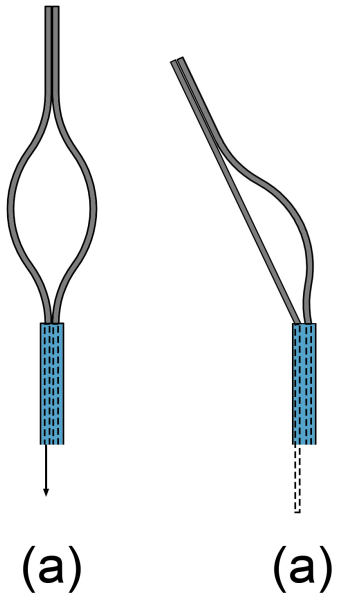

Figure 2.9: Bending of a needle tip consisting of pre-curved fixed elements: The initial tip shape (a) and shape after element retraction (b).

Bevel Tip

The prototype consists of a tube (Vention, Tubing PEBAX 70D, ID=0.46 mm, WT=0.18 mm) together with seven 0.125 mm diameter straight annealed Nitinol wires. When tested into gelatine, the wires tended to spread in various directions (Figure 2.10). This can be explained by the fact that the diameter of the elements decreases, and therefore also the stiffness of each single element. When pushed inside the gelatine, the single elements bent outward by the tip forces.

Pre-curved Elements: Inside

The needle prototype consists of multiple pre-curved 0.25 mm diameter Nitinol wires (Figure 2.11). Each Nitinol wire was pre-curved by Joule heating (for more information on the process of bending the Nitinol wires see Appendix A). When the pre-curved wires were inserted into the cannula, the wires tend to rotate into the same direction to reduce the internal stresses. Therefore, the concept does not work with standard off-the-shelf round wires.

Pre-curved Elements: Fixed Outside

The prototype was made out of four Nitiol wires (OD=0.125 mm). Each wire was pre-curved by Joule heating (Appendix A)). A tube (0.3 ID) was slid over the ends of the wires and fixed by clamping them together. The tip bends by

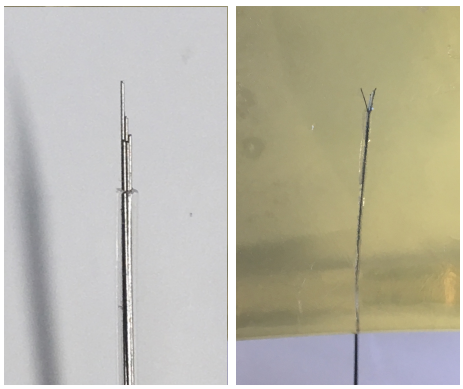

(a) (b)

Figure 2.10: Concept 1: Prototype of bevel tip containing seven straight Nitinol elements. (a) Discrete bevel tip obtained by offsetting the elements. (b) The spreading of the elements when inserted into the gelatine.

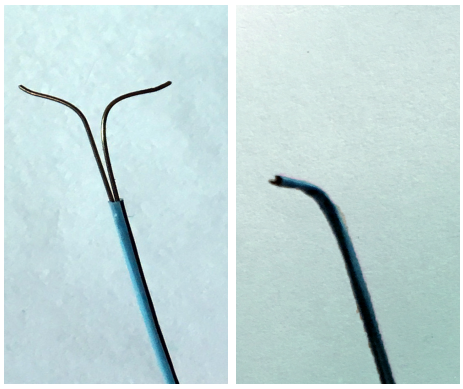

(a) (b)

Figure 2.11: Concept 2: Prototype of two pre-curved elements. (a) The pre-curved elements outside the cannula. (b) Elements tend to go into the same direction when inserted into the cannula.

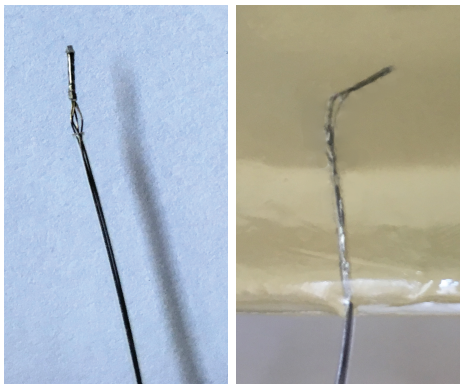

(a) (b)

Figure 2.12: Concept 3: Prototype of four fixed pre-curved elements. (a) Prototype of four pre-curved elements which are fixed at the top. (b) The tip steers inside gelatine by retraction of one of the elements.

retraction of a wire, thereby steering the needle when pushed through the gelatine (Figure 2.12).

2.3.4. Final Concept

Based on the experimental prototypes, we can conclude that the third concept shows the most potential in needle steering. It can steer omnidirectional and can make large tip angles. The concept has multiple elements which are connected to each other at their distal end. The tip bends by retraction of one or more elements. By introducing a small lateral curvature in the elements of the needle, a larger internal moment arm is created, which results in reduced retraction forces compared with straight elements. However, the shape has lots of variables which can be varied, such as the radius of the curvatures (r_1, r_2, r_3), the height of the pre-curved element (h) and the amount of curvatures of the elements (Figure 2.13).

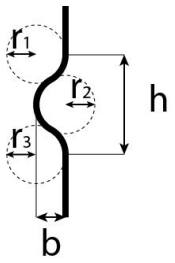

Figure 2.13: Variables in needle tip design containing pre-curved fixed elements: the three radius of the curved element r_1, r_2, r_3, the height h, and width of the curvature b.

To decide on the final dimensions of the tip shape, the element has to be investigated in terms of moment and forces to predict the bending behaviour.

Bending Moment

Most steerable instruments and tendon driven needles make use of a central backbone, together with flexible elements (like cables) at their sides (Figure 2.14 a). The flexible elements are placed as far as possible from their rotating point to create a large moment arm. By pulling and pushing the elements, the generated moment causes bending of the mechanism. When miniaturised, the radius becomes very small, thereby decreasing the moment arm. The decreased moment arm leads to high operating forces when minaturised. In the proposed steering mechanism design, the elements are located next to each other. No central backbone is present, but the elements itself act as one. When two flexible elements are next to each

other and one of the element is pulled, the moment arm is equal to the diameter ($D = 2*r$) of a single element (Figure 2.14 b). In this case, the diameter of a single element is very small (0.125 mm). Therefore, high operating forces are required to create enough moment to cause bending. By introducing a small curvature in an element the internal moment increases by the maximal width of the curvature (d) (Figure 2.14 c), therefore, requiring less operating forces compared to the straight configuration.

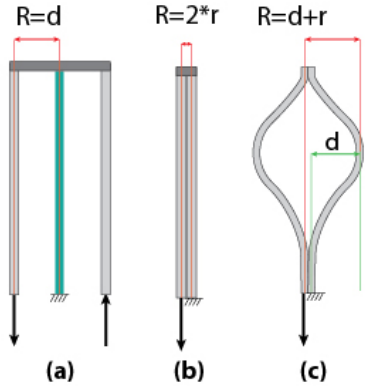

Figure 2.14: Maximum radius R for determine the internal moment for (a) Tendons with central backbone, (b) Two straight elements, and (c) Two curved elements. Where r is the radius of the tendon and d the maximum distance of the central axis of the needle to the centre of the tendon.

Analysing the internal forces and moments when one of the elements is retracted is necessary to investigate the bending behaviour of the pre-curved element. Figure 2.15 shows a schematic representation of the two elements. The force by retracting one element is simplified by a vertical force P on the element. Because the element is slender and flexible, the element wants to deflect laterally by the applied load P.

To say something about the actuation forces we look at the initial bending when one element is retracted. The deflection of a beam for small deflections can be calculated by

$$EI\frac{d^2v}{dx^2} = M(x) \tag{2.1}$$

Where E is the modulus of elasticity of the material, I the moment of inertia, v the displacement, and M the internal moment.

The internal bending moment M can be determined using the method of sections. The free-body diagram of an element section can be seen in Figure 2.15 c. The element enters the tube in point B, which can be seen as a fixed constraint, so that no horizontal or vertical movement or rotations are allowed in point B. We assume point A can move freely in open space.

The curvature can be simplified by a triangular shape shown in Figure 2.15 d.

The curvature of the element can be simplified as a triangular function a where

$$a = \begin{cases} \frac{b}{\frac{1}{2}L}x & \text{if } 0 < x < \frac{1}{2}L \\ b - \frac{b}{\frac{1}{2}L}(x - \frac{1}{2}L) & \text{if } \frac{1}{2}L < x < L \end{cases} \tag{2.2}$$

In this case the internal moment can be calculated by

$$M = P(d + a) \tag{2.3}$$

Where the final formula for the internal moment is

$$M = \begin{cases} P(d + \frac{b}{\frac{1}{2}*L}x) & \text{if } 0 < x < \frac{1}{2}L \\ P(d + b - \frac{b}{\frac{1}{2}*L}(x - \frac{1}{2}L)) & \text{if } \frac{1}{2}L < x < L \end{cases} \tag{2.4}$$

The initial conditions for the displacement v are:

$$v'(L) = \frac{dv}{dx}(L) = 0 \tag{2.5}$$

$$v(L) = 0 \tag{2.6}$$

$$v(1/2 * L) = v(1/2 * L) \tag{2.7}$$

$$v'(1/2 * L) = v'(1/2 * L) \tag{2.8}$$

The differential equation 2.1 can be solved by entering the internal moments in equation 2.4 and the initial conditions in equations 2.5, 2.6, 2.7, and 2.8.

Figure 2.16 shows the deflection (mm) of a single pre-curved element for an element with no curvature (d=0) and a curvature of an element with maximum of 0.25 mm in diameter (d=0.25). The inertia, and force P are taken as a constant and remains the same for both diameters. It shows that when the width of the curvature b is increased and the deflection of the element will increase as well.

When the element deflects (moves to the left), the pulling force on the tip again induced additional moments which cause it to deflect even more.

Dimensions

To minimise the retraction force and maximise the bending of the tip, increasing the width of the curvature (b in figure 2.13) would be beneficial. In our design we limited ourselves

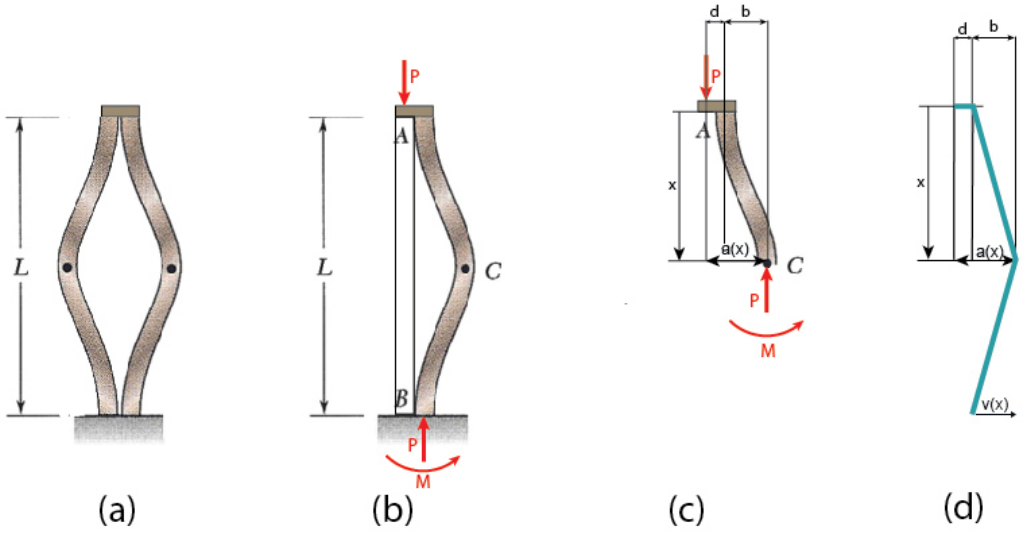

Figure 2.15: Forces and moments on pre-curved element: (a) two pre-curved elements together; (b) one element when the other element is retracted with force P. M is the moment at point of entrance of element into the cannula. (c) section with corresponding force P and moment M; (d) simplification of element curvature by a triangular shape.

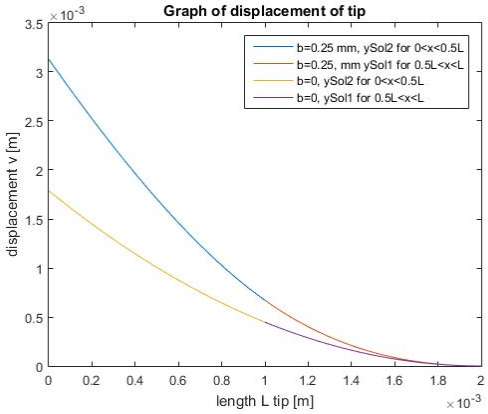

Figure 2.16: Displacement of a single element with a constant force of 3 N, for a element curvature of a maximum width of 0.25 mm (d=0.25) and minimum of 0 mm (d=0).

to a maximum diameter of 0.5 mm, thereby restricting the maximal width of tip design.

The curvatures have to be tangent to have a smooth transition, to prevent as much friction as possible. Therefore, the length of the tip is determined by the radii of the curvatures of the elements ($r1, r2, r3$). For sake of production, it would be beneficial if the radii are equal, so the elements can be curved around a cylinder.

A high radius of curvatures would be beneficial to reduce the retraction forces. Increasing the radius of curvature means that the total length (h) of the tip increases. However, a longer tip results in an larger tip diameter when actuated. Therefore, we aim for a length as short as possible with the outward curvature. The final design has a curvature width of 0.25 mm and has therefore a height of about 1 mm.

Tip configurations

The cannula around the elements keeps the elements together at the point of entrance, therefore the aforementioned pre-curved tip shape can be obtained by various element configurations. The tip designs can be categorised by the amount of curvatures in one single element. Figure 2.17 shows four different tip designs by increasing the amount of curvatures in a single element: zero-curved, one-curved, two-curved and three-curved elements. When inserting the pre-curved fixed elements inside the cannula, the final tip shape is obtained. The one- and two-curved designs have pre-tension when entered inside the cannula, which may be advantageous for tip deflection.

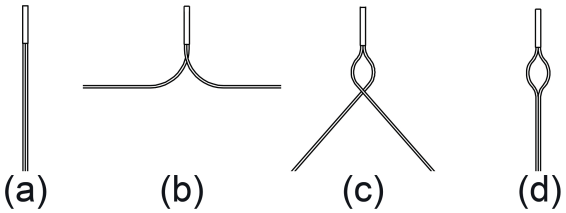

Figure 2.17: four tip designs by varying the amount of pre-curves in the elements: (a) zero-curved; (b) one-curved; (c) two-curved; (d) three-curved.

3

Steering Mechanism: Experimental Selection

3.1. Experiment 1: Comparing Tip Designs

In this experiment, various tip designs were investigated in order to make a proper decision for the final tip design. Four tip designs were tested in this experiment: a tip with zero-curved, one-curved, two-curved and three-curved elements (Figure 2.17). The different tip designs were compared in terms of actuation force and the angle the tip makes relative to the shaft. We want to bend the tip of the needle by using the least amount of pulling force. As described in chapter 2 the retraction force can be reduced by introducing a curvature in the elements. The one-curved and two-curved tip designs have internal stresses which could be advantageous for reducing the element retraction force. However, the pre-curvatures may have influence in the tip behaviour when retracting one of the elements. For example, the curvatures may introduce non-linearities in the bending behaviour. Therefore, the angle of the tip was also examined in order to investigate the bending behaviour of the needle tip.

3.1.1. Experimental Setup

The experimental setup consisted of the needle (two elements), an actuation unit, a load cell, and data acquisition instruments (Figure 3.1).

Needle Tip

Since the needle has to be flexible and bio-compatible, Nitinol wires were used. The material is well known because of its bio-compatibility and its super-elastic properties, and has already a strong founding in medical applications, like steerable needles and stents [31]. Two elements were used to investigate the behaviour of the needle in one plane. Off-the-shelf Nitinol wires were used as elements. Two Nitinol wires (0.125 mm diameter) (Flexmet, Belgium) were attached to each other by gluing a stainless steel tube (ID=0.3 mm, OD=0.5 mm) over the wires. In this case, the tube keeps the wires together and the wires can withstand transverse forces. Directly after application of glue the stainless steel tube was compressed by nose pliers to clamp the wires inside the tube to ensure the wires were fixed well. The wires of the one-curved, two-curved and three-curved tip designs were pre-curved by heating by a rework station (Appendix A). The wires were wrapped around a cylinder with an outer radius of 0.3 mm, and heated by a rework station (Tenma, SMD rework station 220 V) to a temperature of 480 degrees to allow shape setting (see Appendix A). The final prototypes are shown in Figure 3.3.

Actuation Unit

The actuation unit pulls on one of the two elements of the steering mechanism, while the other element was fixed to an additional 3D-printed part mounted to the breadboard (Figure 3.2). The actuation unit consists of a motorised linear stage (Thorlabs MTS25-Z8, 25 mm stage) together with a controller (Thorlabs TDC001 T-Cube DC Servo Motor Controller) (Figure 3.1). A breadboard (Thorlabs) was positioned vertically by mounting it to another breadboard by two aluminium extrusions. The linear stage was mounted on the vertical breadboard to reduce the effect of undesired moments caused by gravitational forces (Figure 3.2 and 3.1).

Data Acquisition

A load cell (FUTEK model LSB200 FSH00102 2 lb) together with an amplifier was used to

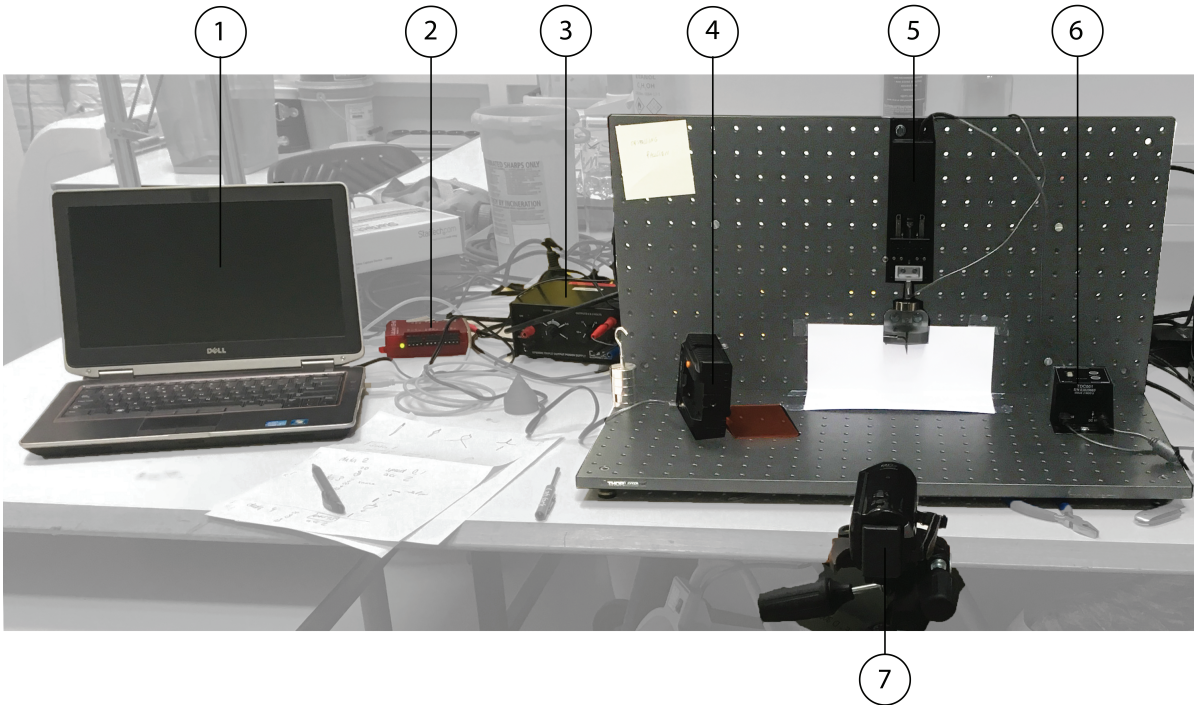

Figure 3.1: Experimental setup: 1. Laptop, 2. USB DAQ device, 3. Amplifier, 4. Light, 5. Motorised linear stage, 6. Servo motor controller 7. Video camera

measure the retraction forces. While calibrating, the load sensor showed nonlinear behaviour for the first 50 g. Therefore, an additional 50 g weight was added to the force sensor to stay in the linear area (see calibration in Appendix B). A USB DAQ device (LabJack U3-HV) was used to read out the data of the load cell into the computer. The load cell was mounted to the motorized linear stage by means of a FDM printed V-shaped part together with three M3 bolts. A video camera (Panasonic HC-V250 video camera) was positioned in front of the linear stage to record the initial and in-between and final position of the needle tip during the trials. A video light (Falcon Eyes Led Video light DV-96V) was used to prevent shades and enhance the image quality for image processing. All data acquisition instruments can be seen in Figure 3.1, and a more detailed experimental setup in Figure 3.2.

3.1.2. Experimental Design

The tip of the steering mechanism bends by retraction of one element. By implementing curvatures in the elements, the forces for retraction can be reduced. In this experiment we want to get more insight in the behaviour of different tip designs by investigating the retraction forces and the needle tip angle.

Dependent and Independent Variables

Dependent Variables
The dependent variables are the element retraction forces [N] needed to bend the tip and the bending angle [degrees] of tip relative to the shaft during retraction of one element (Figure 3.4).

Independent Variables
The independent variables are the amount of retraction of the element [mm], the four needle tip designs (zero-curved, one-curved, two-curved and three-curved elements (Figure 3.3)) and the type of retraction (continuous and step-wise).

The amount of retraction was based on a pilot test. During the pilot test, the three-curved tip showed a 90 degrees angle relative to the needle shaft for a retraction of approximately 1 mm. Therefore, we choose a maximal displacement of 1 mm of pulling, to maximise the effect size without damaging the elements.

Four different tip designs were tested: zero-curved, one-curved, two-curved and three-curved elements (figure 3.3).

Two variations in measurements were conducted: a continuous and step-wise retraction. A continuous retraction means that the stage moves 1 mm up with constant speed.

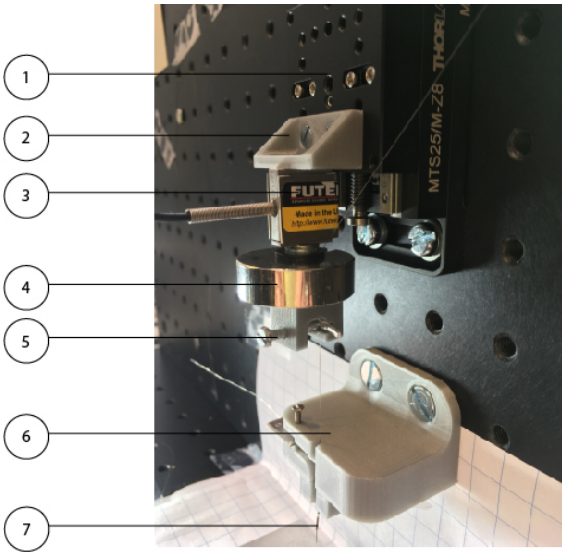

Figure 3.2: Detail Experimental Setup: (1) Motorized linear stage; (2) FDM printed part; (3) Load Cell; (4) Weight of 50 grams; (5) Attachment block element; (6) attachment for cannula and element, (7) Steering Mechanism.

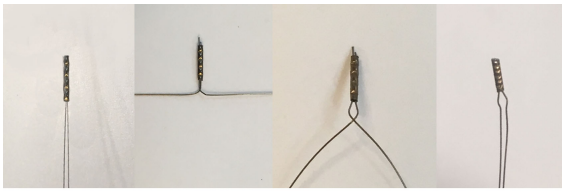

Figure 3.3: Prototypes of two element tip designs: (a) zero-curved; (b) one-curved; (c) two-curved; (d) three-curved.

A step-wise retraction means that the stage moves in steps of 0.1 mm with a dwell time of 2 s in between the step motions. By the step-wise retraction the angle after each step can be easily determined when the needle is not moving, which reduces the measurement error.

Table 3.1 shows the total eight experimental conditions tested. No randomisation between tip designs was performed, because changing tip designs introduces errors in element placement. For each tip design, the continuous experiment was repeated five times and the step-wise experiment was done three times. First the continuous motion experiment was performed, in which the force and displacement was measured. Hereafter, the measurements for the step-wise motion were performed, in which only the displacement was measured. The run table of the experiment can be found in Appendix C.

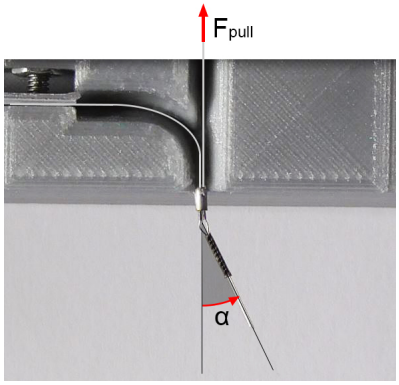

Figure 3.4: Tip with two elements through a cannula. α shows the angle of the needle tip relative to its shaft. The red arrow F_{pull} shows the retraction force when the element is retracted.

Co-founding variables

Co-founding variables are the variables controlled to reduce measurement errors. The co-founding variables were controlled by keeping a constant velocity of 0.1 mm/s and an acceleration of 2 m/s during all trials. All trials were performed in open space, so the tip was allowed to move freely.

Condition	Tip Design (# curvatures)	Measurement
1	0	Continuous
2	0	Stepwise
3	1	Continous
4	1	Stepwise
5	2	Continous
6	2	Stepwise
7	3	Continous
8	3	Stepwise

Table 3.1: Experimental Conditions

Hypothesis

Three hypothesis were formulated:

1. The tip design with no curvatures (zero-curved design) will require higher retraction force than the pre-curved needle tip designs (one-curved, two-curved, three-curved). The curvatures in the elements cause an internal moment, which makes it the retraction force less (See Chapter 2).

2. Increasing the amount of element retraction results in a higher deflection

angle of the tip.

3. Increasing the amount of curvatures in the tip design elements introduces non-linearity in the relation between retraction and angle of the needle tip. i.e. per step of 0.1 mm element retraction the difference in angle deviates (is not constant). The pre-curves in the elements push against the wall of the cannula when retracted, leading to additional forces.

3.1.3. Experimental Procedure

In between the runs the tip designs had to be changed. After the installation of the elements, the force and positioning could be measured.

Changing Tip Designs

Firstly, the elements were inserted into the guiding tubes mounted on a 3D printed part which is attached to the breadboard (Figure 3.2). One of the two wires was fixed by clamping the wire with a screw and plate to the 3D printed part. The second wire was positioned in the 3D printed part which is attached to the force sensor (Figure 3.2). Then the stage was moved into its initial position (20 mm in APT), and the wire was clamped by a screw and plate.

Measuring Force and Positioning

The steps for measuring were as followed:

1. The desired stage positions and speed was loaded into computer software (APT User, Thorlabs).
2. The computer software for reading out the forces (LJStreamUD, LABJACK) was started for recording the forces.
3. The camera for recording the movement of the needle tip were activated.
4. The software program (APT User, Thorlabs) was activated to start the movement of the linear stage, which introduces the retraction of elements.
5. After the trial, the camera was stopped and the force measurement was manually stopped in the program.

3.1.4. Data Analysis

Forces

The load cell measures the force in voltage. In MATLAB (version R2015a), the voltage was converted to Newton by a factor found during calibration of the load cell. The calibration was done by adding 50 g weights to the load cell up to 200 g (Appendix B). In this way, the factor of conversion of voltage to Newton was calculated. All measurements with the same experimental conditions were aligned using MATLAB to compensate for the time lag between them. Of each measurement the maximal force was determined by finding the maximal value in MATLAB. The MATLAB codes used for processing the force files can be found in Appendix F.

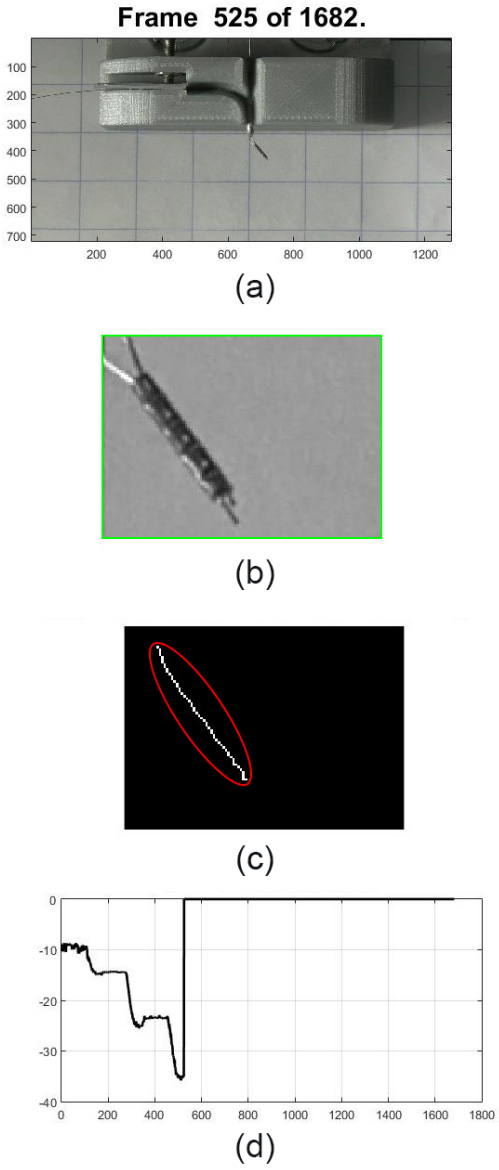

Figure 3.5: Steps in processing the recorded videos: (a) The original image of video frame. (b) The cropped image. (c) A binary skeleton image, where the ellipse represents the main direction (d) The graph of the angle (degrees).

Tip Angle

The recorded video files were first cut in time to remove redundant video material and converted to avi format by VideoPad (NCH Software). In MATLAB, each video frame was cropped to the region of interest to exclude noise of the surrounding area. The cropped image was converted to a binary image, in which the needle tip was processed into a single line (skeleton without branches). From this binary line image the orientation of the line relative to the x-axis was determined by drawing an ellipse around the line and taking the longest axis as main direction of the ellipse (Figure 3.5) The direction is expressed in the angle (degrees) of the tip relative to the shaft. A MATLAB script was written for the video processing, which displays the original frame, the cropped frame, the skeleton and a graph of the angle which changes in real time. Figure 3.5 shows all steps of video processing. The MATLAB files for this program can be found in Appendix F.

3.2. Results

3.2.1. Retraction Forces

The force needed for retracting one of the two elements over a distance of 1 mm during continuous motion was tested for each of the tip designs. Figure 3.6 shows the forces during continuous retraction and Figure 3.7 shows the box plot of the maximal retraction forces. The zero-curved tip design shows the highest retraction forces of a mean value of 2.57 N for a retraction of 1 mm. This force is higher than the force needed with other designs. The one-curved tip required a retraction force of 1.34 N, the two-curved tip 0.85 N and the three-curved tip 1.32 N. (Table 3.2). The two-curved design shows lowest retraction forces (mean=0.85 N), together with the least spread (std=0.02).

The relation between force and retraction is clearly non-linear (Figure3.6). Especially the three-curved and one-curved element designs show two peaks and is clearly non-linear.

3.2.2. Tip Angle

To get more insight in the relation between the retraction of an element and the angle of the tip, four tip designs were evaluated on the angle relative to the shaft of the needle. Figure 3.8 shows the angle of each tip design during continuous retraction. Increasing the amount of element retraction indeed results in a higher deflection angle of the tip. From the graph we can see that the zero-curved ends in a larger total angle displacement than the other tip designs by a element retraction of 1 mm.

Figure 3.9 shows the angle of the tip in time of each tip design during step-wise retraction. Figure 3.10 shows the difference in angle displacement per step of 0.1 mm element retraction. We can see that the relation between retraction and the tip angle is non-linear for all four designs. The zero-curved an one-curved tip designs show similar shape where the step difference increases for a displacement of 0.5 mm, where after the difference in angle decreases.

The three-curved design shows deviation in the angle displacement per step of 0.1 mm retraction. First the step difference increases, than decreases, after the difference increases again. This pattern indicates a higher level of non-linearity. The variation in angle difference per step is for the two-curved tip design the most constant. Therefore, the two-curved designs is the most constant in retraction versus angle.

Table 3.2: Overview of mean and standard deviation of the maximal force for 1 mm retraction of a single element of various tip designs.

	Max. Force	
	Mean	Std.
Tip Design		
zero-curved	2.57	0.068
one-curved	1.34	0.12
two-curved	0.85	0.020
three-curved	1.32	0.083

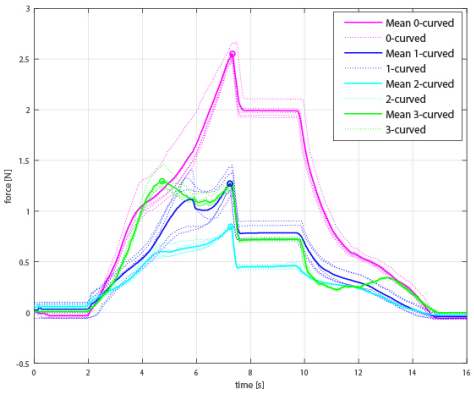

Figure 3.6: Plot of retraction forces over an element displacement of 1 mm for four tip designs: zero-curved, one-curved, two-curved and three-curved elements. The circles represent the maximal retraction force.

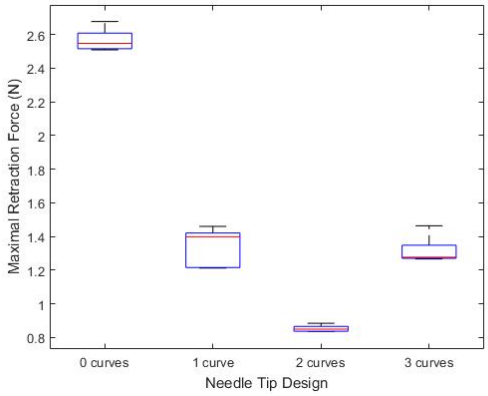

Figure 3.7: Box plot of maximum forces for retraction for 4 tip designs: zero-curved, one-curved, two-curved and three-curved elements.

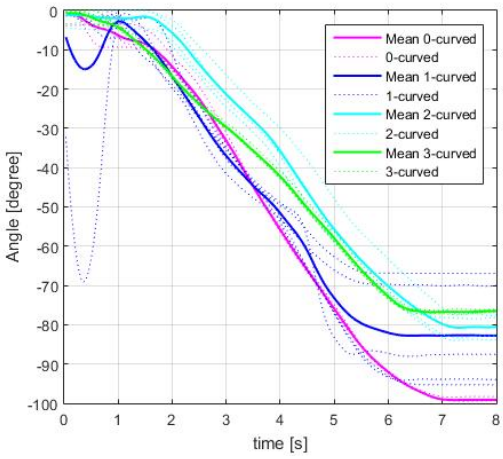

Figure 3.8: Plot of the angle for continuous retraction of 1 mm for 4 tip designs: zero-curved, one-curved, two-curved and three-curved elements.

3.3. Interpretation of Results

3.3.1. Retraction Forces

The zero-curved tip design shows clearly higher retraction forces compared with the curved tip designs as expected. This can be explained by the curvature in the element causing a larger internal bending moment, which decreases retraction force (explained in Chapter 2).

From the results of the experiments, the two-curved design showed the least retraction force. This can be explained by the fact that during retraction, the retracted part of the element inside the tube has no pre-curvatures. When an element is pre-curved and inside the tube, the curvature pushes against the tube wall, causing friction inside the tube.

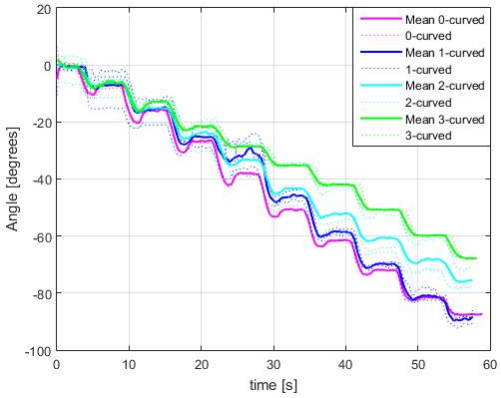

Figure 3.9: Plot of the angle for a step-wise retraction of 1 mm for 4 tip designs: zero-curved, one-curved, two-curved and three-curved elements

3.3.2. Tip Angle

When we look at the angle caused by retraction of the element, the straight zero-curved configuration shows the highest angle to retraction ratio. This can be explained by the fact that the total length of the element is shorter than the pre-curved ones.

When looking at the graphs not all tips start at an initial angle of zero. During clamping of the wire, the wire went a bit up, causing the angle to deviate.

From the graphs in figure 3.9 and 3.8 we can conclude that all tips show non-linear behaviour. The difference in angle seems to follow the tip shape. This can be explained by the additional length of the element by the outward curvature. When retracted the element will elongate first and is not pulling on the other element.

The step between 0.4-0.5 mm retraction shows a deviating tip difference than surrounding values for the zero and one-curved tip designs. This can be explained by the noise which was present during this step. The noise could be causes by internal stresses inside the steering mechanism.

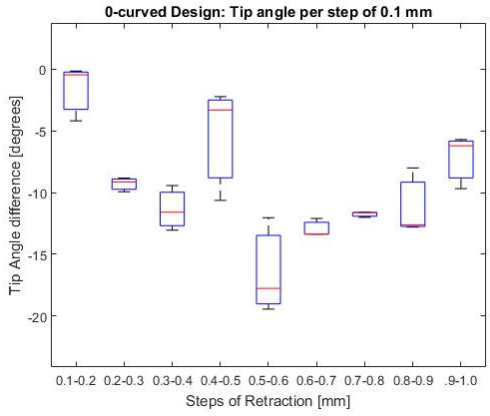

(a)

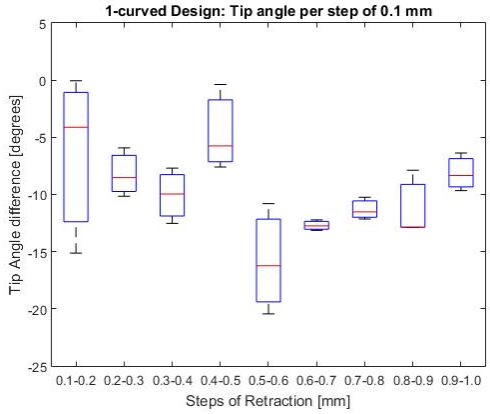

(b)

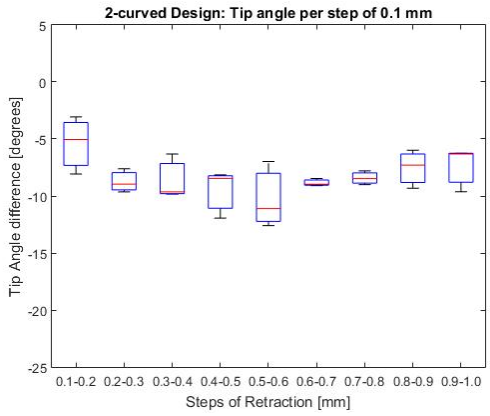

(c)

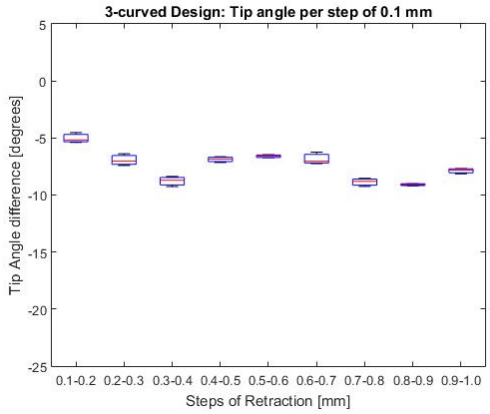

(d)

Figure 3.10: Box plot of angle difference between steps of 0.1 mm retraction for (a) zero-curved, (b) one-curved, (c) two-curved, and (d) three-curved tip designs.

4

Final Design

4.1. Introduction

Chapter 2 proposes a new way of steering a needle by a steering mechanism consisting of multiple of curved elements. To investigate the performance of the steering mechanism, a shaft and a control unit should be added to the steering mechanism to turn it into a working steerable needle. The final proposed needle and control unit is designed as an experimental prototype to investigate the performance of the steering mechanism. The prototype is not intended for the end user. Therefore, the prototye does not have to be ergonomic and intuitive.

4.2. Needle

The needle consists of the steering mechanism, together with a cannula which holds all the elements of the steering mechanism together. The shape and material of the overall needle (body and steering elements) is significant in determining the formation of curves, angles of deflection, and thus influence the level of steerability. Two factors that should be considered in the design choices are the flexural rigidity and buckling of the needle.

4.2.1. Steering Mechanism

Curvature of the Steering Elements

The steering mechanism consist of long, slender cylindrical elements which have a pre-curvature at the tip. The experiment of comparing tip designs showed that the two-curved tip design experienced the lowest amount of retraction forces during element retraction and shows the most linearity in angle displacement per step of 0.1 mm (Chapter 3). Therefore, we continue with a two-curved tip design.

Number of Elements

The number of elements is a trade-of between diameter, stiffness and tip steerability. In the proposed tip design, the tip angle is achieved by retraction of one or more elements. The retraction of an element makes the opposing elements deflect, leading to reorientation of the tip into the direction of the retracted element. A column prefers to bend around the principal axis of the cross section that has the least moment of inertia (the weakest axis). To keep the moments of inertia the same in all directions, the cross-section should be circular. Increasing the number of elements, results in a more homogeneous circular shape, and leads to a better steerability of the tip. However, the overall diameter increases when the number of elements increase (when the diameter of the elements stays the same).

This study of ultra-thin needle steering pushes the boundaries of miniaturisation. To achieve the smallest diameter during the feasibility study, the number of elements will be kept to a minimum. Three elements are the fewest needed to steer in three-dimensional space without rotating the needle. Therefore, a three-element prototype was made.

Material Choice

In previous prototypes we made use of Nitinol wires as elements. This material shows great advantage over other materials because it shows super elastic behaviour. The elements experiences large deformations. Therefore, the material needs to have great elastic properties to bend back to its original shape without plastic deformation.

Joining of Nitinol Elements

Methods to join Nitinol are gluing, welding and soldering. Other mechanical techniques are crimping and swaging. Bonding to Nitinol is challenging because of the tenacious oxides that form on the surface of the Nitinol material [32]. To solder Nitinol, the oxide layer must be removed for optimum solder wetting. Solder

with silver can connect to nitinol if combined with a very aggressive flux. However, both solder and flux have poor biocompatibility, thus soldering is not applicable for a needle which enters human tissue. For welding, TIG-, laser-, e-beam-, resistance- and plasma-welding techniques can be used. These techniques have the advantage that no additional material has to be added. Therefore, welding of the nitinol elements would be the best option.

A laser welding machine was part of our resources. However, the available laser was too strong for such small elements, leading to change in material properties. The Nitinol wires were heated too much by the laser, resulting of loss of the super-elastic behaviour and the Nitinol turned into a brittle material. Therefore, we tried to glue the elements together. Several types of glue (i.e. epoxy, metal glue) were used to try to connect the elements together, however the glued connection seemed to be too weak to hold the transverse forces. Therefore, a stainless steel tube was glued over the tip of the needle, to keep the wires together and to withstand forces perpendicular to the axis of the needle (Figure 4.1a).

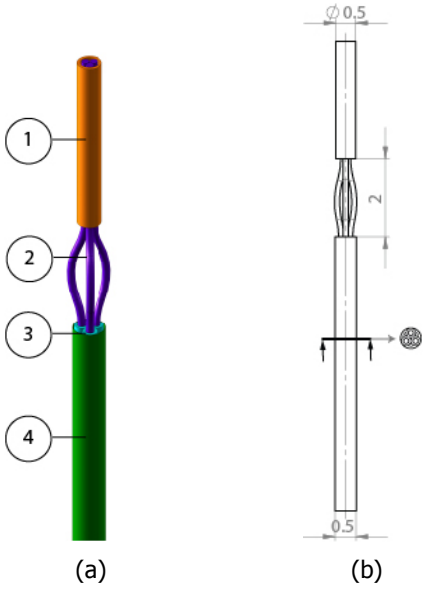

Figure 4.1: Tip design in straight configuration. (a) Tip design: (1) tube; (2) Nitinol element; (3) Nitinol tube; (4) shrinking tube. (b) Schematic drawing tip design including dimensions.

4.2.2. Cannula

The cannula contains the elements of the steering mechanism and keeps them together. The cannula should be tightly fitted around the elements to prevent movement of the elements inside the shaft, which can lead to positioning inaccuracies. The cross-section and material of the cannula, combined with the steering mechanism, determine the proneness to needle buckling. Bodies with low flexural rigidity bend easier than bodies with high flexural rigidity. Therefore, bodies with low flexural rigidity can make small bending curves and follow the tip more easily, thus increasing the steerability of the needle. However, long, low stiffness bodies are prone to buckling. When entering tissue, the needle experiences frictional and cutting forces. The forces on the needle increase during insertion, eventually leading to needle buckling inside the tissue. Therefore, the flexural rigidity of the needle should be sufficient for proper insertion but flexible enough to follow the trajectory of the needle tip.

As mentioned before, a column buckles about the principal axis of the cross section that exhibits the least moment of inertia (the weakest axis). To keep the moments of inertia the same in all directions, circular tubes would make the best columns. Tubes that exactly fit the dimensions of the cross-section of the three elements are difficult to acquire, except for shrinking tubes. Shrinking tubes make a perfect fit by shrinking tightly around the elements. However, plastic shrinking tubes are too thin and flexible and they do not give the minimum rigidity needed to avoid buckling. Therefore, the flexural rigidity of three 0.125 mm diameter Nitinol wires with plastic shrinking tube was too little for proper insertion (>50 mm) without buckling. There are Nitinol tubes with the desired dimensions, but they are too stiff to follow highly curved trajectories.

Because of the lack of flexible, elastic, tight-fit tubes, three thin Nitinol tubes (Johnson Matthey, Nitinol super-elastic tube OD 0.24 mm ID 0.15 mm) were used to make a tight fit with the elements, and to increase the flexural rigidity of the needle 4.1a). The advantage of multiple tubes compared to one single tube, is the fact that they prevent the elements from twisting around each other, reducing steering inaccuracies. An additional advantage is that the tubes can act as a bowden cable for each individual element, all the way to the actuation of the element.

An ultra-thin shrinking tube (Vention, Polyester shrink tubing ID 1.1 mm, wall thickness= 0.0076 mm) keeps all the Nitinol tubes together without drastically increasing the diameter of the needle (Figure 4.1a). A cross-section of the final needle is shown in

Figure 4.2. In this way, the shaft of the needle has a final cross-sectional diameter of 0.5 mm.

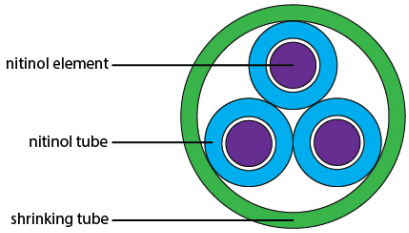

Figure 4.2: Cross-section of the needle with three Nitinol elements (purple), three Nitinol tubes covering the elements (blue), and shrinking tube (green).

4.3. Control Unit

4.3.1. Requirements & Wishes

A control unit capable of moving each element separately, was designed to investigate how the displacement of each individual element influences the steering behaviour of the needle. The main requirements and wishes for this control unit are listed below.

Requirements

1. ***Individual element movement***
   The control unit must be capable of moving the elements individually. This way, the behaviour of the needle can be properly investigated for every possible setting.
2. ***No buckling***
   The elements should not buckle inside the control unit, since it increases positioning errors.
3. ***No permanent connection***
   The connection of the actuation mechanism to the elements should not be permanent. This is in order to allow replacement of the steering mechanism, to change the tip design, or to change the steering mechanism once it is broken.
4. ***Re-configurable control unit up to 6 elements***
   The steering mechanism has to actuate a needle configuration for the minimum requirement of 3 elements. However, the control unit should allow examination of designs up to 6 elements for future purposes. Therefore, the control unit needs to be re-configurable up to six elements.
5. ***Retain setting***
   The setting of the elements should stay the same during tissue insertion. The position of the needle tip is determined by the amount of retraction of each individual element. To provide tissue entering with constant curvature, the elements need to retain the same level of retraction.
6. ***Non-damaging connections***
   The individual elements need to be fixed inside the control unit without damaging the wires. In this way, the elements can be re-positioned and reused.
7. ***Element movement in both directions***
   After an element is retracted to steer the needle, it should be able to return to it's original position in order to ensure continued use. In other words, the movement of the element needs to work in both directions.

Wishes

1. ***Attachment via M3 bolt***
   The control unit needs to be attached to the linear stage through an already excising aluminium block by means of an M3 bolt. This block then makes the connection between the linear stage and the control unit.
2. ***High accuracy***
   The displacement of the elements must be as accurate as possible to finally improve the of the needle tip placement.
3. ***Easy element replacement***
   Replacement of the steering mechanism should be as easy as possible to provide removal of the elements without taking too much effort.
4. ***Make use of rapid prototyping***
   In order to work within the time limits for this project, the techniques for rapid prototyping (3D-printing, laser cutting) are very useful.

4.3.2. Actuation Elements

Each element needs to move independently. Therefore, the initial focus is on the actuation of a single element. Later, the same actuation mechanism can be applied to the intended design by adding up to the maximal number of six elements.

Movement of Elements

The maximum displacement of an element is in the order of 1 millimetre to steer the needle tip 90 degrees (see Chapter 3). Such small displacements are difficult to control manually without transmissions. Therefore, increasing the input-to-output displacement is desirable for accurate positioning.

Some options for increasing the input-output displacement are the usage of a worm and wheel, a lead screw, rack and pinion, a crank and slider, and a cam and follower. We chose to use a lead screw, because the mechanism is limited in size and in number of parts, is easy to operate, while it increases the input-output ratio depending on the pitch of the lead screw. The materials for a lead screw are also easy to aquire by off-the-shelf screws and by tapping a thread in another part. The rotation of the lead screw can be precisely controlled by a wheel that is connected to the top of the lead screw. The wheels can easily be manually rotated using finger movement.

Attachment of Element

The diameter of an element is very thin (0.125 mm) and is difficult to attach to the actuation mechanism because of their minimal amount of surface area. Some ideas to attach the wires are knotting, clamping, gluing or using a shape slot. The attachment might not be permanent, because the elements need to be replaceable. Therefore, clamping and a shape slot would be good options. However, by adding a shape slot the steering mechanism is not retractable anymore. Therefore, we choose for clamping to attach the elements (Figure 4.5).

Buckling prevention

The elements of the steering mechanisms are long and flexible and are therefore prone to buckling. Along the needle shaft, the elements are protected from buckling by the Nitinol tubes encompassing them. However, the Nitinol cannot cover the travel space necessary to move the element back and forth. Therefore, a concentric tube was added to minimise the unsupported length of the Nitinol tube (Figure 4.3). The rigid tube is connected by glue to the attachment block and has a tight fit around the Nitinol tube (OD Nitinol tube=0.24 mm, ID rigid tube=0.3 mm) which minimises the movement of the Nitinol tube.

Total Actuation Mechanism

Figure 4.4 shows a schematic overview of the actuation mechanism. The lead screw is inserted in a rectangular block (Figure 4.4). The block has an inner thread with the same pitch as the lead screw. The rectangular block is fitted in a shape lock, preventing it to rotate. Rotation of the wheel, and thereby the rotation the screw, results in a linear movement up or down of the block, depending on the rotational direction of of the wheel. Each element is clamped inside the block by a brass part pushed inward by a set screw. The brass part prevents damage created by torsional forces of the set screw during rotation. This mechanism provides the control of the displacement of each element.

The pitch of the screw determines the ratio between the amount of wheel rotation and the corresponding height translation of the block.

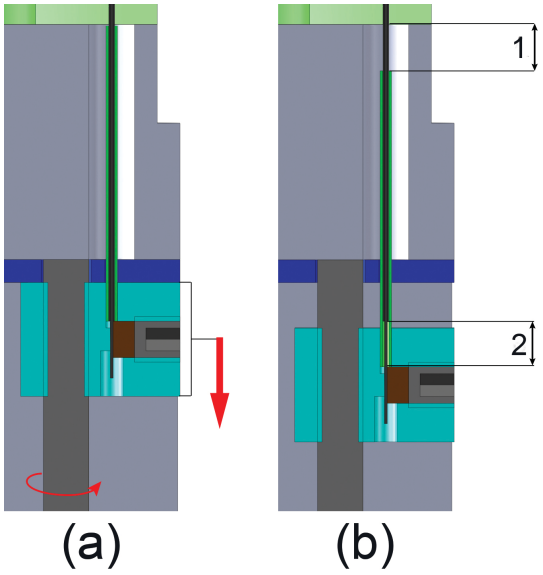

Figure 4.3: Minimising buckling length when actuated. (a) shows the movement of the block by rotation of the lead screw represented by the red arrows. (b) Shows the position after rotation where (1) shows the unsupported length of the Nitinol tube and (2) the unsupported length of the element inside the rigid tube (green).

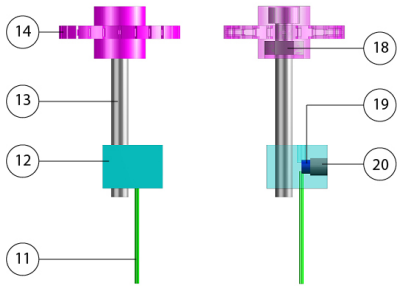

Figure 4.4: 3D drawing of the actuation mechanism: (14) wheel; (13) screw M2x20; (12) rectangular block; (11) rigid tube; (18) nut M2; (19) brass part; and (20) set screw M1.6.

In the final design, a M2x20 screw was used, with a pitch of 0.4 mm. Therefore, each rotation results in a translation into movement of 0.4 mm of the block. The wheel contains little and large grooves, of which each large groove (movement of 90 degrees) corresponds to 0.1 mm displacement, and each little groove (movement of 15 degrees) corresponds to a displacement of 1/60 mm.

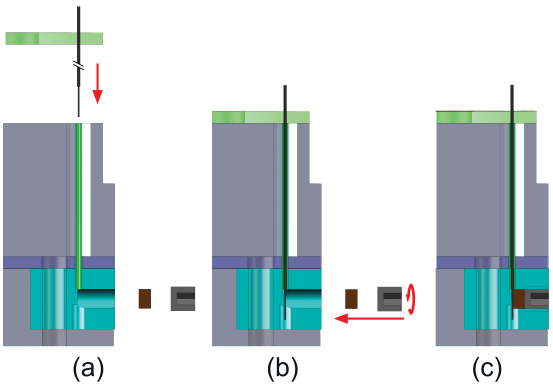

Figure 4.5: Attachment of a single element into the rectangular block by a set screw: (a) The element together with the Nitinol tube are inserted into the rigid tube; (b) the brass part together with the setscrew are inserted into the rectangular block; (c) clamping of element.

4.3.3. Body

The main body of the control unit is a cylindrical part with slots for the attachment blocks (Figure 4.7). Section 4.3.2 discusses the actuation of a single element. However, the prototype needs to individually actuate elements up to a maximum of six elements. Therefore, the number of actuation mechanisms were increased to a total of six. The six actuation mechanisms are configured in a circular configuration, so that every actuation unit corresponds to its element in the circular configuration inside the needle.

The long rectangular slots of the body prevent rotation of the attachment blocks. Cylindrical spare outs at the top provide insertion of the protrusions of the wheels to stabilise the wheel. The wheel is established between the back plate and main body. The back plate and the body are kept together by means of three bolts, capturing the wheel. Rings are positioned around the bolts in order to keep a set distance between the body and back plate, thereby preventing blocking of the wheel rotation caused by clamping (Figure 4.7).

4.3.4. Guiding of Elements

The elements need to be guided from the control unit towards the needle tip of the ultra-thin needle. Since the Nitinol tubes act as a bowden cables, they can span a distance over two fixed points. The Nitinol cables are glued to a thin disc positioned at the top of the main body. By grooves inside the conical cap, the tubes are guided towards the top, from where the tubes come together into the needle shaft. The tubes were glued to the top of a guidance cap to prevent motion of the tubes. The conical cap together with the disc was mounted to the base by three M3 bolts (Figure 4.7).

4.3.5. Needle Protection

Unintended large lateral deflection of the needle can occur caused by unexpected forces, such as buckling or bumping into an object during needle insertion or transportation. Large needle deflections cause high stress concentrations at the point of entry of the needle into the control unit. This might result in damage of the needle by plastic deformation. Therefore, the final cap has, as a safety precaution, rounded edges at the point of entry to avoiding sharp curvatures (Figure 4.7). When the needle experiences large deflections, the needle curves along the rounded edge of the cap, decreasing stress concentrations compared to a sharp edge.

4.4. Prototype

The prototype of the final design consists of the needle and the control unit. The needle consists of three longitudinally aligned elements, made of super-elastic, straight annealed (heat treatment at 400°C to 550°C in straightened configuration), polished surfaced Nitinol wires of 0.125 mm outer diameter (Flexmet BVBA, Belgium). The shape setting of the pre-curvature at the tip was created by carefully heating the elements to a temperature of 480 degrees Celsius by a rework station (Tenma SMD rework station 220V) while curved around a 0.3 mm diameter rods (Appendix A). A tube (Stainless steel, 0.3 mm ID, 0.5 OD) was glued around the tip ends, to join the three curved elements together. All three wires were individually guided by Nitinol tubes towards the control unit. The Nitinol tubes were covered with shrinking tube (Vention, Polyester shrink tubing ID 1.1 mm, wall= 0.0076 mm) to keep them together. The total length of the needle shaft is 180 mm measured from the control unit up to the steering mechanism. The steering

mechanism curvature has a length of 2 mm, and width of 0.5 mm. The tube at the needle tip has a length of 3 mm.

The control unit was made with rapid prototyping methods, such as additive manufacturing, laser cutting. The body of the control unit and the rectangular blocks were 3D printed in stainless steel (type 316L) by additive manufacturing by means of laser metal fusion (Sisma, type Mysint100). The metal printer delivers a rough surface finish, and needs post-processing to remove support structures and to enhance the surface structure. First the support structures were cut away, and subsequently the part was sanded and polished.

The wheels and the two caps were printed in polymeric material (acrylate, R05 red) by additive manufacturing. We made use of digital light processing (Envisiontec Type: perfactory 4 mini xl), to have a high precision part with a smooth surface finish. The disk and star were made by means of laser cutting. The complete bill of materials (BOM), together with the Engineering Drawings, can be found in appendix E.

The prototype of the needle and control unit is shown in (Figure 4.8). A close-up of the needle tip is shown in Figure 4.9. The tip of the needle showed bending when one of the wheels was rotated (Figure 4.10). The prototype of the assembled actuation mechanism is shown in Figure 4.11.

Table 4.1: Overview of all parts of the prototype and their quantity (QTI).

Item No.	Name	QTI
1	Shrinking Tube	1
2	Protection Cap	1
3	Screw M3x10	3
4	Cable Guidance Cap	1
5	Nitinol Cable	3 / 6
6	Disc	1
7	Element	3 / 6
8	Screw M2x5	3
9	Body	1
10	Star Plate	1
11	Rigid Tube	3 / 6
12	Rectangular Block	6
13	Lead Screw M2x20	6
14	Wheel	6
15	Ring	3
16	Back Plate	1
17	Screw M2x10	3 / 6
18	Nut M2	3 / 6
19	Brass Part	3 / 6
120	Set Screw M1.6	3 / 6

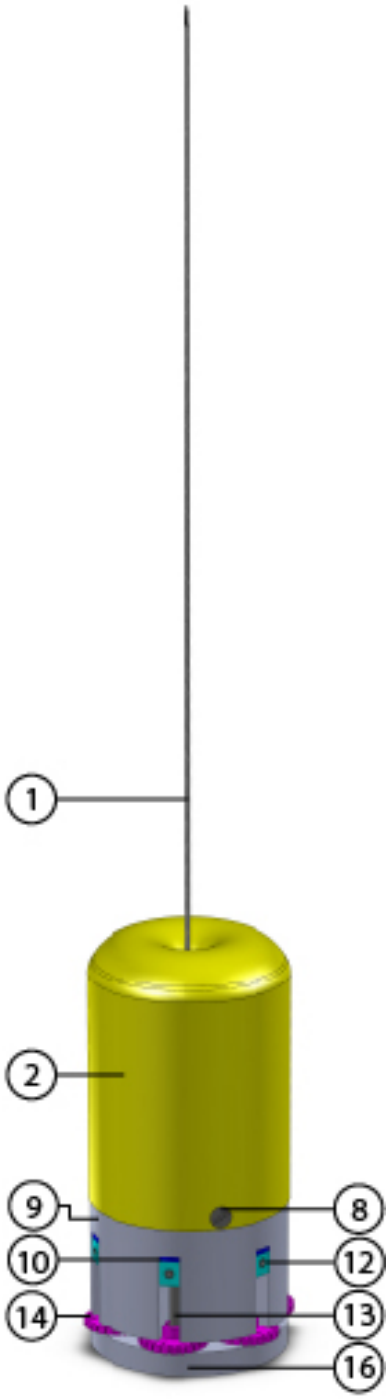

Figure 4.6: 3D drawing of the control unit: (1) shrinking tube; (2) protection cap; (3) bolt M3x10; (5) Nitinol tube; (7) element; (8) screw M2x5; (9) body; (12) rectangular block; (13) lead screw M2x20; (14) wheel; (15) ring; (16) back plate; (17) screw M2x10.

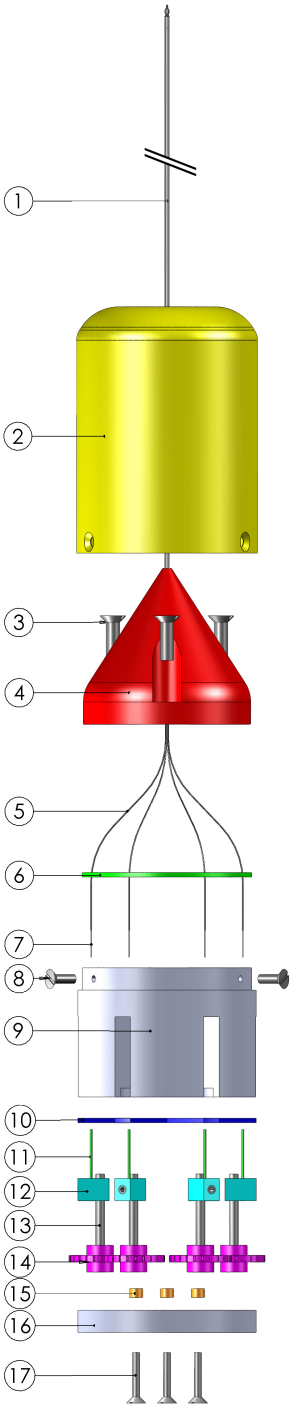

Figure 4.7: Exploded view of control unit: (1) shrinking tube; (2) protection cap; (3) bolt M3x10; (4) conical guidance cap; (5) Nitinol tube; (6) disc; (7) element; (8) screw M2x5; (9) body; (10) star plate; (11) rigid tube; (12) rectangular block; (13) lead screw M2x20; (14) wheel; (15) ring; (16) back plate; (17) screw M2x10.

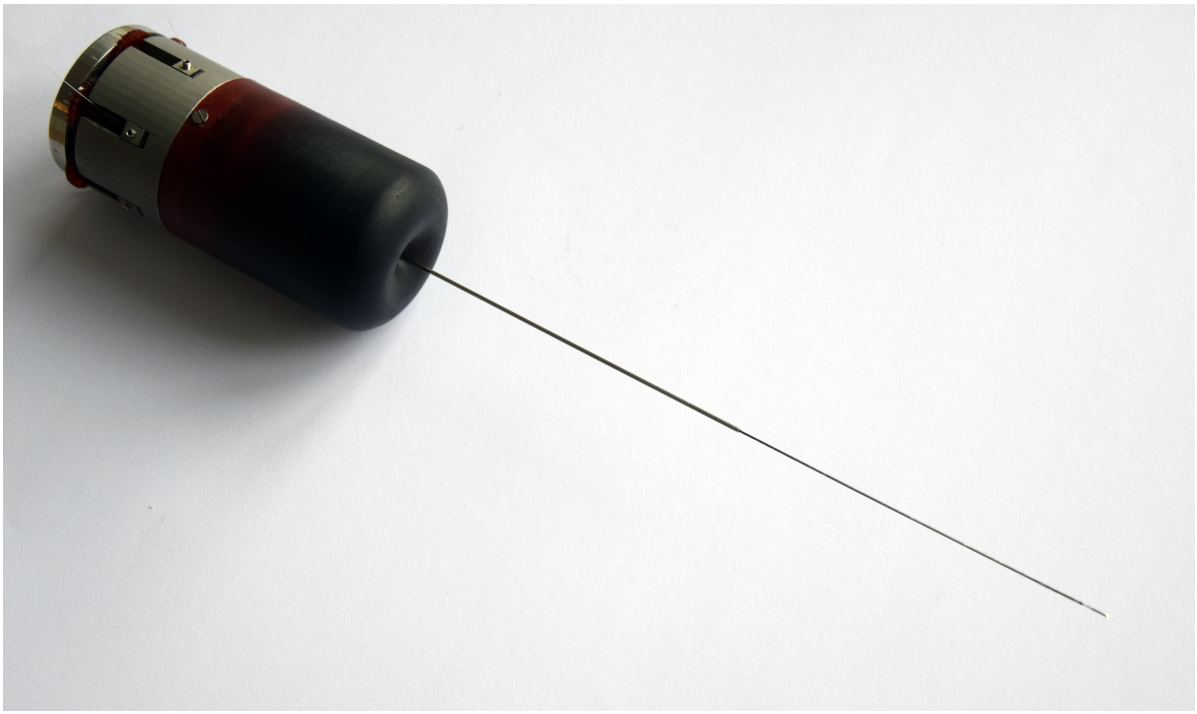

Figure 4.8: Prototype of needle and control unit.

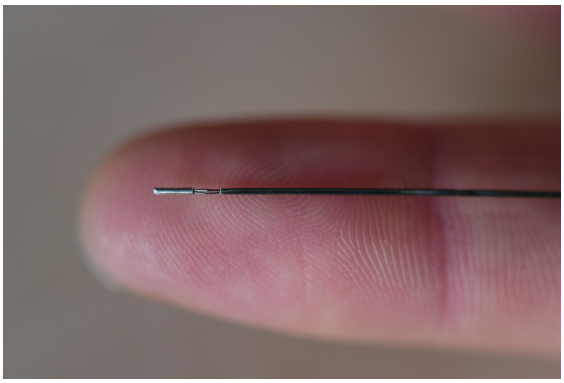

Figure 4.9: Close-up of the final needle tip design in straight position.

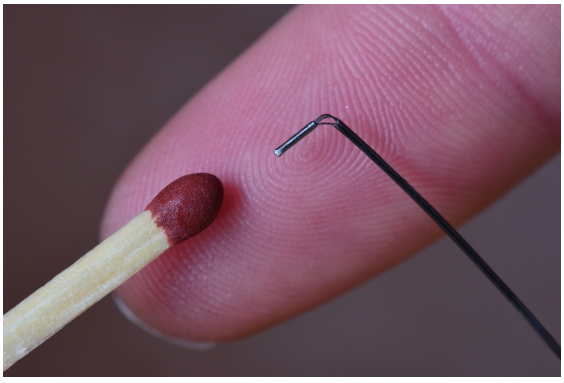

Figure 4.10: Close-up of the needle tip after element retraction leading to a bend tip position.

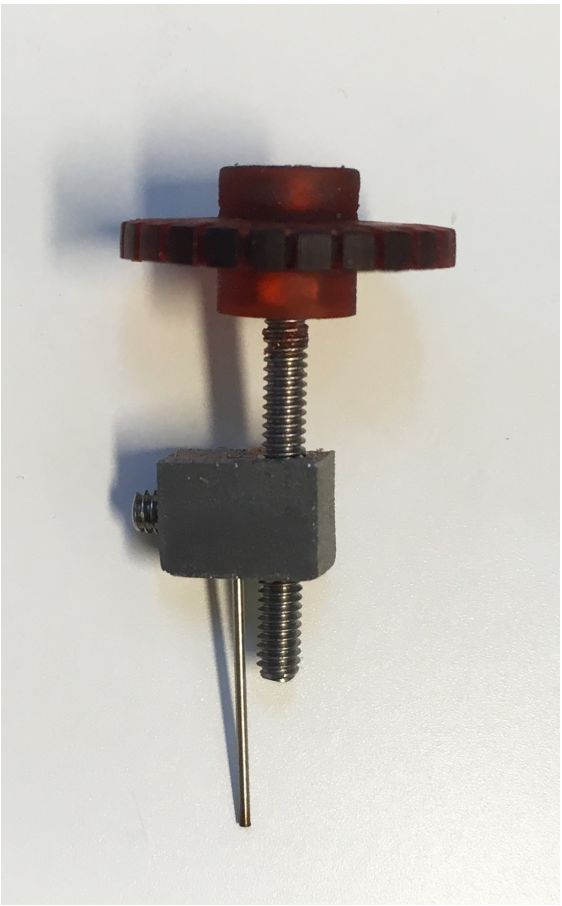

Figure 4.11: Prototype of the element actuation mechanism.

5

Final Evaluation

5.1. Experiment 2: Needle Performance

Two experiments were conducted to investigate the performance of the needle. The first experiment was performed to investigate the steering direction of the prototype. After this experiment, the steerability in terms of deflection was measured for various amounts of element retraction.

5.1.1. Experimental Setup

The experimental setup shown in Figure 5.1 was used to measure the steering direction and the deflection of the needle when inserted into artificial tissue by a vertical linear motion. The experimental setup consists of the final needle prototype (described in chapter 4), the actuation unit for needle insertion, a gelatine phantom, a buckling prevention mechanism and data acquisition instruments.

Actuation Unit

A motorised linear stage (Aerotech ACT115, model MTC300) was used to insert the needle into the phantom. The linear stage is controlled by the Soloist CT (Aerotech) controller in combination with the MATLAB program 'soloist' by D. van Gerwen, TU Delft. The linear stage is placed vertically, to reduce the effect of undesired moments and forces caused by gravity. The prototype was mounted on the linear stage by means of an aluminium block acting as mounting plate. The prototype was connected with a M3 bolt to the aluminium mounting plate which, in turn, was attached by four M4 bolts to the linear stage (Figure 5.1).

Gelatine Phantom

Gelatine phantoms were prepared by mixing hot tap water (80 degrees) and gelatine powder (Dr. Oetker Professional, The Netherlands) into transparent containers with a dimension of 120 x 80 x 120 mm (HEMA, The Netherlands). The gelatine was poured in the containers in liquid state, and stored in a fridge overnight (5 degrees Celsius) to harden.

Buckling Prevention

To avoid buckling of the needle outside the tissue during insertion, two concentric rigid tubes were placed over the longitudinal axis of the needle. When the needle is pushed into the phantom, the tubes will slide into each other leaving no space for lateral motion of the needle, therefore prevent buckling of the needle. The outer tube (OD =2 mm, ID= 1.1 mm) and the inner tube (OD=1 mm, ID= 0.6 mm) were both made out of stainless steel.

Data Acquisition

The combination of two views in different planes of the needle are enough to calculate the position in three-dimensional space. Therefore, two cameras (Panasonic HC-V250 video camera) were used to record the path of the needle in the phantom in two planes. One camera was positioned in front of the phantom, and the other at the right side of the phantom (Figure 5.1). A video lighting solution (Falcon Eyes Led Video light DV-96V) was placed behind a white paper behind the phantom, used to enhance the image quality required for image processing.

5.1.2. Experimental Design

In this experiment, the effect of element displacement on the steering direction and deflection was evaluated for a needle with three elements, to investigate the performance of the needle.

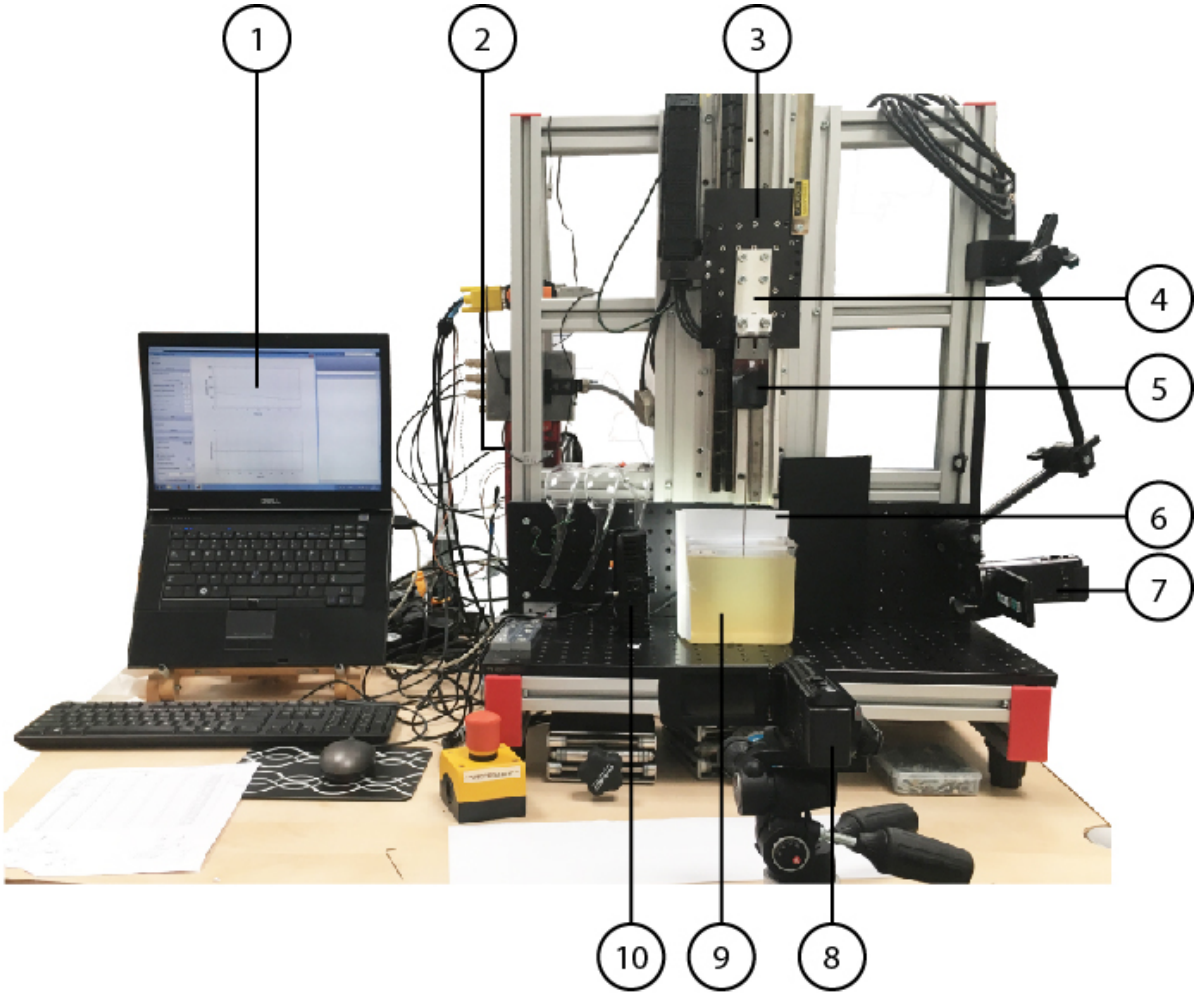

Figure 5.1: Experimental Setup: (1) laptop; (2) controller; (3) linear stage; (4) aluminium mounting plate; (5) prototype; (6) white paper; (7) camera for recording side view; (8) camera for recording front view; (9) gelatine phantom, (10) video lighting.

Variables

Dependent Variables

Steering Direction

The steering direction is the direction in which the needle steers relative to its initial insertion axis. The steering direction is measured in terms of the angle (degrees) with a fixed axis in perpendicular plane to the needle shaft (see Figure 5.2).

Needle Deflection

The curvature of a needle can be expressed by the needle deflection: the more the needle deflect the higher the curvature of the needle. The deflection was measured by taking the euclidean distance, which is the distance from initial axis of insertion to the final position of the needle tip (Figure 5.2) in the plane perpendicular to needle insertion.

Independent Variables

In the experiment, the independent variables are the element configuration (EL1, EL2, EL3) and the retraction of each element [mm]. The element configuration is determined by which element is actuated. The prototype has three movable elements:

- Movement element 1 [EL1]
- Movement element 2 [EL2]
- Movement element 3 [EL3]

For this experiment we use 3 levels of retraction for an element. By trial and error, three levels of element retractions were determined. A maximum of 1,2 mm element retraction corresponded to a needle insertion with maximum deflection without buckling. One

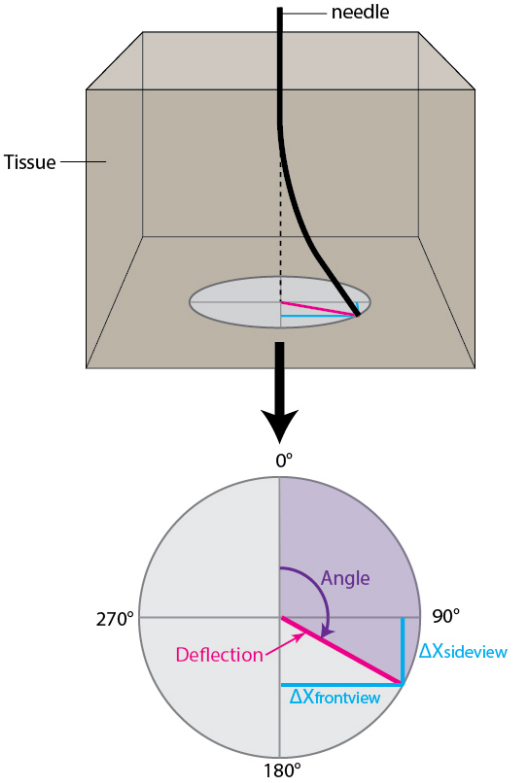

Figure 5.2: Schematic representation of measuring steering direction and needle deflection. The angle was measured in respect to a set inital axis (to the back of the gelatine box). The deflection was measured by the Euclidean distance, where $\Delta X_{frontview}$ and $\Delta X_{sideview}$ are the recorded horizontal distances in two perpendicular planes.

turn (four large grooves in the wheel) of the wheel corresponds to 0.4 mm linear movement. Therefore, the retraction levels are defined as follows:

- Level 1: 0.4 mm retraction (1 wheel turn)
- Level 2: 0.8 mm retraction (2 wheel turns)
- Level 3: 1.2 mm retraction (3 wheel turns)

Steering Direction

EL1, EL2 and EL3 were used for retraction. Because steering does not occur when all three elements are actuated, only single and double element actuation were performed, leading to a total of six experimental conditions. The steering direction is not dependent on the amount of retraction. Therefore, only one level of retraction was used (Level 2, which corresponds with 0.8 mm retraction). Combining the element configuration (EL1, EL2, EL3) together with one level of retraction (Level 2) results in six experimental conditions for the steering direction experiment (Table 5.1). All conditions are visual represented in Figure 5.3.

Table 5.1: Experimental Conditions for the Steering Direction Experiment

	Retraction Level		
Exp. Co.	EL1	EL2	EL3
1	2	0	0
2	2	2	0
3	0	2	0
4	0	2	2
5	0	0	2
6	2	0	2

Table 5.2: Experimental Conditions for the deflection Experiment

	Retraction Level		
Exp. Co.	EL1	EL2	EL3
1	1	0	0
2	2	0	0
3	3	0	0
4	1	1	0
5	2	2	0
6	3	3	0
7	2	1	0
8	3	1	0
9	3	2	0

Needle Deflection

For the deflection experiment, only EL1 and EL2 were taken in consideration, because other configurations lead to the same relative configuration (i.e., a rotated or mirrored version). EL 1 will be single actuated by three levels of retraction (three conditions), both EL1 and El2 will be pulled in three different levels of retraction (three conditions). Additionally, three in-between conditions were added leading to a total of nine experimental conditions (Table 5.2). All nine experimental conditions are shown in Figure 5.4.

Each experiment was performed five times, resulting in a total of 30 runs for the steering direction experiment, and a total of 45 runs for the deflection experiment. The run tables of both experiments can be found in Appendix C.

Co-founding Variables

The concentration of gelatine phantom was 10 wt% for all experiments. The insertion speed for needle insertion was 2 mm/s, to be able to intervene quickly and prevent damage to the needle in case something went wrong. The Insertion depth from initial to final

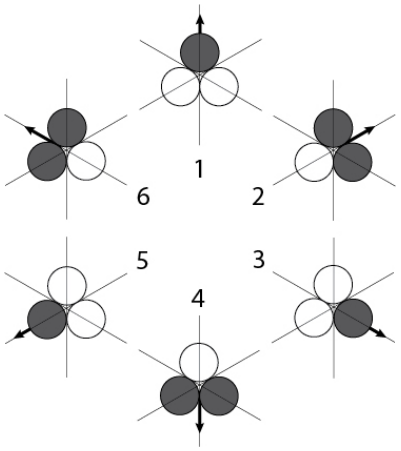

Figure 5.3: Element representation of the experimental conditions for the steering direction experiment: Grey corresponds to Level 2 retraction of that element, the arrow indicates the hypothesised steering direction.

position was 65 mm for all experiments. For each experiment, a total of five containers of gelatine were used for needle puncturing. To decrease influence of minor changes in gelatine containers, each measurement within an experimental condition was performed in a different container.

For the steering direction experiment, the needle was inserted in a circle in the middle of the gelatine phantom based on the hypothesised steering direction (Figure 5.5 (a)). In this way, the needle has enough space to deflect laterally. For the deflection experiment, all needle deflections will go in approximately the same direction. Therefore, two rows of insertion points were defined, in which the path crossing was limited (Figure 5.5 (b)).

Hypothesis

For both steering direction and deflection experiments hypotheses were formulated:

Experiment 1: Steering direction

1. The needle will steer in the same direction as the retracted element. All combinations of retracted elements with their expected steering direction are shown in figure 5.3. This means that the angle between single element retraction is 120° (EC1,EC3,EC5), between double element retraction is 120° and between single and double element retraction is 60° (EC1-EC2-EC3-...-EC6-EC1). The steering direction is vissually represented by the arrows in Figure 5.3.

Experiment 2: Deflection

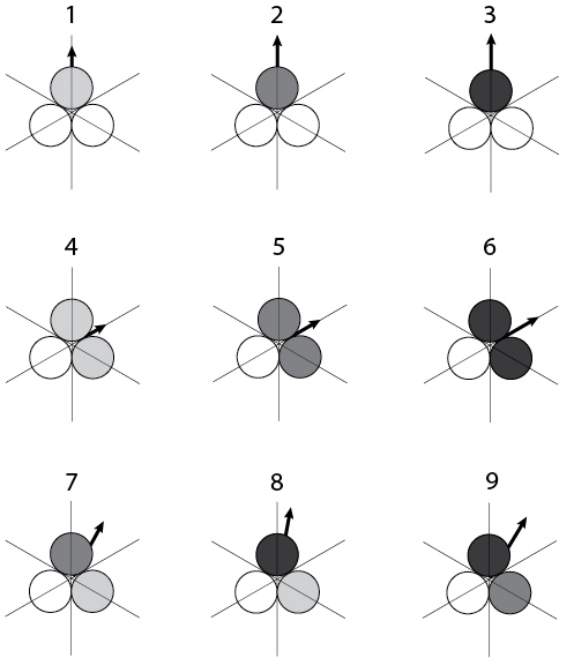

Figure 5.4: Element representation of the experimental conditions for the deflection experiment:
Each colour represents the amount of retraction: light grey is Level 1; medium grey is Level 2; dark grey is Level 3. The arrow indicates the hypothesised steering direction.

1. The deflection increases with an increase in the amount of retraction of the elements (Figure 5.4).

2. Retraction of one element will cause more needle deflection than retraction of two elements. When one element is retracted, two elements are in bend position (instead of one for two element retraction), which causes more force on the tissue than one bend element.

5.1.3. Experimental Procedure

The gelatine samples were used directly after taking them out of the refrigerator, to ensure there is no influence by the samples heating up to room temperature. A white paper with a reference mark was attached with scotch tape to the back of the gelatine box. The gelatine box was placed on the breadboard positioned under the linear stage.

After positioning the gelatine phantom to its desired position the coocentric tubes (for buckling prevention) were placed on the gelatin phantom. To ensure the steering tip entered the phantom before steering, the needle was first inserted inside the phantom for about 10 mm (initial position 150 mm of linear stage) in straight configuration. After insertion,

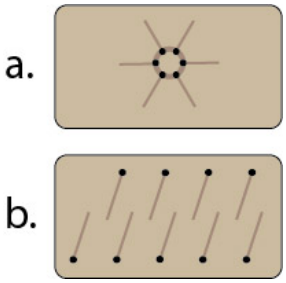

Figure 5.5: Top view of the gelatine container showing insertion points for the needles with their expected trajectory, for steering direction experiment (a) and deflection experiment (b).

pictures were taken with both video cameras to capture the initial position from the front- and side-plane. Then, the wheels were rotated to obtain the element configuration for the desired experimental condition. After configuring the elements, the program 'Soloist' was activated, thereby, inserting the needle 65 millimetres into the gelatine phantom by the linear stage. Photographs with both cameras (Front and Side) were taken at the end of each trial of the final position of the needle inside the gelatine phantom. After each trial, the needle was retracted out of the phantom by the linear stage.

After retraction the needle was configured in its initial straight configuration where all elements have zero retraction. After each trial, the gelatine phantom was changed or re-positioned manually. Both the steering direction and the needle deflection experiment took about half a day each, and were performed on different days.

5.1.4. Data Analysis

To extract the steering direction and the deflection, the images taken by the cameras (front and side) were post-processed in MATLAB. All steps are shown in Figure 5.6.

1. **Cropping images**
   All images were post-processed by cropping them to their region of interest to reduce influence of noise. First the region of interested was manually selected of the images of the final needle position. Both the final and initial needle images were cropped with the same rectangular cropping frame.

2. **Post-processing final position images**
   After cropping, the cropped images of the final positions were post-processed by sharpening the images and adjusting the contrast. Then the image processing toolbox was used to convert the images to binary black and white images. A line (skeleton) was extracted from the binary images and additional noise was removed.

3. **Retract begin point and endpoint**
   The coordinates of the beginning and end points were retracted from the line. For the steering direction the maximal vertical (y) value of the endpoints was used to find the end point. For the deflection experiment the maximal horizontal (x) value was used so it also works for high curvatures where the needle goes up again.

4. **Further cropping and post-processing of initial images**
   The begin point was used to crop the images of the initial position of the needle. A rectangular of 60 by 150 pixels was used to crop the image of initial positions to reduce the influence of noise. Then the same post-processing of sharpening, contrast adjusting were applied and a transformation to a binary image was made to create a line of which the coordinates of the endpoint was extracted.

5. **Calculation difference in x and y value**
   The end points of both initial and final needle images were used to calculate the difference in the amount of pixels in horizontal (Δx) and vertical (Δy) position between the initial and final needle tip position. The differences in x and y positions are in pixels. Therefore, the actual displacement in millimetres can be calculated by multiplication by a scaling factor for both front and side view.

   The scaling factor for the front view was calculated by a reference in the front-view picture. The actual needle displacement in y direction for both front and side view should be the same. Therefore, the scaling factor for the side view was calculated by equating the length of the difference in y value (Δy). For the steering direction, a scaling factor for the side view was calculated for each single measurement. In the deflection experiment some experimental conditions led to a high curvature. When a needle had a high curvature, the needle went up, leading to a small distance from

initial position to final position of the needle tip. The small distance introduces errors in the scaling factors. Therefore, the median value of all scaling factors per experimental condition was used as scaling factor in the deflection experiment.

6. **Calculate steering direction or needle deflection**

   Determine Steering Direction
   The steering direction was calculated by taking the tangent between both differences in x coordinates of the initial and final needle tip position from both front and side view (Figure 5.2). The angle theta is the counterclockwise angular displacement in degrees from the positive x-axis.

   Determine Needle Deflection
   The deflection is the distance from the origin to a point in the x-y plane. By the Pythagorean theorem the deflection of the needle was calculated from both x values from the front and side view (see Figure 5.2).

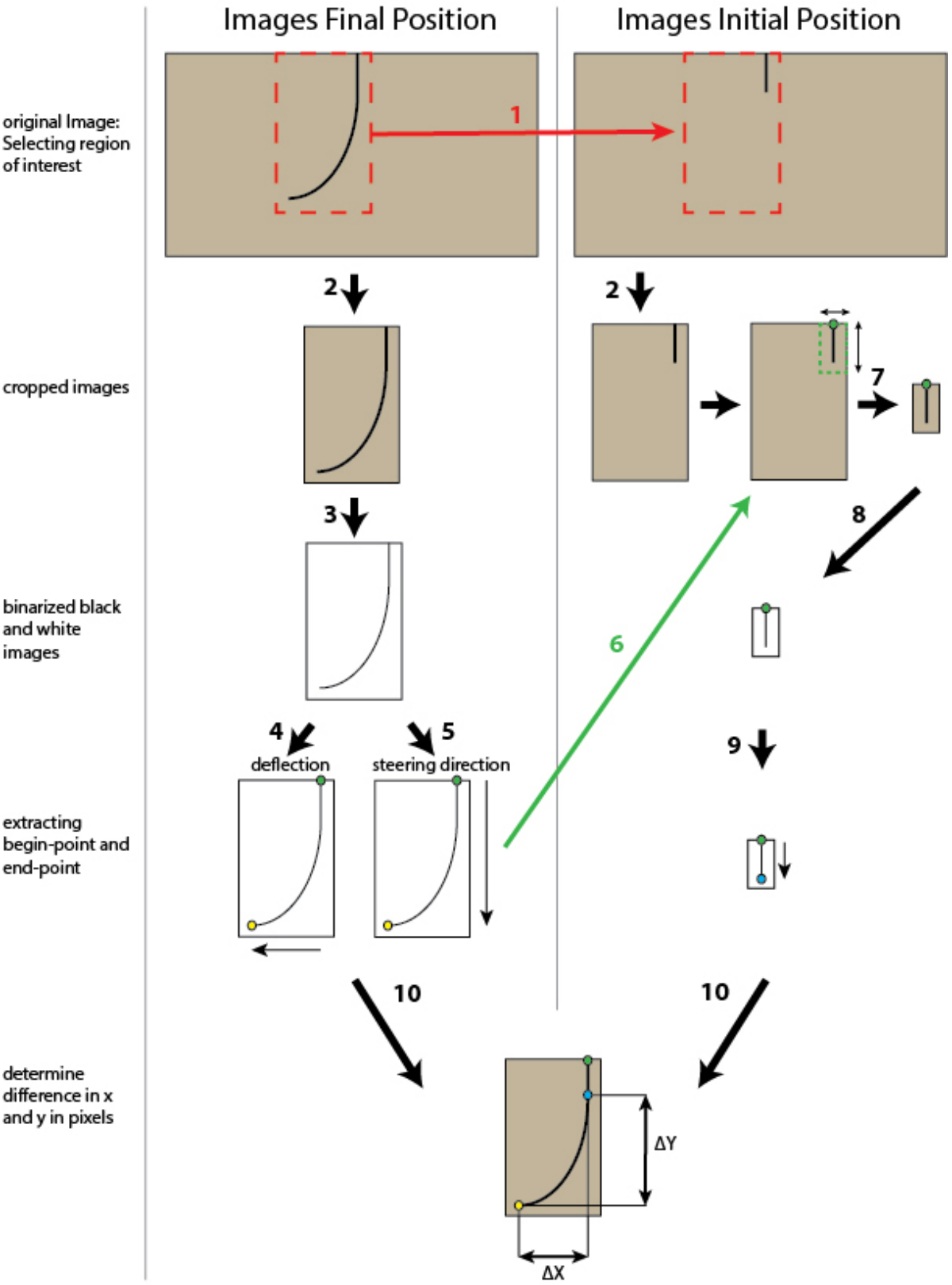

Figure 5.6: Steps of image processing of pictures of needle in gelatine (final and initial position) to determine out the difference in x and y values: (1) transferring manually selected rectangular (red); (2) Cropping images by red rectangle; (3) transformation to a binary image; (4) read out begin (green dot) and end points (yellow dot) by the maximum x value; (5) read out begin (green dot) and end points (yellow dot) by the maximum y value; (6) use begin point final position to select region of interest in initial position; (7) cropping initial position image to region of interest; (8) transformation to a binary image; (9) read out begin (green dot) and end points (blue dot) of the initial needle position by the maximum y value; (10) determine difference in horizontal and vertical position by end points.

5.2. Results

5.2.1. Needle Steering Direction

Figure 5.7 shows an example of the front view image of the needle prototype insertion into the gelatine phantom.

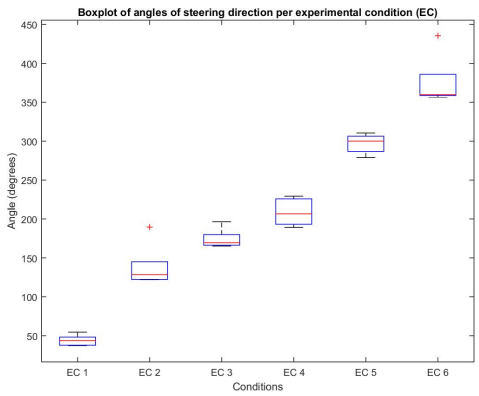

Figure 5.7: Image of needle insertion into the gelatin phantom with a retraction of 0.8 mm of element 1 and element 2(EC 4).

Figure 5.8 shows the results of the steering direction of each experimental condition. It defines the needle steering direction by the angle between a set initial axis (Figure 5.2) and the projection of begin and end coordinates of the needle on a plane perpendicular to the initial axis of the needle.

Figure 5.9 shows the steering direction and the magnitude of deflection for all six experimental conditions relative to the initial position of the needle as seen from the top view of gelatine box.

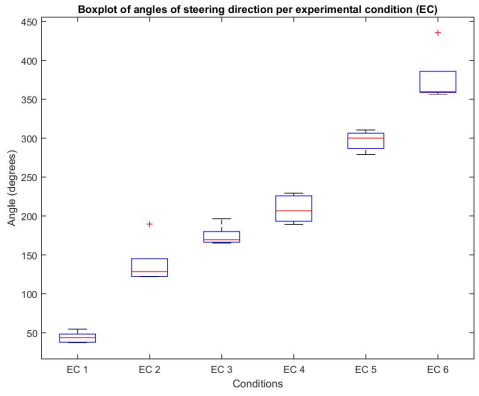

Figure 5.8: Box plot of angle (degrees) of steering direction.

The tip consists of three elements configured in a circular manner. Therefore, the needle is rotational symmetrical over a rotation angle of 120° and 240°. When element 1 is retracted

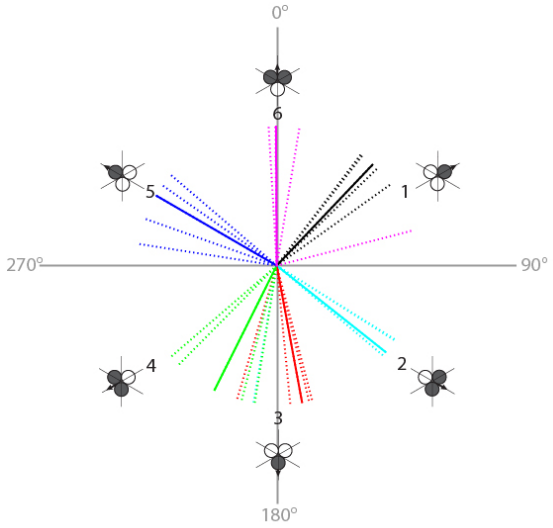

Figure 5.9: Steering directions of all six experimental conditions.

Table 5.3: Median, mean and standard deviation results of steering direction (degrees).

Condition No. *(EL1, EL2, EL3)*	**Median** *[deg]*	**Mean** *[deg]*	**Std** *[deg]*
1. (2 0 0)	43.55	43.83	7.05
2. (2 2 0)	128.43	138.53	28.79
3. (0 2 0)	169.50	174.46	12.82
4. (0 2 2)	206.58	208.84	17.78
5. (0 0 2)	300.11	296.83	12.65
6. (2 0 2)	359.70	376.16	33.54

(EC1) the needle steers to an angle with a median of 43.55°, and when element 2 is retracted (EC3) the needle steers towards an angle with a median of 169.50 ° to its initial axis. The difference between the median of the two angles is 125.95°. Between the angle of element 2 retraction (EC3) and the angle of element 3 retraction (EC5) the difference in median is 130.61°, and the difference in median angle between element 3 and 1 the difference in median angle is 103.44 °. When two elements are retracted the difference in median is respectively 78.15° (between EC2 en EC4), 206.87° (between EC4 and EC6) and 128.73° (between EC6 and EC2).

When we look at the standard deviation of the results, the standard deviation of single element retractions (EC1, EC3, EC5) is less than the standard deviation of double element actuation (EC2, EC4, EC6) (Table 5.3).

5.2.2. Needle Deflection

Figure 5.10 shows the results of the steering direction of each experimental condition. Figure 5.11 shows the same results but then categorised on single element actuation, double element actuation with same level of retraction, and double element actuation with different levels of retraction.

Increasing the amount of retraction of the elements resulted in a larger deflection of the needle (Figure 5.10). The median deflection for one element retracted to level 1 (0.4 mm), level 2 (0.8 mm) and level 3 (1.2 mm) were respectively 38.3 mm, 54.12 mm and 61.68 mm. The median of the deflection for two-element retraction to level 1, level 2 and level 3 were respectively 45.26 mm, 50.27 mm and 55.53 mm (Table 5.4).

One element retraction showed higher median of deflection than two element retraction for level 2 (0.8 mm) and level 3 (1.2 mm) retraction, when the elements were actuated with the same level of retraction. However, for level 1 (0.4 mm) element retraction, the double element actuation showed a higher deflection than the single element actuation (Table 5.4).

When we look at the standard deviation of the results, the standard deviation of level 1 (0.4 mm) retraction showed larger standard deviation than the level 2 (0.8 mm) and level 3 (1.2 mm) retractions (Table 5.4) in case of single element retraction.

Table 5.4: Median, mean and standard deviation results of deflection experiment.

Condition No. *(EL1, EL2, EL3)*	**Median** *[mm]*	**Mean** *[mm]*	**Std** *[mm]*
1. (1 0 0)	38.31	42.70	11.84
2. (2 0 0)	54.12	52.85	4.45
3. (3 0 0)	61.68	58.77	6.11
4. (1 1 0)	45.26	45.21	5.58
5. (2 2 0)	50.27	48.89	6.28
6. (3 3 0)	55.53	56.02	1.86
7. (1 2 0)	53.50	55.09	6.90
8. (1 3 0)	57.58	58.25	2.10
9. (2 3 0)	62.76	64.03	3.49

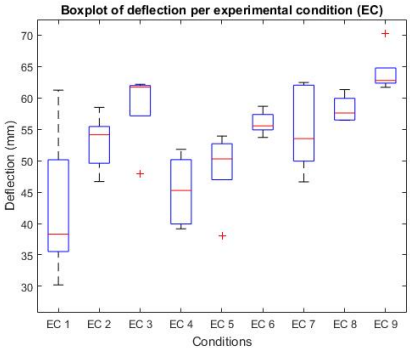

Figure 5.10: Box plot of deflection for all experimental conditions.

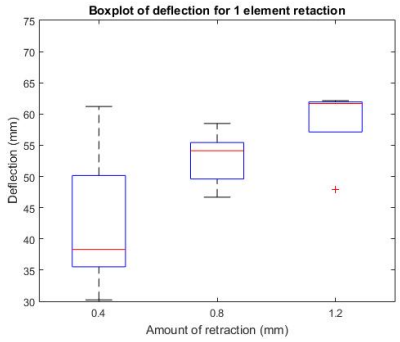

(a)

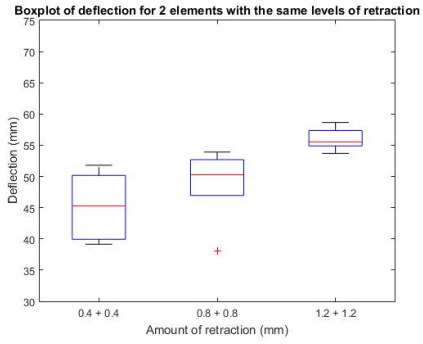

(b)

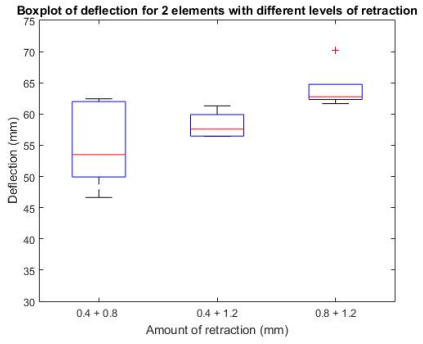

(c)

Figure 5.11: Box plots of deflection: (a) Box plot of deflection caused by 1 element retraction, (b) Box plot of deflection caused by 2 element retractions, (c) Box plot of deflection caused by 2 elements with different levels of retraction.

6 Discussion

6.1. Concept of Steerable Needle

In this thesis, we present a novel approach for the design of an ultra-thin steerable needle. Decreasing the diameter of needles can be advantageous in percutaneous procedures, because it reduces tissue damage and post-operative pains. Needles under 1 mm diameter are limited in steering in three-dimensional space without the use of axial rotation [9]. However, axial rotation of needles results in needle twisting, which induces inaccuracies in needle steering. Therefore, the goal of the study was to design an ultra-thin steerable needle which can steer omnidirectional without the use of axial rotation. To compete with standard bevel needles, we set ourselves the limit of a maximum needle diameter of 0.5 mm.

The proposed needle is inspired by previous work in the field of ovipositor-inspired needles. The wasp ovipositor consists of multiple long, slender, interlocking elements. Steering is achieved by offsetting the segments, resulting in an asymmetric tip. In this way, the needle can steer without the need for axial rotation of the needle. Previous work of Scali et al. [18] showed steering of a 1.2 mm needle consisting of multiple long elements configured in a quasi-bevel tip. The small diameter was achieved by using wires instead of cylindrical needle segments as elements.

The needle design makes use of multiple long sliding wires to steer in 3D without the need of axial rotation of the needle. Steering is achieved by on-demand bending of the needle tip. The needle prototype consists of three pre-curved Nitinol wires, which are fixed at their distal ends. Pulling one or more wires results in tip deflection, which allows steering in three-dimensional space without the need of axial rotation. The Nitinol wires are guided by Nitinol tubes to increase the flexural rigidity for proper needle insertion. The prototype of the needle has a diameter of 0.5 mm along the shaft, which meets our requirement of a maximal diameter. However, by little imperfections in the shrinking tube it can vary slightly from the set 0.5 mm. The performance of the needle prototype was evaluated in terms of steering direction and deflection in porcine gelatine phantoms.

6.2. Interpretation of Results

6.2.1. Steering Direction

The tip consists of three elements configured in a circular way. Therefore, we expect the needle to be rotational symmetrical over a rotation angle of 120° and 240°. We hypothesised that the needle will steer in the same direction as the element retraction. One-element retraction showed good rotational symmetry (difference in median of 125.95°, 130.61°, 130.61°). However, two-element retractions showed less rotational symmetry (i.e. difference in median of 78.15°, 206,87°, and 128,73°). When we look at the standard deviation, the two element retraction shows higher values for the standard deviation (28.79 mm, 17.78 mm, 33.54 mm) than one element retraction (7.05 mm, 12.82 mm, 1.65). These differences in spread and rotational symmetry for two-element retraction can be explained by the fact that both elements need to be retracted with the same amount of retraction to steer in the hypothesised direction. When one element is a bit more retracted than the other, the steering direction will slightly deviate from the intended direction. With the retraction of one element, there is only one variable which can be controlled and therefore, it will steer in the same direction.

6.2.2. Needle Deflection

Increasing the amount of retraction of the elements resulted in a higher deflection of the needle, which is in line with our hypothesis. The median deflection for one element retraction of Level 1 (0.4 mm), Level 2 (0.8 mm) and Level 3 (1.2 mm) were respectively 38.3, 54.12 and 61.68 mm. The median deflection for two element retractions for Level 1, Level 2 and Level 3 were 45.26 mm, 50.27 mm and 55.53 mm.

We hypothesised that one element retraction will lead to a higher deflection than two element retraction with the same level of retraction. However, the results show no consistent difference between the amount of deflection. One element retraction showed higher deflection than two element retraction for level 2 (0.8) mm and level 3 (1.2 mm) retraction, when the elements were actuated with the same level of retraction. However, for level 1 (0.4 mm) element retraction, the double element actuation showed a higher deflection than the single element actuation. Therefore, we can conclude that it does not make a significant difference.

The difference in deflection between Level 1 and level 2 turns out to be bigger than the deflection difference between Level 2 and level 3 deflections (Figure 5.11). This can be explained by the high curvature of the needle shaft with the level 3 retraction (i.e. 1.2 mm). By level 3 element retraction, the needle path was highly curved, which resulted in upward motion of the needle (see Figure 6.1). After reaching point A the deflection still increases but the amount of deflection per insertion length decreases (i.e. the slope of the path).

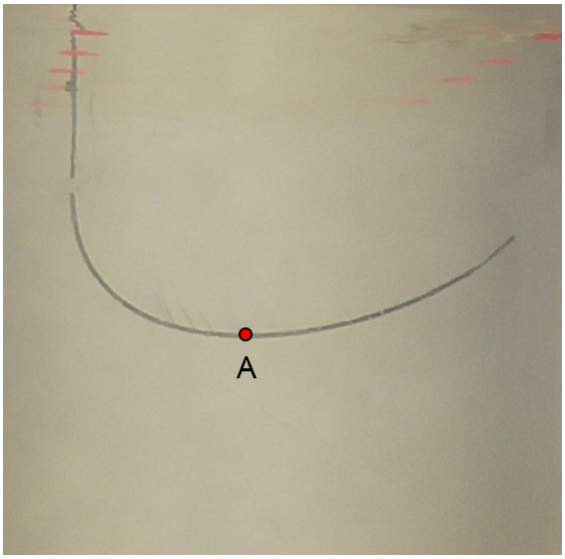

Figure 6.1: Level 3 retraction results in high curvature of the needle, resulting in an upwards needle path when it passes point A

6.3. Contribution and Relevance

In contrast to other steerable needles on dimensions below 1 mm, the proposed needle can steer omnidirectional without the use of axial rotation [18]. The needle does not cause any additional tissue damage as bevel and pre-curved needles do caused by duty cycling. Of needle designs with a dimension smaller than 1 mm, the Nitinol bevel tip needle of Majewicz et al. [33] has similar dimensions (0.58 mm) and shows a small bending radius of 34 mm. Our wish was to reach at least the same radius of curvature. In this thesis we used the deflection of the needle as indication of the curvature of the needle. To be able to compare the radius of curvature of other needles with our design, we took a measurement of maximal median of needle deflection. The deflection had a maximum median of 62,76 mm (EC6), corresponding to an median horizontal (y) value of 18,08 mm, for an insertion of 65 mm of the needle. When defined as a constant arc, the radius would be approximately 33,2 mm. Therefore, we can imply that our proposed needle is the first needle which can steer omnidirectional and has higher curvature than similar 0.5 mm diameter needles. Also it is the first needle which can steer omnidirectional without the use of rotation on such dimensions (diameter < 1 mm).

6.4. Limitations

6.4.1. Experiment

Concentric Tubes

During the experiment the needle was inserted by a motorized linear stage. To prevent buckling of the needle during insertion, two concentric tubes were added around the shaft of the needle to minimise the unsupported length. The concentric tubes slide over each other during needle insertion. In our experiment the smallest tube showed friction with the needle shaft, which eventually could lead to damage of the shrinking tube covering the needle. Therefore, the smallest tube was fixed to the prototype, while the bigger diameter tube could slide. However, the big tubes leaves space for small lateral needle displacement, causing inaccuracies during needle insertion.

Cameras

Two cameras were used to record the needle insertion in two perpendicular planes. However, camera lenses introduce bias in visual information by the perspective. For example, objects further from the camera appear smaller than objects close to the camera. We tried to limit the bias by calculating the scaling factor for images of the side camera based on information from the images of the front camera (so both measurements have the same vertica (y) value in mm). However, we did not take into account the bias of the front camera.

Gelatine Concentration

All experiments were performed in 10 wt% gelatine phantoms. However, biological tissue has different mechanical properties than porcine gelatine. The gelatine phantom is homogeneous, while real tissue shows deviations in stiffness of the tissue because of tissue layers. To say something about the needle steering in tissues with different stiffness, a small experiment was performed. In the small experiment, the needle was inserted with the same element configuration and retraction in containers with 5 wt%, 10 wt% and 15 wt% porcine gelatine. We hypothesised that a higher concentration of gelatine results in more resistance in terms of cutting and friction forces, therefore leading in smaller radius of curvature i.e. higher delfection. For lower concentration of gelatine, we expected less needle deflection. No quantitative measurement was done, but the deflection was only evaluated in a qualitative way by comparing images taken by a camera in front of the phantom.

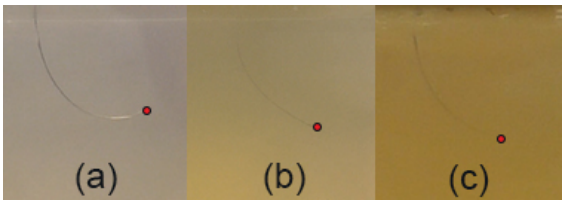

Figure 6.2: Try-out needle insertion with (a) 5 wt% gelatine, (b) 10 wt% gelatine, and (c) 15 wt% gelatine. The red dots show the final needle tip deflection.

The results show that the opposite seems to be true. The needle showed larger deflection in 5 wt% gelatine phantoms than the 10% and 14% gelatine concentrations (Figure 6.2). This result can be explained by the fact that the needle tip presses against the surrounding gelatine. For low gelatine concentrations the tissue deforms more easily than higher gelatine concentrations. Therefore, the needle tip will bend easier in lower concentrations gelatin leading to a higher deflection.

Multiple Curvatures

During the final needle experiment we investigated the performance of the needle by looking at its steering direction and deflection. The experiments were done by inserting the needle with a constant element retraction. Because the element retraction did not change during the experiment, the needle showed only single curved paths and no multiple curved paths. By varying the element configuration during needle insertion, the needle could follow a path with multiple curves. To verify the possibilities of multiple curves for the proposed needle, a few trials were performed where the element configuration was varied during insertion. Results showed that the needle can make multiple curves during insertion (Figure 6.3).

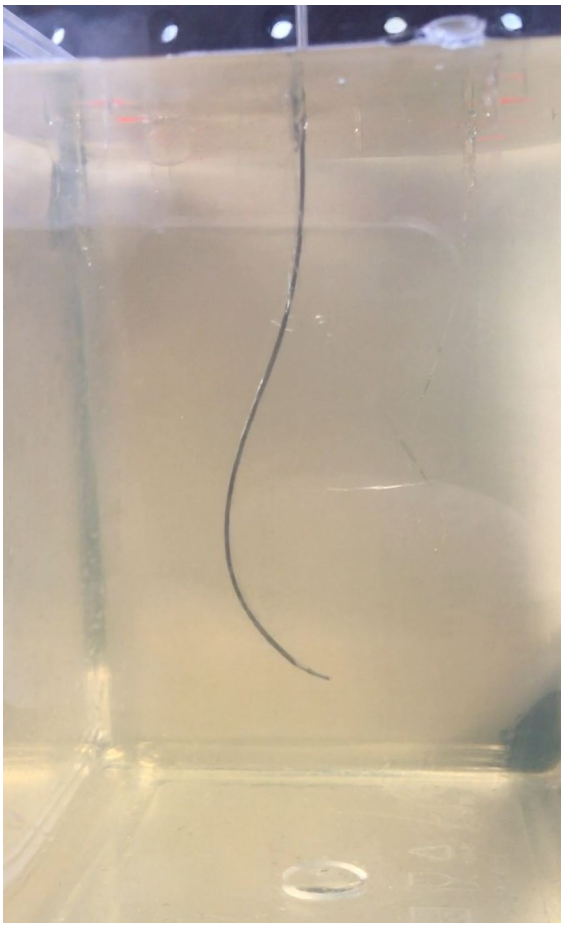

Figure 6.3: Try-out Multiple-curves

6.4.2. Needle Design

Prototype

For the prototype we were limited in material supply. The availability of flexible tubes for covering the three elements was limited. Therefore three Nitinol tubes were added around the elements to get a sufficient flexural rigidity to insert the needle for at least 50 mm. The three Nitinol tubes were covered with a shrinking tube to hold them together. The Nitinol tubes make the steering mechanism itself non-retractable, unless the Nitinol tubes are retracted as well, leaving the very thin shrinking tube behind. The study showed that it was possible to steer with a minimum of three elements. However, replacement of the three nitinol tubes with one single cannula is can be beneficial to leave a more rigid tube behid for insertion of drugs and instruments.

Curvature

In an ideal situation, the needle can be inserted deep inside the tissue and high curvature can be reached without buckling. However, in the proposed needle design there is a trade of between curvature and insertion depth. The prototype makes use of 3 elements, which is the minimum for omnidirectional steering without the use of axial rotation. For the prototype, we added Nitinol tubes around the elements to increase the flexural rigidity to reach higher insertion depths without needle buckling. The steerable tip is able to make needle tip angles over 90 degrees relative to the shaft of the needle (See Chapter 3). However, the shaft of the prototype is too stiff to follow the large needle tip angle, thereby cutting the tissue (Figure 6.5). When the tip angle was further increased, the tip angle was too high, resulting in buckling of the needle tip (Figure 6.4). Hence, the deflection of the needle is not limited by the tip design, but by the flexural rigidity of the shaft of the needle.

6.5. Future Work

6.5.1. Additional Technologies

The proposed needle design allows high steerability of ultra-thin needles without the need of axial rotation. However, needle placement is also dependent of other technologies that help to perform a successful procedure. Technologies for needle visibility is one technology which can increase the success of needle steering. To steer a needle to a target, one should know the position of the needle in real time to be able to correct for its path, if necessary. Imaging guidance can help to steer the needle into the desired direction. However, this study does not look into image guidance possibilities, such as visibility for MRI or CT imaging. Neither, additional technologies to control the needle are taken into account, such as computational modelling and robotic actuation. Therefore, it can be a point for a future work to look into visibility of the needle.

Flexible ultra-thin instruments could be interesting technological development which can increase the success of procedures combined with ultra-thin steerable needles. The proposed needle is able to make highly curved trajectories.

However, this high curvature is not applicable for each procedure, depending following steps after needle placement. When the needle reaches its target, the steering mechanism is retracted out of the cannula, leaving a open lumen behind. Through this lumen instruments can be inserted, and fluids can be injected. However, the instruments (such as grippers and biopsy tools) fed through the cannula should be thin and flexible enough to follow the curved trajectory of the needle cannula. Therefore, investigation in flexible ultra-thin instruments is needed to fully integrate ultra-thin flexible needles in procedures such as ablations and biopsies.

6.5.2. Optimising Tip Design

The tip of the needle prototype consists of a tube which is glued around the distal end of the elements. Experiments were performed to weld the elements together. However, the available laser was to strong resulting in an brittle connection. Welding seems to be a good solution for attachment because no additional material is needed. However, further research has to be done to properly connect the elements at their tip. In our prototype the top of the tip is flat, which results in an increased cutting force compared to conical tip designs. The tip can be optimised to reduce the cutting forces by making the tip conical.

6.5.3. Self Propelling Needle

The limiting factor in further decreasing the diameter and curvature of the needle is its proneness to buckling. Buckling causes lateral slicing of the tissue during tissue penetration as described by Kyle et al. [15]. The buckling problem may be solved by using a mechanism that is able to penetrate without the application

of a net push force. Previous studies show promising designs of needle insertion without net push force [28][9]. However, these designs show no or low steerability. Combining the proposed steering mechanism with an insertion without net push forces allows omnidirectional ultra-thin needle steering with high curvature without needle buckling, and therefore allows deep tissue insertion.

6.6. Application

6.6.1. Needle Steering

The exposed curved elements at the tip induce a local compliance because of the low bending stiffness of the small wires relative to the shaft. Due to the compliance of the needle tip, it cannot penetrate dense tissue layers without buckling. However, active steering is not always necessary during insertion. Therefore, the steering mechanisms does not have to be present all the time during needle insertion. While inserting the needle straight into the tissue, the steering mechanism can be inside the cannula, so the flexural rigidity of the needle tip increases. The increased stiffness of the tip allows the needle to make straight trajectories and decreases the chance of tip buckling. The pre-curved elements needs to be pushed out of the cannula to enable needle steering.

The demanded freedom in steering direction and radius of curvature is dependent on specific medical applications. In some cases, such as in brachytherapy, the needle has only to compensate for the movement of tissues and organs in the environment and the required deflection is relatively small (e.g., between 2 mm and 6 mm) [34]. However, when a target is blocked by sensitive structures such as blood vessels, the demanded needle deflection is much higher (e.g., 30 mm) over a relatively short distance from the insertion point (e.g., 80 mm) [23] [18].

In most cases, the needle insertion is done in such way that the needle travels the least difficult path toward its target. The initial insertion of the needle towards the target can often be travelled by a straight pathway. The proposed needle has a diameter of 0.5 mm, which fits a standard 21 gauge needle (ID=0.514 mm). So for percutaneous procedures, a rigid straight needle can be inserted first, to penetrate the first tissue layers and reach the area as close as possible to the target. After insertion of the rigid needle, the steerable needle can be fed through the cannula of the rigid needle to allow final steering towards the target. In case of mispuncture of a straight rigid needle, the steerable needle can adjust for a small deviation close to the tip of the rigid needle by insertion of the steerable needle through the cannula of the rigid needle.

Because the tip can be reoriented on demand, it allow steering in other mediums such as fluids and open air. Therefore the steering mechanism can also be used for other medical procedures, such as endovascular procedures, eye surgery and lung examinations.

Figure 6.4: Tip buckling with high element retraction

Figure 6.5: Tissue cutting with high element retraction

6.7. Design Proposal: Intuitive Steering

The control unit in this thesis is designed for investigation of the needle performance. Therefore, the proposed needle is not intuitive, nor ergonomic. A new control unit needs to be designed to increase intuitiveness and the ergonomics.

Firstly, to steer intuitively the action needs to be repeatable, which means that the

same action will lead to the same end-result. Secondly, one should understand how to steer it. A joystick would meet the requirement to steer in omnidirectional space in an intuitive way. An design proposal for an intuitive control unit can be seen in Figure 6.6. A swivel mechanism was used to allow element retraction without pulling the opposite elements (Figure 6.7). The top part can swivel to allow element retraction.

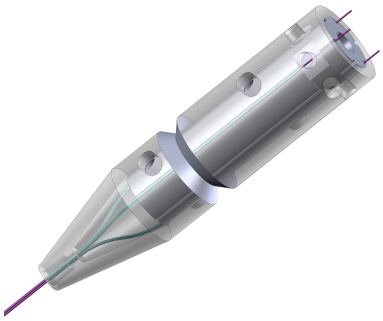

Figure 6.6: Solidworks model of design for intuitive steering.

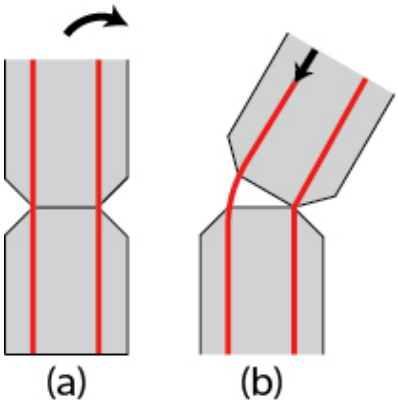

Figure 6.7: Retraction of element by swivel mechanism. The red lines represent the elements. (a) Mechanism in straight configuration. The black arrows indicate the movement of the joystick (b) Swivel mechanism in bend position. The arrow indicates the element movement.

An additional step for future design could be to add a mechanism where the steerable tip is only outside the cannula when steering is needed. A proposal for such a mechanism can be seen in Figure 6.8. By pressing on the sides of the joystick, the element are pushed forward, thereby, sliding the steering mechanism outside the cannula.

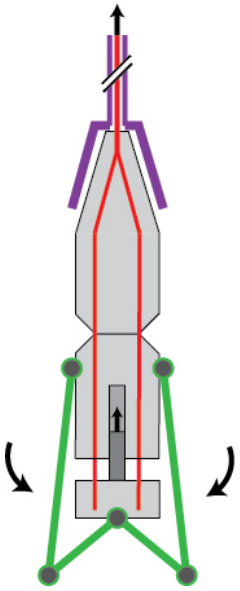

Figure 6.8: Intuitive design. The red lines represent the elements of the steering mechanism. By squeezing the sides of the joystick (green) the elements are pushed forward, leading to the steerable tip to come out of the cannula (purple). The black arrows represent the motion of the flaps, and the elements.

7

Conclusions

In this study, a novel ultra-thin needle design was presented with a diameter of 0.5 mm. The needle consistis of a flexible cannula with a steering mechanism. The steering mechanism consists of three pre-curved Nitinol wires, which are fixed at their distal ends. Pulling one or more wires results in tip deflection, which allows steering in three-dimensional space without the need of axial rotation.

Needle insertion experiments with the prototype were performed in soft tissue phantoms made of porcine gelatine to evaluate the performance of the needle in terms of steering direction and curvature.

The results of the experiments showed that the needle steered into the expected direction by retracting an element, with limited variation (ranging from 7.05 to 33.54 degrees). The needle deflection increased whith higher levels of retraction of the elements. Results show a maximal deflection of 62.76 mm as maximal median for a needle insertion of 65 mm without needle buckling. This value corresponds to a radius of curvature of 33 mm, when the needle path is considered as constant arc.

The proposed needle showed good potential in omnidirectional steering with high curvature and it is able to follow multi-curved trajectories. When looking at ultra-thin (<1mm) needles, the proposed needle is the first needle which can steer omnidirectional without rotation, and shows higher curvature than similar 0.5 mm diameter needles. Future improvements can be done to refine the design and make it user-friendly. Possibly, this will allow our needle to compete with ultra-thin standard bevel-tip and pre-curved needles.

Bibliography

[1] T. Xu, S. M. Hutfless, M. A. Cooper, M. Zhou, A. B. Massie, and M. A. Makary, *Hospital cost implications of increased use of minimally invasive surgery,* JAMA Surgery **150**, 489 (2015).

[2] A. K. Geim and H. A. M. S. ter Tisha, *Detection of earth rotation with a diamagnetically levitating gyroscope,* Physica B: Condensed Matter **294–295**, 736 (2001).

[3] G. Wan, Z. Wei, L. Gardi, D. B. Downey, and A. Fenster, *Brachytherapy needle deflection evaluation and correction,* Medical Physics **32**, 902 (2005).

[4] N. Ehrhart, *Principles of tumor biopsy.* Clinical techniques in small animal practice **13**, 10 (1998).

[5] S. KENNEDY, A. READER, J. NUSSTEIN, M. BECK, and J. WEAVER, *The Significance of Needle Deflection in Success of the Inferior Alveolar Nerve Block in Patients with Irreversible Pulpitis,* Journal of Endodontics **29**, 630 (2003).

[6] R. J. Roesthuis, Y. R. van Veen, A. Jahya, and S. Misra, *Mechanics of needle-tissue interaction,* in *International Conference on Intelligent Robots and Systems, IROS 2011* (IEEE Robotics and Automation Society, 2011) pp. 2557–2563.

[7] V. K. Bui, S. Park, J.-O. Park, and S. Y. Ko, *A novel curvature-controllable steerable needle for percutaneous intervention,* Proceedings of the Institution of Mechanical Engineers, Part H: Journal of Engineering in Medicine **230**, 727 (2016), pMID: 27206444.

[8] N. J. Van De Berg, D. J. Van Gerwen, J. Dankelman, and J. J. Van Den Dobbelsteen, *Design Choices in Needle Steering - A Review,* IEEE/ASME Transactions on Mechatronics **20**, 2172 (2015).

[9] M. Scali, T. P. Pusch, P. Breedveld, and D. Dodou, *Needle-like instruments for steering through solid organs : A review of the scientific and patent literature,* (2016), 10.1177/0954411916672149.

[10] S. P. DiMaio and S. E. Salcudean, *Needle insertion modeling and simulation,* Ieee Transactions on Robotics and Automation **19**, 864 (2003).

[11] N. Abolhassani, R. Patel, and M. Moallem, *Needle insertion into soft tissue: A survey,* Medical Engineering and Physics **29**, 413 (2007), arXiv:arXiv:1011.1669v3 .

[12] S. P. DiMaio and S. E. Salcudean, *Needle steering and motion planning in soft tissues,* IEEE Transactions on Biomedical Engineering **52**, 965 (2005).

[13] L. Barbé, B. Bayle, M. De Mathelin, and A. Gangi, *Needle insertions modelling: Identifiability and limitations,* in *IFAC Proceedings Volumes (IFAC-PapersOnline)*, Vol. 6 (2006) pp. 129–134.

[14] .

[15] K. B. Reed, A. Majewicz, V. Kallem, R. Alterovitz, K. Goldberg, N. J. Cowan, and A. M. Okamura, *Robot-Assisted Needle Steering,* IEEE robotics & automation magazine / IEEE Robotics & Automation Society **18**, 35 (2011).

[16] A. Grant and J. Neuberger, *Guidelines on the use of liver biopsy in clinical practice,* Gut **45**, iv1 (1999).

[17] D. Glozman and M. Shoham, *Flexible needle steering for percutaneous therapies,* Computer Aided Surgery **11**, 194 (2006).

[18] M. Scali, D. Kreeft, P. Breedveld, and D. Dodou, *Design and evaluation of a wasp-inspired steerable needle,* (2017).

[19] K. B. Reed, A. M. Okamura, and N. J. Cowan, *Modeling and control of needles with torsional friction,* IEEE Transactions on Biomedical Engineering **56**, 2905 (2009).

[20] R. J. Roesthuis, N. J. van de Berg, J. J. van den Dobbelsteen, and S. Misra, *Modeling and steering of a novel actuated-tip needle through a soft-tissue*

simulant using fiber bragg grating sensors, 2015 IEEE International Conference on Robotics and Automation (ICRA), , 2283 (2015).

[21] S. Y. Ko, L. Frasson, and F. Rodriguez Y Baena, *Closed-loop planar motion control of a steerable probe with a programmable bevel inspired by nature,* IEEE Transactions on Robotics **27**, 970 (2011).

[22] S. C. Ryu, Z. F. Quek, J. S. Koh, P. Renaud, R. J. Black, B. Moslehi, B. L. Daniel, K. J. Cho, and M. R. Cutkosky, *Design of an optically controlled MR-compatible active needle,* IEEE Transactions on Robotics **31**, 1 (2015).

[23] T. K. Adebar, J. D. Greer, P. F. Laeseke, G. L. Hwang, and A. M. Okamura, *Methods for Improving the Curvature of Steerable Needles in Biological Tissue,* IEEE Transactions on Biomedical Engineering **63**, 1167 (2016).

[24] P. J. Swaney, J. Burgner, H. B. Gilbert, and R. J. Webster, *A flexure-based steerable needle: High curvature with reduced tissue damage,* IEEE Transactions on Biomedical Engineering **60**, 906 (2013), arXiv:NIHMS150003 .

[25] L. L. Howell, *Introduction to Compliant Mechanisms,* in *Handbook of Compliant Mechanisms* (2013) pp. 1–13.

[26] A. Majewicz, S. Marra, M. van Vledder, M. Lin, M. Choti, D. Song, and A. Okamura, *Behavior of tip-steerable needles in ex vivo and in vivo tissue,* I E E E Transactions on Biomedical Engineering **59**, 2705 (2012).

[27] J. Vincent and M. King, *The mechanism of drilling by wood wasp ovipositors,* Biomimetics (USA) (1995).

[28] T. Sprang, P. Breedveld, and D. Dodou, *Wasp-inspired needle insertion with low net push force,* in *Biomimetic and Biohybrid Systems: 5th International Conference, Living Machines 2016, Edinburgh, UK, July 19-22, 2016. Proceedings*, edited by N. F. Lepora, A. Mura, M. Mangan, P. F. Verschure, M. Desmulliez, and T. J. Prescott (Springer International Publishing, Cham, 2016) pp. 307–318.

[29] N. J. van de Berg, J. Dankelman, and J. J. van den Dobbelsteen, *Design of an actively controlled steerable needle with tendon actuation and fbg-based shape sensing,* Medical Engineering & Physics **37**, 617 (2015).

[30] T. Push, *From the Wasp Ovipositor to a 3D Steerable Needle for Solid-Tissue Interventions*, master thesis, Technical University Delft (2017).

[31] T. Duerig, a. Pelton, and D. Stöckel, *An overview of nitinol medical applications,* Materials Science and Engineering: A **273-275**, 149 (1999).

[32] I. Corporation, *Soldering to Nitinol kernel description,* (2017).

[33] A. Majewicz, T. R. Wedlick, K. B. Reed, and A. M. Okamura, *Evaluation of robotic needle steering in ex vivo tissue,* in *Proceedings - IEEE International Conference on Robotics and Automation* (2010) pp. 2068–2073, arXiv:NIHMS150003 .

[34] N. N. Stone, J. Roy, S. Hong, Y. C. Lo, and R. G. Stock, *Prostate gland motion and deformation caused by needle placement during brachytherapy,* Brachytherapy **1**, 154 (2002).

[35] H. B. Gilbert and R. J. Webster, *Rapid, Reliable Shape Setting of Superelastic Nitinol for Prototyping Robots,* IEEE Robotics and Automation Letters **1**, 98 (2016).

A

Shape Setting Nitinol

Shape setting of Nitinol wires is a complex process. Nitinol needs high temperatures (500 degrees) to set them in a desired shape. For pre-curving the elements of the steering mechanism, we tried shape setting by means of Joule heating, and by heating it by a rework station.

A.1. Joule Heating

Gilbert et al. [35] proposed an electrical technique that uses Joule heating to obtain the high shape setting temperatures. This high power heating prevents unintended ageing of the material and provides a consistent and accurate results for the rapid creation of prototypes [35].

The temperature of the Nitinol sample can be determined by the measurement of the resistance, which is available during heating if the applied voltage and current are measured.

To reach a high temperature without burning the wire, the fixture should have a low thermal conductivity to minimize heat loss. In addition, the fixture must not interfere with the electrical path, which means that an insulator is needed. Options of insulating materials with low conductivity are for example ceramics and wood. We decided to make the fixure out of MDF plates because MDF has a low thermal conductivity of about 0.25 W/M0K, and is easy to engrave with the use of a laser cutter. Figure A.1 shows the fixtures made of MDF.

Figure A.2 shows the electric circuit used for heating up the wires.

By heating up the elements to a temperature of 500 degrees for a very short time (2 seconds), the wires were pre-curved. However, by the high temperature the nitinol elements tend to degrade in performance. Also small residues of the MDF were stuck to the nitinol elements, which created friction when sliding the elements through tubes.

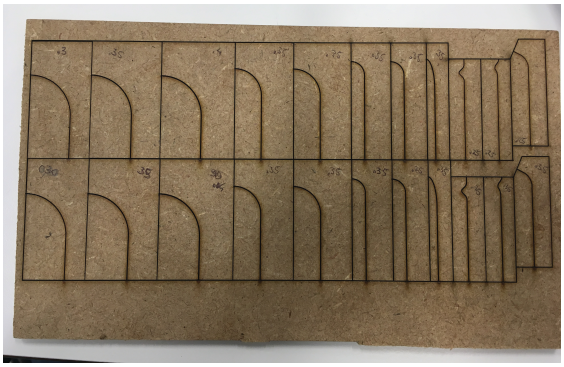

Figure A.1: MDF fixure for curving Nitinol elements with Joule heating.

A.2. Heating by rework station

A rework station (Tenma SMD rework station 220V) was used to heat up the elements. The maximum temperature the rework station could reach was 480 degrees Celsius. It turned out that this temperature was enough to set the shape in the nitinol wires. The rework station with the clamped wires are shown in Figure A.3.

The shape setting of the pre-curvature at the tip was created by carefully heating the elements to a temperature of 480 degrees Celsius by the rework station, while curved around a cilindrical objects.

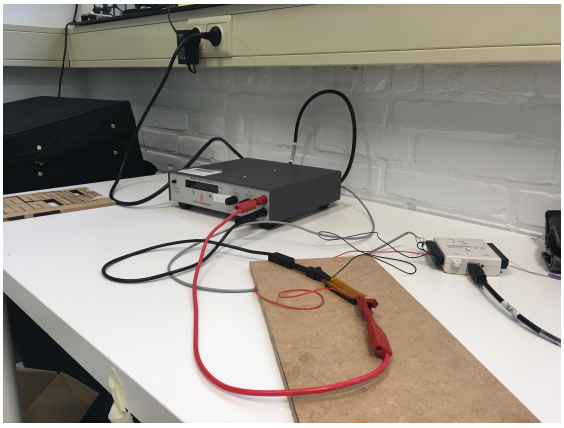

Figure A.2: Setup for Joule heating.

Figure A.3: Setup for heating with a rework station.

B

Calibration Load Cell

Table B.1: My caption

Grams	Newton	Test 1		Test 2		Test 3		average Delta	average Factor
		Volt	Delta	Volt	Delta	Volt	Delta		factor
0	0	.46	0.16	.46	0.16	.46	0.16	0.16	3.065625
50	0.4905	.62	0.59	.62	0.58	.62	0.58	0.583333	0.840857
100	0.981	1.21	0.57	1.20	0.58	1.20	0.58	0.576667	0.850578
150	1.4715	1.78	0.59	1.78	0.58	1.78	0.59	0.586667	0.83608
200	1.962	2.37	0.56	2.36	0.59	2.37	0.56	0.57	0.860526
250	2.4525	2.93	0.57	2.95	0.55	2.93	0.57	0.563333	0.87071
300	2.943	3.50		3.50		3.50			
								Total average 0.576	Total average 0.85175

This appendix shows the calibration of the force sensor. To calibrate the force sensor 50 g weights were added to the force sensor up to a weight of 300 g. After adding weight the voltage of the force sensor was measured. Delta is the difference in Volt between the previous measurement. The test was performed three times. Then the average difference (delta) in volt per 50 g was calculated.

The average factor was calculated by dividing the difference in Newtons by the volt difference.

The final average factor used in matlab was determined by averaging over all measurements, with exclusion of the first one.

C

Experiments: Run Tables

Table C.1 shows the order in which the tip experiments were performed for the experimental selection of the needle tip design.

Table C.2 and C.3 show the runtables of the experiments for the final evaluation of the prototype. Table C.2 shows the order in which the experiments for the steering direction were performed, and Table C.3 shows the order in which the experiments for the needle deflection were performed.

Table C.1: Run table for experimental selection of tip shapes

Run	Tip type	Type of experiment
1	0	Continuous
2	0	Continuous
3	0	Continuous
4	0	Continuous
5	0	Continuous
6	0	Steps
7	0	Steps
8	0	Steps
9	1	Continuous
10	1	Continuous
11	1	Continuous
12	1	Continuous
13	1	Continuous
14	1	Steps
15	1	Steps
16	1	Steps
17	2	Continuous
18	2	Continuous
19	2	Continuous
20	2	Continuous
21	2	Continuous
22	2	Steps
23	2	Steps
24	2	Steps
25	3	Continuous
26	3	Continuous
27	3	Continuous
28	3	Continuous
29	3	Continuous
30	3	Steps
31	3	Steps
32	3	Steps

Table C.2: Run table for steering direction experiment

Run	Cond.	EL1	EL2	EL3	Hyp.
1	3	0	2	0	120°
2	6	2	0	2	300°
3	2	2	2	0	60°
4	3	0	2	0	120°
5	4	0	2	2	180°
6	6	2	0	2	300°
7	1	2	0	0	0°
8	3	0	2	0	120°
9	4	0	2	2	180°
10	5	0	0	2	240°
11	5	0	0	2	240°
12	4	0	2	2	180°
13	4	0	2	2	180°
14	2	2	2	0	60°
15	1	2	0	0	0°
16	2	2	2	0	60°
17	5	0	0	2	240°
18	1	2	0	0	0°
19	2	2	2	0	60°
20	1	2	0	0	0°
21	4	0	2	2	180°
22	5	0	0	2	240°
23	3	0	2	0	120°
24	6	2	0	2	300°
25	6	2	0	2	300°
26	1	2	0	0	0°
27	2	2	2	0	60°
28	5	0	0	2	240°
29	3	0	2	0	120°
30	6	2	0	2	300°

Table C.3: Run Table: Deflection

Run No	Cond.	EL1	EL2	EL3	Gel.
1	5	2	2	0	1
2	4	1	1	0	2
3	4	1	1	0	3
4	7	2	1	0	4
5	8	3	1	0	5
6	6	3	3	0	6
7	3	3	0	0	7
8	7	2	1	0	8
9	2	2	0	0	9
10	3	3	0	0	1
11	9	3	2	0	2
12	6	3	3	0	3
13	7	2	1	0	4
14	2	2	0	0	5
15	6	3	3	0	6
16	1	1	0	0	7
17	8	3	1	0	8
18	5	2	2	0	9
19	5	2	2	0	1
20	8	3	1	0	2
21	5	2	2	0	3
22	2	2	0	0	4
23	3	3	0	0	5
24	7	2	1	0	6
25	1	1	0	0	7
26	4	1	1	0	8
27	9	3	2	0	9
28	8	3	1	0	1
29	7	2	1	0	2
30	1	1	0	0	3
31	8	3	1	0	4
32	6	3	3	0	5
33	1	1	0	0	6
34	9	3	2	0	7
35	5	2	2	0	8
36	2	2	0	0	9
37	4	1	1	0	1
38	9	3	2	0	2
39	6	3	3	0	3
40	3	3	0	0	4
41	4	1	1	0	5
42	9	3	2	0	6
43	2	2	0	0	7
44	1	1	0	0	8
45	3	3	0	0	9

D

Results Tip Experiment: Angles Stepwise retraction

This appendix shows the box plots of the angle per step for the zero-curved, one-curved, two-curved and three-curved tip design.

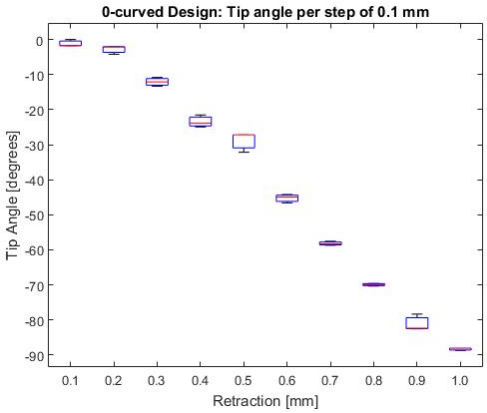

Figure D.1: Box plot of the angle for a step-wise retraction of 1 mm with steps of 0.1 mm for the zero-curved tip design

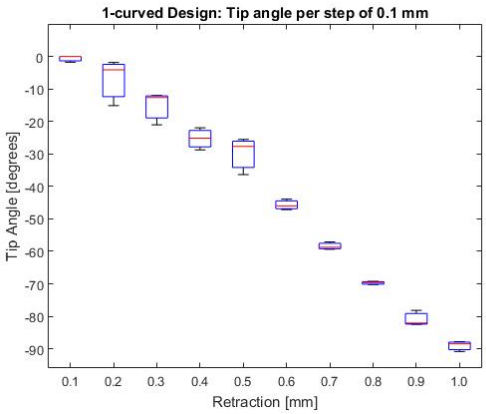

Figure D.2: Box plot of the angle for a step-wise retraction of 1 mm with steps of 0.1 mm for the one-curved tip design

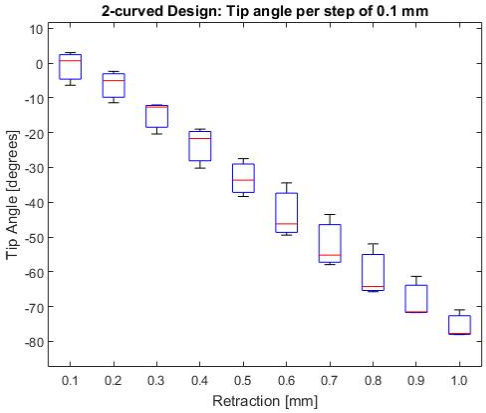

Figure D.3: Box plot of the angle for a step-wise retraction of 1 mm with steps of 0.1 mm for the two-curved tip design

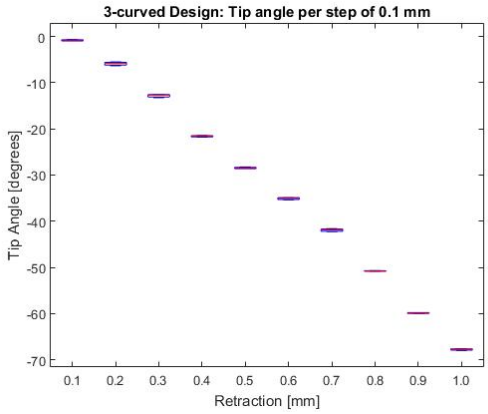

Figure D.4: Box plot of the angle for a step-wise retraction of 1 mm with steps of 0.1 mm for the three-curved tip design

E

Engineering Drawings

This appendix contains the engineering drawings for the control unit. Standard tubes were not included. All drawings were made by Solidworks.

Table E.1: Bill of Materials

Item No.	Name	production method	Material	QTI
1	Shrinking Tube	off-the-shelf	Polyester	1
2	Protection Cap	digital light processing	Acrylate, R05 red	1
3	Screw M3x10	off-the-shelf	steel	3
4	Cable Guidance Cap	digital light processing	Acrylate, R05 red	1
5	Bowden Cable	off-the-shelf	Nitinol	3 or 6
6	Disc	lasercutting	Stainless Steel plate	1
7	Element	off-the-shelf + heating	Nitinol	6
8	Screw M2x5	off-the-shelf	Stainless Steel	3
9	Body	laser metal fusion	Stainless Steel 316L	1
10	Tube	off-the-shelf + cutting	Stainless Steel	3 or 6
11	Attachment Block	laser metal fusion	Stainless Steel 316L	6
12	Screw M2x20	off-the-shelf	Stainless Steel	6
13	Wheel	digital light processing	Acrylate, R05 red	6
14	Ring	off-the-shelf + cutting	Stainless Steel 316L	3
15	Body Backpart	laser metal fusion	Stainless Steel 316L	1
16	Screw M2x10	off-the-shelf	Stainless Steel	3

9

Mat.: AISI Type 316L stainless steel
Aantal: 1

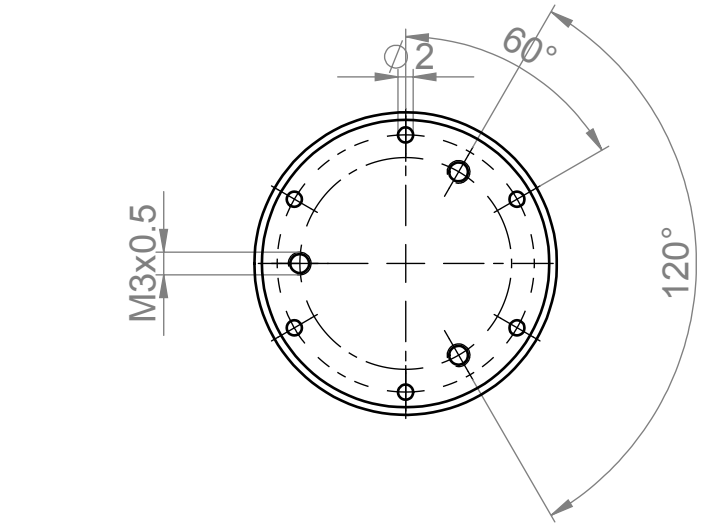

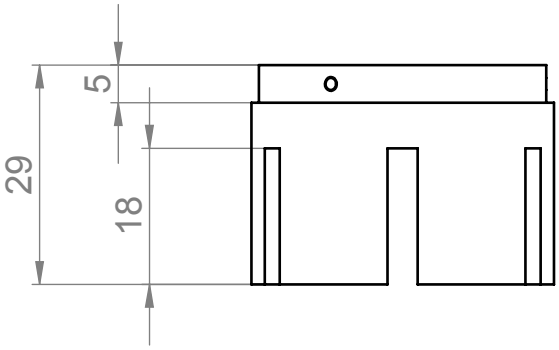

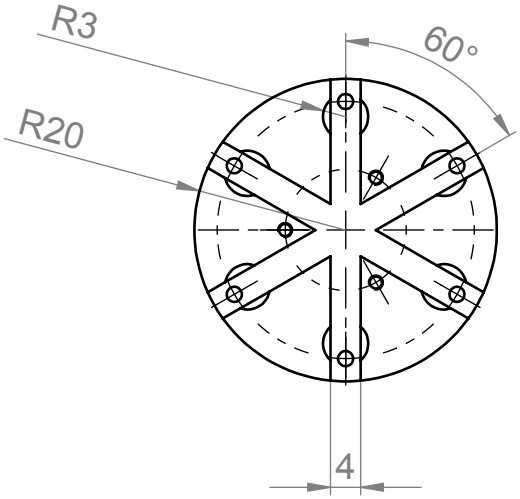

benaming Body				maateenheid mm	
				formaat A4	tekeningnummer 2
SolidWorks Student Edition. For Academic Use Only.	schaal 1:1	datum 26-7-2017	gewicht 221 gram		
TU Delft Industrial Design Engineering	getekend Paulien Veldhoven 4130669				groep -

15

Mat.: AISI Type 316L stainless steel
Aantal: 1

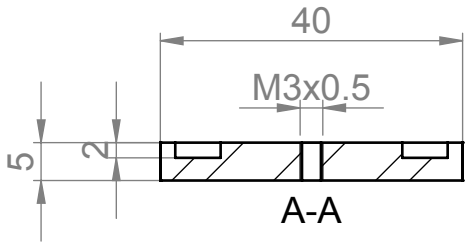

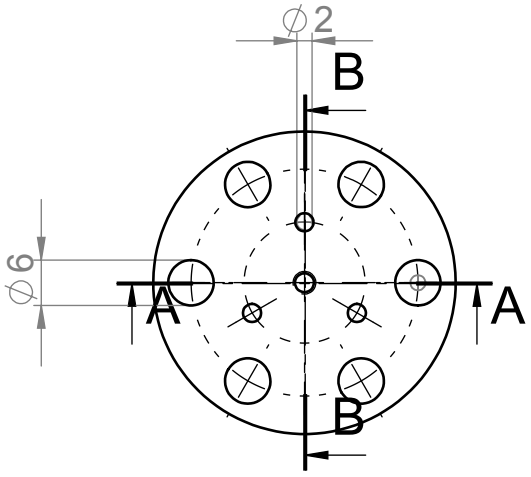

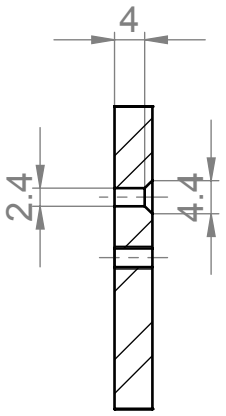

benaming BodyBackPart					maateenheid mm
				formaat A4	tekeningnummer 3
SolidWorks Student Edition. For Academic Use Only.	schaal 1:1	datum 26-7-2017	gewicht 47 gram		
TU Delft Industrial Design Engineering	getekend Paulien Veldhoven 4130669				groep -

2

Mat.: Kunststof: R05 red
Aantal: 1

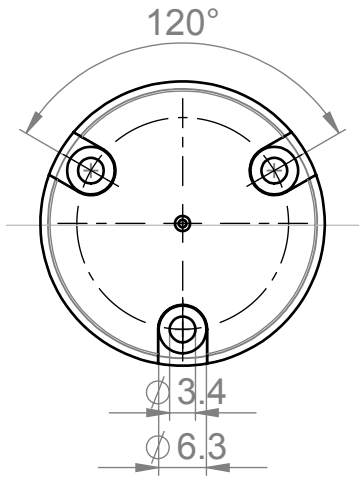

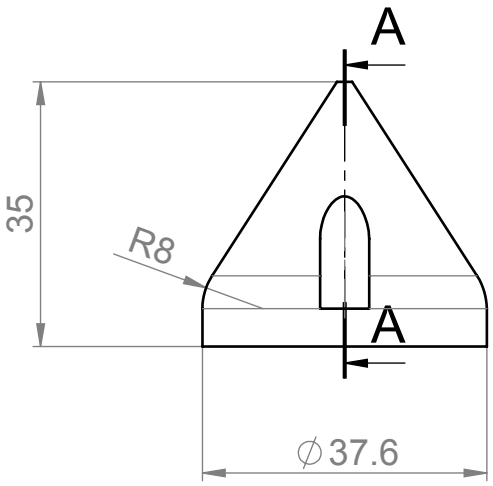

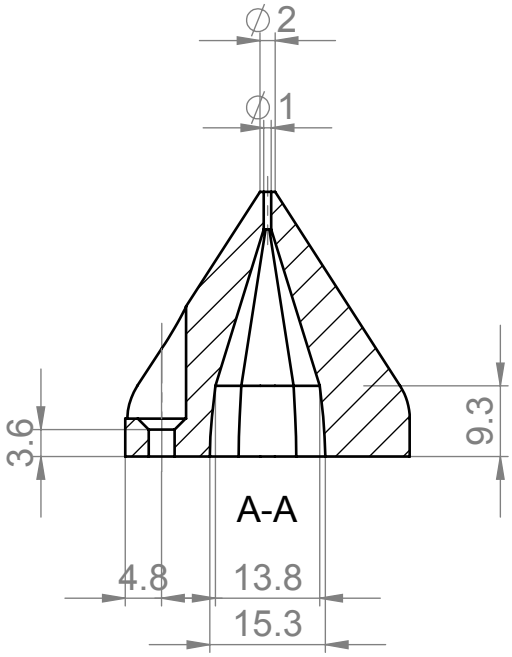

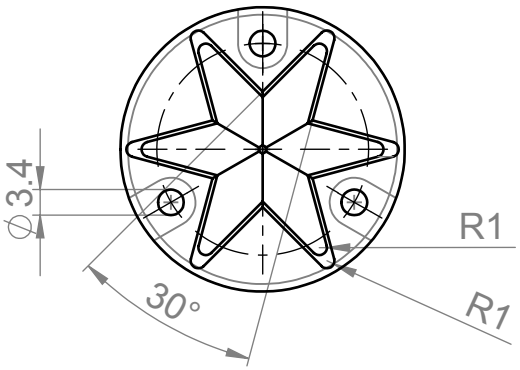

benaming CableGuidenceCap					maateenheid mm
				formaat A4	tekeningnummer 1
SolidWorks Student Edition. For Academic Use Only.	schaal 11	datum 26-7-2017	gewicht 11 gram		
TU Delft Industrial Design Engineering	getekend Paulien Veldhoven 4130669				groep -

6

Mat.: AISI 316 Stainless Steel Sheet (SS
Aantal: 1

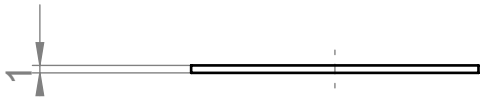

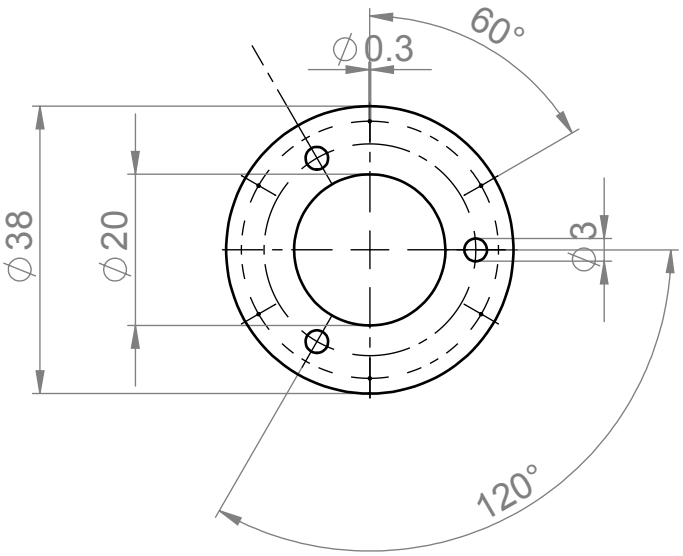

benaming Disc					maateenheid mm
				formaat A4	tekeningnummer 5
schaal 1:1	datum 26-7-2017	gewicht 6 gram			
getekend Paulien Veldhoven 4130669					groep -

TU Delft
Industrial Design Engineering

2

Mat.: Acrylic (Medium-high impact)
Aantal: 1

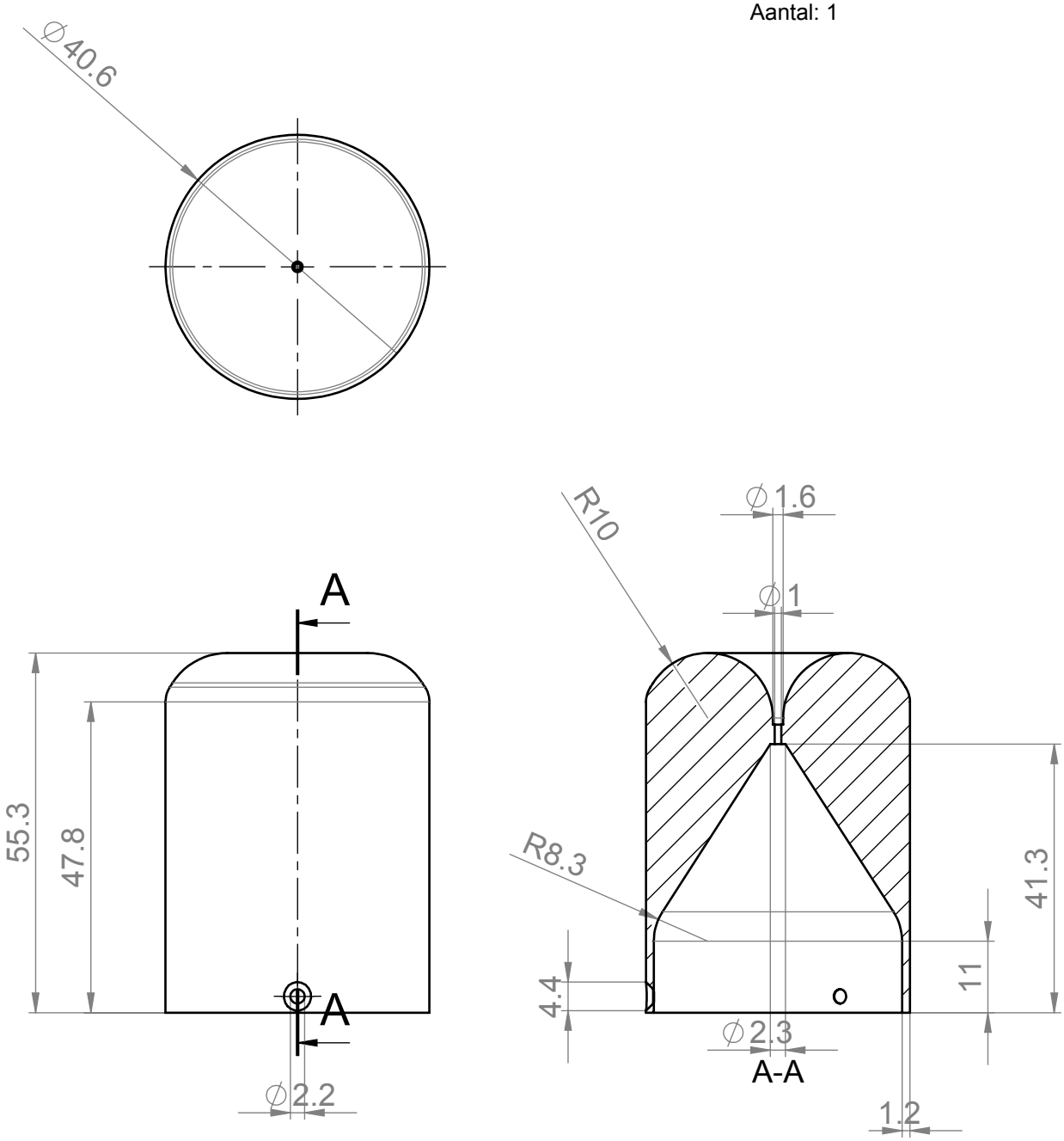

benaming ProtectionCap			maateenheid mm
		formaat A4	tekeningnummer 4
schaal 1:1	datum 26-7-2017	gewicht 51 gram	
getekend Paulien Veldhoven 4130669			groep -

TU Delft
Industrial Design Engineering

12

Mat.: AISI Type 316L stainless steel
Aantal: 6

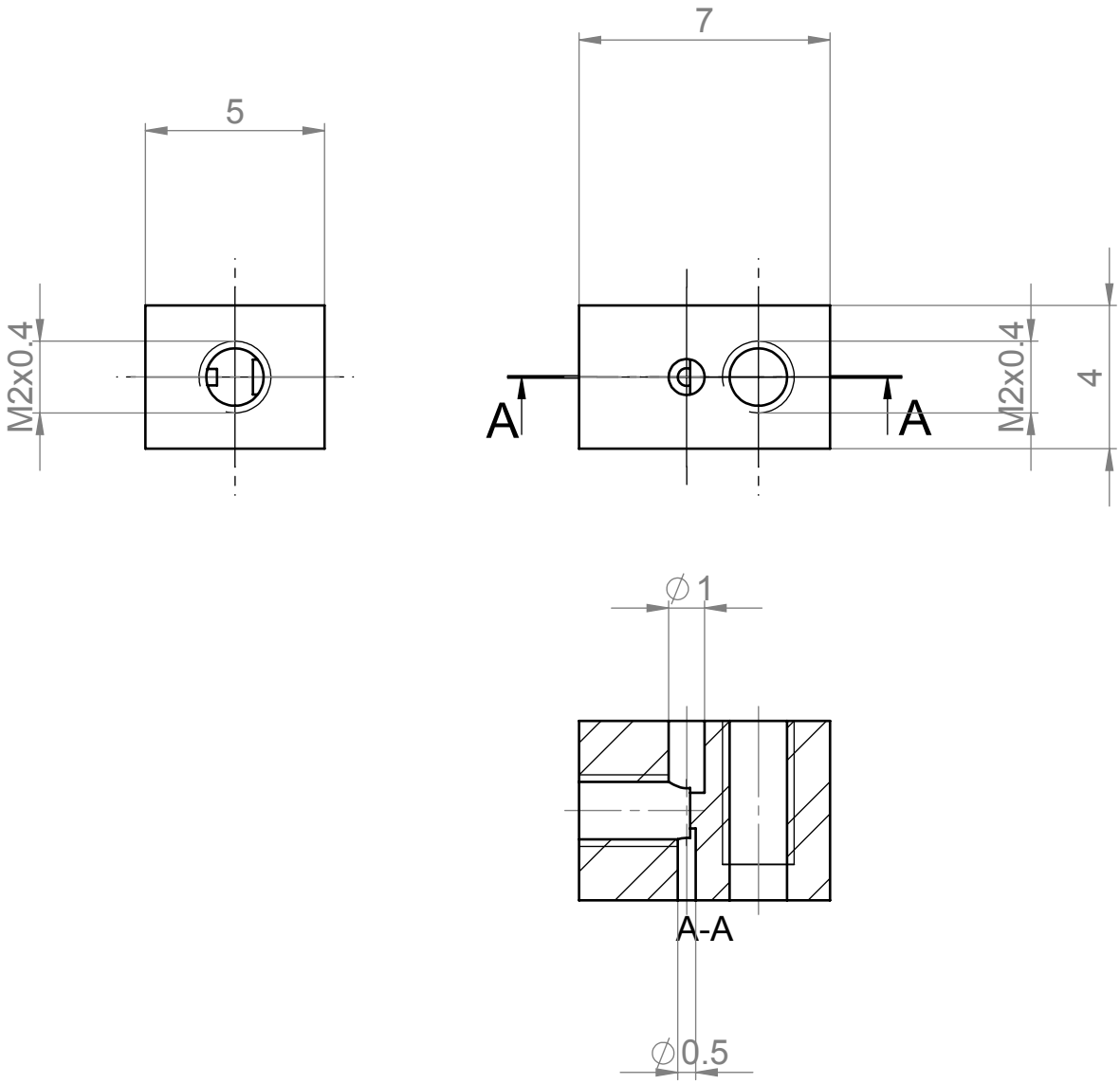

benaming	Attachment Block			maateenheid	mm
				formaat	tekeningnummer
SolidWorks Student Edition. For Academic Use Only.	schaal 5:1	datum 16-11-2017	gewicht 1 gram	A4	12
TU Delft Industrial Design Engineering	getekend Paulien Veldhoven 4130669			groep	-

14

Mat.: Acrylic (Medium-high impact)
Aantal: 6

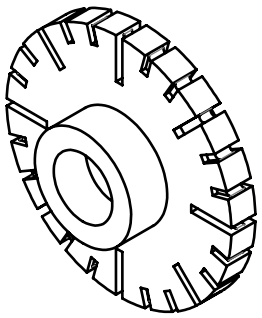

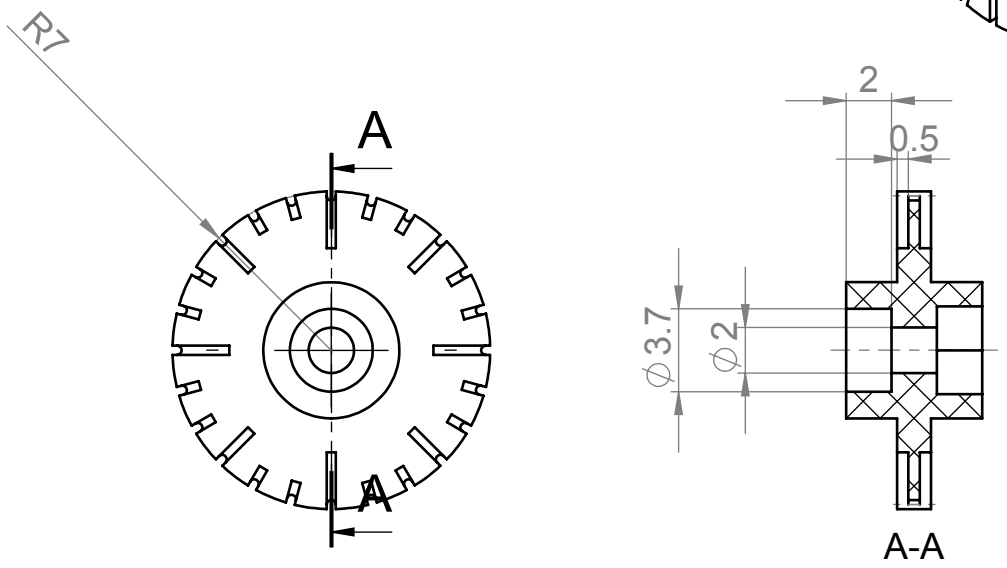

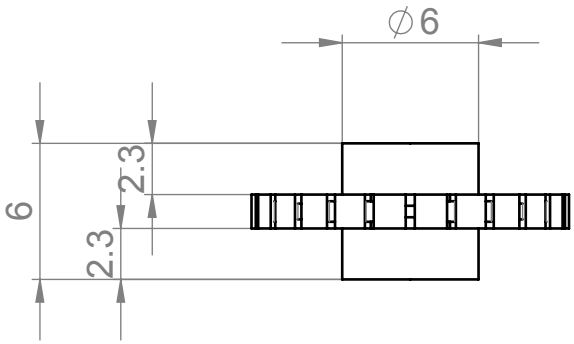

benaming Wheel					maateenheid mm
				formaat A4	tekeningnummer 1
SolidWorks Student Edition. For Academic Use Only.	schaal 3:1	datum 17-11-2017	gewicht 0 gram		
TU Delft Industrial Design Engineering	getekend Paulien Veldhoven				groep

10

Mat.: AISI 316 Stainless Steel Sheet (SS
Aantal: 1

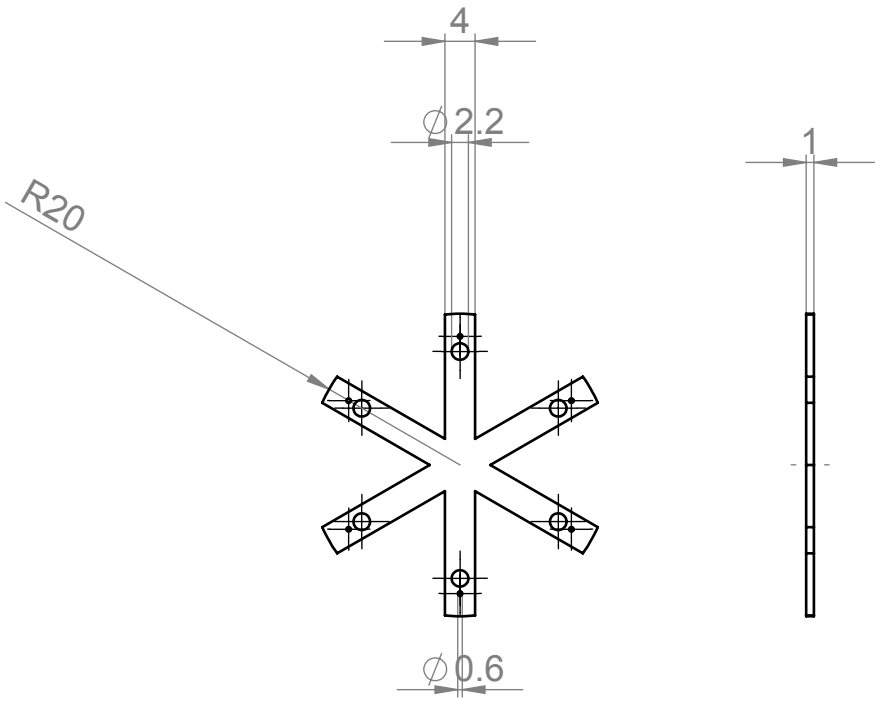

benaming Star				maateenheid mm
			formaat A4	tekeningnummer 1
TU Delft Industrial Design Engineering	schaal 1:1	datum 17-11-2017	gewicht 3 gram	
	getekend Paulien Veldhoven 4130669			groep

```
clear; close all; clc

% Processing load cell data files
%
% Author: P Veldhoven
% Created: 2017 May


% Select files to analyze
[filenames,dirname] = uigetfile('*.dat','Select data files (hold down shift or
ctrl)','multiselect','on');
if ~iscell(filenames)
    filenames = {filenames}; % Ensure that "filenames" is a cell array (if
there is only one file)
end
filenames = sort(filenames); % Ensure filenames are sorted in alphabetical
order


%% Analysis loop: Reading out Forces and time from data
pqn = length(filenames); % Total number of runs

VoltAll = [];
MaxForce= [];
Forci=[];
for file_id = 1:pqn

    % Construct current file path
    filename = filenames{file_id}; % Name of i-th file
    filepath = fullfile(dirname,filename); % Construct path to file

   tempstruct=readtable(filename,'delimiter', '\t', 'Headerlines',6); %read
file starting from line 6
   varnames = fieldnames(tempstruct);

   % Assign the first field of tempstruct to the variable "Time"
   run_dataTime = tempstruct.(varnames{1});
   DataTime =  strrep(run_dataTime, ',', '.');
   Time=cellfun(@str2num,DataTime); %create numbers instead of strings

   % Assign the second field of tempstruct to the variable "Volt"run_dataVolt
= tempstruct.(varnames{2});
   DataVolt =  strrep(run_dataVolt, ',', '.');
   Volt=cellfun(@str2num,DataVolt); %create numbers instead of strings

    %callibration from Volt to Newton
    ForceZ = 0.85 * (Volt-.62)+0.5 -0.395;%5; %NEED TO CHECK per experiment!

    %safe Time and Force in cell array
    Times{file_id} = Time;
    Forces{file_id}=ForceZ;

    [M,I]= max(ForceZ);  % maximum force without filter
    [Mf,If]= max(maf(ForceZ,10));    %maximum force with moving average filter
```

```
    %Max= [M;Mf]; voor beide met en zonder maf-filter
    Max= [Mf];
    MaxForce = [MaxForce Max];

    TimeMax = Time(I);
    TimeMaxf = Time(If);

 %Plot of force measurement
figure
    ks = 10; % Moving average filter kernel size [-]
    grey = [0.4 , 0.4 , 0.4] ;
        hl(1) = line(Time,ForceZ,'color', 0.6*ones(1,3)); %
        hl(2) = line(Time,maf(ForceZ,ks),'color','r');
        ylabel('force [N]')

        hold on
        plot(TimeMax,M,'o','color','b');
        plot(TimeMaxf,Mf,'o','color','r');
        ylabel('force[N]')
        hold off

    xlabel('time [s]')
    grid on
    box on
    title(filename,'interpreter','none')
    legend(hl,{'raw',sprintf('moving avg. filtered (kernel size = %u)',ks)})
    disp('Waiting... Hit any key to continue.')
    pause % Pause until keystroke ...
    close % ... then close the figure
    clc
end

%% Allignment of data to compensate for lag of measurements
[F1,F2,D2] = alignsignals(Forces{1},Forces{2},[]);
[F1,F3,D3] = alignsignals(F1,Forces{3},[]);
[F1,F4,D4] = alignsignals(F1,Forces{4},[]);
[F1,F5,D5] = alignsignals(F1,Forces{5},[]);

%assign new time vector per dataset
T1= (1:(length(F1)))/500;
T2= (1:(length(F2)))/500;
T3= (1:(length(F3)))/500;
T4= (1:(length(F4)))/500;
T5= (1:(length(F5)))/500;

%% Calculate Mean values and make all vectors same length
M = {F1,F2,F3,F4,F5}; %create one cell array of all force vectors
m=max(cellfun(@length,M)); %maximal length of individual cells
n=length(M); %length of cell array M (amount of columns)
V=zeros(m,n); %creates a matrix with zeros in the maximal sizes of length and
width
mask=zeros(m,n);

%create matrix where length of each array is the same
```

```
for i=1:length(M)
    vi=M{i}; %length of seperate cell array
    V(1:length(vi),i)=vi; %enter values in new array
    mask(1:length(vi),i)=ones(size(vi)); % create ones in array where values
are present
end

MeanV = sum(V.*mask,2)./sum(mask,2); %calculate average of all Force vectors
over time


   %% Opslaan van variablen per conditie
   % (variabele naam varieert per conditie: c1=1 curve, c2=two curves,
c3=three curves)
    T1c1=T1;
    T2c1=T2;
    T3c1=T3;
    T4c1=T4;
    T5c1=T5;

    F1c1= F1;
    F2c1=F2;
    F3c1=F3;
    F4c1=F4;
    F5c1=F5;

    MeanVc1=MeanV;
     TVc1=T3;
%%    Plot all forces including mean

ks=20; %kernel size for moving average filter

figure
    hl(1) = line(T1c0,maf(F1c0,ks),'LineStyle', ':', 'color', 'm'); % 0 curves
    hl(2) = line(T2c0,maf(F2c0,ks),'LineStyle', ':','color','m');
    hl(3) = line(T3c0,maf(F3c0,ks),'LineStyle', ':','color','m');
    hl(4) = line(T4c0,maf(F4c0,ks),'LineStyle', ':','color','m');
    hl(5) = line(T5c0,maf(F5c0,ks),'LineStyle', ':','color','m');
    hl(6) = line(TVc0,maf(MeanVc0,ks),'LineWidth',1.5,'color','m');

    hl(7) = line(T1c1(1:8000),maf(F1c1(1001:9000),ks),'LineStyle',
':','color', 'b'); % 1 curve
    hl(8) = line(T2c1(1:8000),maf(F2c1(1001:9000),ks),'LineStyle',
':','color','b');
    hl(9) = line(T3c1(1:8000),maf(F3c1(1001:9000),ks),'LineStyle',
':','color','b');
    hl(10) = line(T4c1(1:8000),maf(F4c1(1001:9000),ks),'LineStyle',
':','color','b');
    hl(11) = line(T5c1(1:8000),maf(F5c1(1001:9000),ks),'LineStyle',
':','color','b');
    hl(12) =
line(TVc1(1:8000),maf(MeanVc1(1001:9000),ks),'LineWidth',1.5,'color','b');

    hl(13) = line(T1c2(1:8450),maf(F1c2(551:9000),ks),'LineStyle',
':','color', 'c'); % 2 curves
```

```
    hl(14) = line(T2c2(1:8450),maf(F2c2(551:9000),ks),'LineStyle',
':','color','c');
    hl(15) = line(T3c2(1:8450),maf(F3c2(551:9000),ks),'LineStyle',
':','color','c');
    hl(16) = line(T4c2(1:8450),maf(F4c2(551:9000),ks),'LineStyle',
':','color','c');
    hl(17) = line(T5c2(1:8450),maf(F5c2(551:9000),ks),'LineStyle',
':','color','c');
    hl(18) =
line(TVc2(1:8450),maf(MeanVc2(551:9000),ks),'LineWidth',1.5,'color','c');

    hl(19) = line(T1c3(1:8050),maf(F1c3(951:9000),ks),'LineStyle',
':','color', 'g'); % 3 curves
    hl(20) = line(T2c3(1:8050),maf(F2c3(951:9000),ks),'LineStyle',
':','color','g');
    hl(21) = line(T3c3(1:8050),maf(F3c3(951:9000),ks),'LineStyle',
':','color','g');
    hl(22) = line(T4c3(1:8050),maf(F4c3(951:9000),ks),'LineStyle',
':','color','g');
    hl(23) = line(T5c3(1:8050),maf(F5c3(951:9000),ks),'LineStyle',
':','color','g');
    hl(24) =
line(TVc3(1:8050),maf(MeanVc3(951:9000),ks),'LineWidth',1.5,'color','g');
        ylabel('force [N]')
   legend([ hl(6)  hl(1) hl(12)  hl(7) hl(18)  hl(13) hl(24)  hl(19)],'Mean 0-
curved','0-curved', 'Mean 1-curved','1-curved','Mean 2-curved','2-
curved','Mean 3-curved','3-curved')
    xlim([0 16])
    xlabel('time [s]')
    grid on
    box on


%% Plot of Maximal Retraction Forces Per Needle Tip Design
MaxForces=[MaxForce0' MaxForce1' MaxForce2' MaxForce3']
labels = {'0 curves','1 curve','2 curves','3 curves'};

% Open figure and change some properties
figure('color','white','name','Maximal Forces per measurement')
% Plot observations as black circles
figure
line(1:4,MaxForces,'linestyle','none','marker','o','color','r')

% Title
 title('Maximal Forces of Data')

% Adjust the axes
set(gca,'xlim',[0 6],'xtick',1:4,'xticklabel',labels,'box','on')
axis([0 5 0 3])
ylabel('Maximal Force [N]')


%% Boxplot of Maximal Retraction Forces Per Needle Tip Design
figure
boxplot(MaxForces, labels)
```

```
xlabel('Needle Tip Design')
ylabel('Maximal Retraction Force (N)')
```

Reading out and processing data of forces

```
%DETERMINE ANGLE OF THE TIP

%This file reads out .avi movie files, crops each frame to a set
 region of
%interest, and processes the ROI, to finally show the angle the needle
%makes relative to the shaft in a plot.

clc;    % Clear the command window.
close all;  % Close all figures (except those of imtool.)
imtool close all;  % Close all imtool figures.
clear;  % Erase all existing variables.
workspace;  % Make sure the workspace panel is showing.
fontSize = 22;

% Open the 'filename'.avi  movie.
% First get the folder that it is stored in.
folder = fileparts(which('Dat8Vid9Steps.avi')); % Determine where
 folder is located.
movieFullFileName = fullfile(folder, 'Dat8Vid9Steps.avi');

% Check to see that movie file exists.
if ~exist(movieFullFileName, 'file')
 strErrorMessage = sprintf('File not found:\n%s\nYou can choose a new
 one, or cancel', movieFullFileName);
 response = questdlg(strErrorMessage, 'File not found', 'OK - choose a
 new movie.', 'Cancel', 'OK - choose a new movie.');
 if strcmpi(response, 'OK - choose a new movie.')
  [baseFileName, folderName, FilterIndex] = uigetfile('*.avi');
  if ~isequal(baseFileName, 0)
   movieFullFileName = fullfile(folderName, baseFileName);
  else
   return;
  end
 else
  return;
 end
end

try
 videoObject = VideoReader(movieFullFileName)
 % Determine how many frames there are.
 numberOfFrames = videoObject.NumberOfFrames;
 vidHeight = videoObject.Height;
 vidWidth = videoObject.Width;

 numberOfFramesWritten = 0;
 % Prepare a figure to show the images in the upper half of the
 screen.
 figure;
 %  screenSize = get(0, 'ScreenSize');
 % Enlarge figure to full screen.
 set(gcf, 'units','normalized','outerposition',[0 0 1 1]);
```

```
 % Loop through the movie, writing all frames out.
 % Each frame will be in a separate file with unique name.
 angles = zeros(numberOfFrames, 1); %make array with zeros with
 dimensions of the numbers of frames

 for frame = 1 : numberOfFrames
  % Extract the frame from the movie structure.
  thisFrame = read(videoObject, frame);

  % Display it
  hImage = subplot(2, 2, 1);
  image(thisFrame);
  caption = sprintf('Frame %4d of %d.', frame, numberOfFrames);
  title(caption, 'FontSize', fontSize);
  drawnow; % Force it to refresh the window.


%IMAGE PROCESSING PART

%1 CROPPING

%A=thisFrame; %original image
%A = thisFrame(576:672, 891:1141, 2); %cropped image
%A = thisFrame(370:507, 552:700, 2); %cropped image for DAT6 (minyx,
 minxy )
A = thisFrame(348:507, 723:800, 2); %cropped image for DAT6Vid10 enzo
 ookwel dat7 (minyx, minxy )
%W=image(A);
% W=imcrop(A);

%2 FROM PICTURE TO SKELETON
%I = rgb2gray(A); %convert to grayscale image
W=imadjust(A,stretchlim(A), [0 1]); %adjust contraast
imBW=im2bw(W, 0.4); %create black and white image
imBWinv = ~imBW;  % complement the image (objects of interest must be
 white)
%imBWc = bwmorph(imBWinv,'close',Inf); %closing, which is dilation
 followed by erosion
imBWc = bwmorph(imBWinv,'bridge',Inf);%closes ner pixels
%thin=bwmorph(imBWc, 'thin', Inf);
skelet= bwmorph(imBWc, 'skel', Inf); %create skeleton
spur = bwmorph(skelet, 'spur', 30); %trim branches
clean= bwmorph(spur, 'clean'); %remove isolated pixels
%figure
%imshow(clean)
[L, num]= bwlabel(clean);

%DETERMINE ANGLE
angle = regionprops(double(clean), 'Orientation') ;

angles(frame)= abs(angle.Orientation)-90;
        %angles(frame)= -(angle.Orientation)-90;
```

```
%PLOTTING ANGLES
        % Plot the angle.
  hPlot = subplot(2, 2, 2);
  hold off;
  plot(angles, 'k-', 'LineWidth', 2);
  hold on;
  grid on;

  % Put title back because plot() erases the existing title.
  title('angle orientation', 'FontSize', fontSize);
  if frame == 1
   xlabel('Frame Number');
   ylabel('Angle');
   % Get size data later for preallocation if we read
   % the movie back in from disk.
   [rows, columns, numberOfColorChannels] = size(thisFrame);
        end

  % Update user with the progress.  Display in the command window.
  if writeToDisk
   progressIndication = sprintf('Wrote frame %4d of %d.', frame,
 numberOfFrames);
  else
   progressIndication = sprintf('Processed frame %4d of %d.', frame,
 numberOfFrames);
  end
  disp(progressIndication);
  numberOfFramesWritten = numberOfFramesWritten + 1;


  subplot(2, 2, 3); %Plot cropped image
  imshow(A);
  title('cropped image', 'FontSize', fontSize);


  subplot(2, 2, 4); %plotting cleaned skeleton of needle
  imshow(clean);
  title('skeleton of Binarized Difference Image', 'FontSize',
 fontSize);
 end



end
```

Published with MATLAB® R2015a

Table of Contents


```
clc;    % Clear the command window.
close all;  % Close all figures (except those of imtool.)
imtool close all;  % Close all imtool figures.
clear;  % Erase all existing variables.
```

Categorising images per experimental condition

```
%For Front Images
%pqn = length(filenames); % Total number of runs
runs = 30;

for file_id = 1:(runs)
      %read out images from files (select map for front images in
 path)
    FimInit{file_id}=imread(sprintf('%d 1.jpg',file_id));
    FimFinal{file_id}=imread(sprintf('%d 2.jpg',file_id));
end

%  Categorize per condition

%For Front Images
FCond1= {FimFinal{7}, FimFinal{15},FimFinal{18},
 FimFinal{20},FimFinal{26}};
FCond2= {FimFinal{3}, FimFinal{14},FimFinal{16},
 FimFinal{19},FimFinal{27}};
FCond3= {FimFinal{1}, FimFinal{4},FimFinal{8},
 FimFinal{23},FimFinal{29}};
FCond4= {FimFinal{5}, FimFinal{9},FimFinal{12},
 FimFinal{13},FimFinal{21}};
FCond5= {FimFinal{10}, FimFinal{11},FimFinal{17},
 FimFinal{22},FimFinal{28}};
FCond6= {FimFinal{2}, FimFinal{6},FimFinal{24},
 FimFinal{25},FimFinal{30}};
FConds={FCond1, FCond2, FCond3, FCond4, FCond5, FCond6};
```

```
FCond1In= {FimInit{7}, FimInit{15},FimInit{18},
 FimInit{20},FimInit{26}};
FCond2In= {FimInit{3}, FimInit{14},FimInit{16},
 FimInit{19},FimInit{27}};
FCond3In= {FimInit{1}, FimInit{4}, FimInit{8},
 FimInit{23},FimInit{29}};
FCond4In= {FimInit{5}, FimInit{9}, FimInit{12},
 FimInit{13},FimInit{21}};
FCond5In= {FimInit{10},FimInit{11},FimInit{17},
 FimInit{22},FimInit{28}};
FCond6In= {FimInit{2}, FimInit{6},FimInit{24},
 FimInit{25},FimInit{30}};
FCondsInit={FCond1In, FCond2In, FCond3In, FCond4In, FCond5In,
 FCond6In};
```

For Side Images

```
runs = 30;

for file_id = 1:(runs)

    %read out images from files (select map for side images in path)
    SimInit{file_id}=imread(sprintf('%d 1.jpg',file_id));
    SimFinal{file_id}=imread(sprintf('%d 2.jpg',file_id));
end

SCond1= {SimFinal{7}, SimFinal{15},SimFinal{18},
 SimFinal{20},SimFinal{26}};
SCond2= {SimFinal{3}, SimFinal{14},SimFinal{16},
 SimFinal{19},SimFinal{27}};
SCond3= {SimFinal{1}, SimFinal{4},SimFinal{8},
 SimFinal{23},SimFinal{29}};
SCond4= {SimFinal{5}, SimFinal{9},SimFinal{12},
 SimFinal{13},SimFinal{21}};
SCond5= {SimFinal{10}, SimFinal{11},SimFinal{17},
 SimFinal{22},SimFinal{28}};
SCond6= {SimFinal{2}, SimFinal{6},SimFinal{24},
 SimFinal{25},SimFinal{30}};
SConds={SCond1, SCond2, SCond3, SCond4, SCond5, SCond6};

SCond1In= {SimInit{7}, SimInit{15},SimInit{18},
 SimInit{20},SimInit{26}};
SCond2In= {SimInit{3}, SimInit{14},SimInit{16},
 SimInit{19},SimInit{27}};
SCond3In= {SimInit{1}, SimInit{4}, SimInit{8},
 SimInit{23},SimInit{29}};
SCond4In= {SimInit{5}, SimInit{9}, SimInit{12},
 SimInit{13},SimInit{21}};
SCond5In= {SimInit{10},SimInit{11},SimInit{17},
 SimInit{22},SimInit{28}};
SCond6In= {SimInit{2}, SimInit{6},SimInit{24},
 SimInit{25},SimInit{30}};
```

```
SCondsInit={SCond1In, SCond2In, SCond3In, SCond4In, SCond5In,
 SCond6In};
```

cropping images

```
for i=1:length(FConds)
    for j=1:length(FConds{i})
      SCond=SConds{i};
      FCond= FConds{i};

      [X,Y,Fcropped,Frect] = imcrop(FCond{j});
      [X,Y,Scropped,Srect] = imcrop(SCond{j});
      FCr{j}= Fcropped;
      SCr{j}= Scropped;

      Frect(4)=150; %150 pixels down from top of cropping final
 position
      Srect(4)=150;

      FInCr{j} = imcrop(FCondsInit{i}{j},Frect);
      SInCr{j} = imcrop(SCondsInit{i}{j},Srect);
    end

    FCrCond{i}=FCr;
    SCrCond{i}=SCr;

    FInCrCond{i}= FInCr;
    SInCrCond{i}= SInCr;

end

 save('FCroppedImages.mat', 'FCrCond')
 save('FInCroppedImages.mat', 'FInCrCond')

 save('SCroppedImages.mat', 'SCrCond')
 save('SInCroppedImages.mat', 'SInCrCond')
```

Image processing: cropped images of final position

```
%Image Processing for Front View Cropped Images
% Do for FCrConds, SCrConds, FCrInitConds, SInitConds


for n=1:length(FCrCond)
    CrCond= FCrCond{n};
    CrCondIn=FInCrCond{n};

    for m=1:length(CrCond)
        W=imadjust(CrCond{m},stretchlim(CrCond{m}), [.1 .9]); %
 contrast stretch
        imBW=im2bw(W, 0.4); %create binary black and white image
```

```
        imBWinv = ~imBW;  % complement the image (objects of interest
must be white)
        imBWc1 = bwmorph(imBWinv,'bridge',Inf); %connecting close
pixels
        imBWc = bwmorph(imBWc1,'close',Inf); % closing
        imBWr=bwmorph(imBWc,'majority', 2); % get rid of noise larger
than 2 pixels
        skelet= bwmorph(imBWr, 'skel', Inf); %create skeleton
        spur = bwmorph(skelet, 'spur', 1); %trim branches of skeleton
        clean1= bwmorph(spur, 'clean'); %remove isolated pixels

        endPoints = bwmorph(clean1, 'Endpoints');    % Find first and
last points of skeleton
        [rows, columns] = find(endPoints);

        %figure
        %imshow(clean1);
        %hold on;
        %plot(columns,rows,'g*');

        %determine endpoint
        [yf{m}, no]=max(rows); %find maximum value in rows (y value)
        xf{m}=columns(no); %find corresponding value in columns (x
value)

      %determine first point to crop initial image
      [yfmin{m}, no]=min(rows); %find point of minimal value in rows
(y value)
      xmin=columns(no); %find corresponding value in columns (x
value)

      xfmin{m}=xmin;
      % figure
      %imshow(clean1);
      % hold on;
      % plot(xfmin,yfmin,'g*');

        figure
        imshow(clean1);
        hold on;
        plot(xf{m},yf{m},'g*');

    % Plotting final results on original cropped imange
        figure
        imshow(CrCond{m});
        hold on;

        plot(xf{m}, yf{m},'g*');
    title(['Final Cond.' 'condition n=' num2str(n) ',image m='
num2str(m)])

   end

   %save in cell
```

```
    Xf{n}=xf;
    Yf{n}=yf;

    Fyfmin{n}=yfmin;
    Fxfmin{n}=xfmin;

end
```

Image processing: cropped imanges of initial positions

```
for n=1:length(FInCrCond)
    CrCondIn=FInCrCond{n};
    xfmin=Fxfmin{n};
    yfmin= Fyfmin{n};

    for m=1:length(CrCondIn)
        A=imcrop(CrCondIn{m},[xfmin{m}-30 yfmin{m} 60 150]); %cropping
 frm begin point with rectangle of 60x150
        W=imadjust(A,stretchlim(A), [0.01 .99]); % contrast stretch
        imBW=im2bw(W, .6); %create binary black and white image
        imBWinv = ~imBW;  % complement the image (objects of interest
 must be white)
        imBWc1 = bwmorph(imBWinv,'bridge',Inf); %connecting close
 pixels
        imBWc = bwmorph(imBWc1,'close',Inf); % closing
        imBWr=bwmorph(imBWc,'majority', 2); % get rid of noise larger
 than 2 pixels
        skelet= bwmorph(imBWr, 'skel', Inf); %create skeleton
        spur = bwmorph(skelet, 'spur', 1); %trim branches of skeleton
        clean2= bwmorph(spur, 'clean'); %remove isolated pixels
        endPoints = bwmorph(clean2, 'Endpoints');    % Find last
 points of skeleton
        [rows, columns] = find(endPoints);

        %figure
        %imshow(clean2);
        %hold on;
        %plot(columns,rows,'g*');

        [yfIn{m}, no]=max(rows); %find maximum value in rows (y value)
        xfIn{m}=columns(no);  %find corresponding value in columns (x
 value)

        %Plotting points on binarized image for check
        figure
        imshow(clean2);
        hold on;
        plot(xfIn{m},yfIn{m},'g*');

        %Plotting results on original cropped image
        figure
```

```
        imshow(CrCondIn{m});
        hold on;
        plot((xfIn{m}+(xfmin{m}-10)),yfIn{m},'g*');
        title(['Initial Cond.' 'condition n=' num2str(n) ',image m='
 num2str(m)])

        %Determine difference between points
        Diffx{m}=Xf{n}{m}-(xfIn{m}+xfmin{m}-30); %ADJUST WITH CROPPING
 RECTANGLE
        Diffy{m}=Yf{n}{m}-yfIn{m};
    end

    %Xf{n}=xf;
    %Yf{n}=yf;

    %save values
    XfIn{n}=xfIn;
    YfIn{n}=yfIn;

    XFDiff{n}=Diffx;
    YFDiff{n}=Diffy;
    %imProc{n}=improc;
end
```

Image processing Side View

```
%same as processing Front view
%only names are different: So XS instead of XF
```

determine factor for frontview

```
imshow(FCondsInit{1}{1})
        [x1 y1] = getpts;
imshow(FCondsInit{1}{1})
        [x2 y2] = getpts;

FactorFront= 120/sqrt((x2-x1)^2+(y2-y1)^2);
```

deterimine factor for sideview

```
FactorSide1= cell2mat(YFDiff{1,1}).*FactorFront./
cell2mat( YSDiff{1,1});
FactorSide2= cell2mat(YFDiff{1,2}).*FactorFront./
cell2mat( YSDiff{1,2});
FactorSide3= cell2mat(YFDiff{1,3}).*FactorFront./
cell2mat( YSDiff{1,3});
FactorSide4= cell2mat(YFDiff{1,4}).*FactorFront./
cell2mat( YSDiff{1,4});
FactorSide5= cell2mat(YFDiff{1,5}).*FactorFront./
cell2mat( YSDiff{1,5});
FactorSide6= cell2mat(YFDiff{1,6}).*FactorFront./
cell2mat( YSDiff{1,6});
```

Plotting of angles

```
[Theta1, rho1]= cart2pol(cell2mat(XFDiff{1,1})*FactorFront,
 cell2mat(XSDiff{1,1}).*FactorSide1);
[Theta2, rho2]= cart2pol(cell2mat(XFDiff{1,2})*FactorFront,
 cell2mat(XSDiff{1,2}).*FactorSide2);
[Theta3, rho3]= cart2pol(cell2mat(XFDiff{1,3})*FactorFront,
 cell2mat(XSDiff{1,3}).*FactorSide3);
[Theta4, rho4]= cart2pol(cell2mat(XFDiff{1,4})*FactorFront,
 cell2mat(XSDiff{1,4}).*FactorSide4);
[Theta5, rho5]= cart2pol(cell2mat(XFDiff{1,5})*FactorFront,
 cell2mat(XSDiff{1,5}).*FactorSide5);
[Theta6, rho6]= cart2pol(cell2mat(XFDiff{1,6})*FactorFront,
 cell2mat(XSDiff{1,6}).*FactorSide6);

% determine mean values
Mean1=median(Theta1);
Mean2=median(Theta2);
Mean3=median(Theta3);
Mean4=median(Theta4);
Mean5=median(Theta5);
Mean6=median(Theta6);
%stXf=std(XFront)

%make all vectors same length for plotting
Dist2=10;

%transform in cartesian vectors for plotting
[Mx1,My1] = pol2cart(Mean1,Dist2);
[Mx2,My2] = pol2cart(Mean2,Dist2);
[Mx3,My3] = pol2cart(Mean3,Dist2);
[Mx4,My4] = pol2cart(Mean4,Dist2);
[Mx5,My5] = pol2cart(Mean5,Dist2);
[Mx6,My6] = pol2cart(Mean6,Dist2);

Dist=10*ones(1,5);
Zero=zeros(1,5);
[x1,y1] = pol2cart(Theta1,Dist);
[x2,y2] = pol2cart(Theta2,Dist);
[x3,y3] = pol2cart(Theta3,Dist);
[x4,y4] = pol2cart(Theta4,Dist);
[x5,y5] = pol2cart(Theta5,Dist);
[x6,y6] = pol2cart(Theta6,Dist);

% Plotting steering directions

figure
plotv([x1; y1],'k:'); hold on
plotv([Mx1; My1],'k-');
plotv([x2; y2],'c:');
plotv([Mx2; My2],'c-');
plotv([x3;y3],'r:');
plotv([Mx3;My3],'r-');
```

```
plotv([x4;y4],'g:');
plotv([Mx4;My4],'g-');
plotv([x5;y5],'b:');
plotv([Mx5;My5],'b-');
plotv([x6;y6],'m:');
plotv([Mx6;My6],'m-');

xlim([-11 11])
ylim([-11 11])
pbaspect([1 1 1])

%legend('EC1','EC2','EC3','EC4','EC5','EC6')
```

Boxplots of steering direction

```
tu=90;

Deflection=[rho1' rho2' rho3' rho4' rho5' rho6'];


Anglerad= [Theta1' Theta2' Theta3' Theta4' Theta5' Theta6'];
Angledeg=Anglerad./(2*pi).*360;
AngleAll=[Angledeg-tu];
Angle360= mod(AngleAll, 360); %-180/pi *

%adjust for increasing values
Angle360(:,6)=AngleAll(:,6);

%boxplot
labels = {'EC 1','EC 2','EC 3','EC 4', 'EC 5', 'EC 6'};

figure
boxplot(Deflection, labels)
xlabel('Conditions')
ylabel('Deflection (mm)')
title('Boxplot of deflection per experimental condition (EC)' )

figure
boxplot(360 -Angle360, labels)
xlabel('Conditions')
ylabel('Angle (degrees)')
title('Boxplot of angles of steering direction per experimental
 condition (EC)' )
```

Published with MATLAB® R2015a